SISSA

PhD in Astrophysics

Curriculum of Astroparticle Physics

Academic Year 2007/2008

PhD Thesis

High-energy astrophysics, cosmic rays and fundamental physics

Candidate:
Luca Maccione

Supervisors:
Stefano Liberati
Annalisa Celotti

To my parents

To my syster

To Elisa

High-energy astrophysics, cosmic rays and fundamental physics

Luca Maccione — *Ph.D. thesis*

Supervisors: S. Liberati and A. Celotti

Abstract

This thesis is devoted to the study of phenomenological consequences of theoretical models of Quantum Gravity. In particular, this work is focused on the study of possible violations of Lorentz invariance, which may arise if, owing to quantum gravity effects, the high-energy structure of the space-time is different from the smooth, continuous one we are used to in our low-energy world. After a brief description of the most widely known models accounting for Lorentz invariance violations, particular focus will be given to astrophysical tests of Lorentz invariance. These are motivated by the fact that some astrophysical objects are able to accelerate particles to extremely high energies, unreachable to terrestrial experiments. This consideration naturally leads us to look at the radiation of the Crab Nebula, one of the most powerful objects in our Galaxy. We first understand how the violation of Lorentz invariance affects the physical processes at the basis of the production of electromagnetic radiation by this object. Then, we compare our prediction for the Lorentz violating spectrum to observational data, exploiting the vast multi-wavelength information on the Crab Nebula radiation. Furthermore, we take advantage of the recent development of new technology to improve on our analysis of the Crab Nebula radiation by extending our research to the effects of Lorentz violation onto hard X-ray polarization.

After this investigation we shall move to study the physics of cosmic rays, the most energetic particles ever experienced on Earth. Our interest in this physics is twofold: on the one hand, we want to understand more about their properties and their propagation. To this aim, we develop a new model of propagation for cosmic rays in our Galaxy, exploiting as much as possible of the multi-channel information available at present. On the other hand, according to the multi-channel perspective, we try to understand the consequences of Lorentz symmetry violation on the properties of ultra-high-energy cosmic rays.

Contents

List of Figures

List of Tables

Acknowledgments

There are many people I should and would like to thank here. First of all, special thanks are to the two special persons who guided me during these few years spent at SISSA: my supervisors. I thank them not only for what they taught me about physics, for their physical insights, for the discussions we pleasantly had together, but also for their human qualities and their friendly support. I think the mission of a Professor should be not only to teach his professional topic, but also to make students grow in a more general sense. I feel they succeeded.

I cannot of course forget to thank my family. It would be meaningless to thank my parents, my sister Laura, for something, given that all I did was possible just because of them. I just thank them with all my hearth because they are, and because they are so. I thank Elisa, my wife, because she has been always very close to me, although some hundreds kilometers distant. We already traveled a lot, we will travel even more in the future, but together.

I cannot forget Dario, who I know since at least 4 years and whom it has been a pleasure to work with, John, for discussing with me lot of physics, and also for his kind hospitality in Heidelberg, and Piero.

I gratefully thank all my friends, for never making me feel alone. Carmelo and Barbara for their amusing initiatives, my flatmate Luca and Walter for always discussing with me many interesting questions, Lorenzo, Sara, Marcella, Marco and all the others.

A final thought to Lorena, our sector secretary, for her patient help in many administrative cases and for her infectious smile.

September 2008

Luca Maccione

Preface

Local Lorentz Invariance (LI) is fundamental to both of the two pillars of our present physical knowledge: the standard model of particle physics and general relativity. Nonetheless, the most recent progress in theoretical physics, in particular towards the construction of a theory of Quantum Gravity (QG), has led to a new perspective, in which both the above mentioned theories are seen as effective ones to be replaced by a theory of some more fundamental objects at high energies. From this perspective it is conceivable that even fundamental space-time symmetries (such as local LI) could cease to be valid in the vicinity of the Planckian regime.

There is little doubt that our low energy world is Lorentz invariant to great accuracy. LI has actually driven our intuition in the construction of successful physical theories over the last century, and has been continuously verified by increasingly high energy experiments built on Earth.

However, from a theoretical point of view, there is no reason why Lorentz symmetry should not be an attractive infrared fixed point of the fundamental theory "ultimately" describing the high-energy world. This would yield the LI world we live in, and a Lorentz violating high-energy one where the complete theory is defined. Moreover, from a purely logical point of view, it is clear that the hypothesis of *exact* Lorentz invariance at arbitrarily large energy is empirically not so strongly motivated given that an infinite volume of the Lorentz group is (and will always be) experimentally untested, since the Lorentz group is non-compact, unlike the rotation one.

Actually, the above reasoning is by itself not very specific, as it does not provide any argument by which we should expect any departure from Lorentz symmetry due to QG. However, there are other arguments that lead us to suspect that there could be a failure of Lorentz symmetry in the proximity of the Planck scale. Indeed, in recent years we have witnessed a growing interest in the possible high energy violations of local Lorentz Invariance as well as a flourishing of observational tests. Although Lorentz symmetry breaking is not firmly established as a necessary feature of QG, the possibility that Planck-scale induced Lorentz violation (LV) effects could provide an

observational window into QG phenomena deserves careful consideration.

From this perspective, it is crucial to set up tests that can probe Lorentz symmetry at higher and higher energies. Since QG effects are expected to be revealed in physical reactions involving very high energies, particle accelerators can be thought of as suitable experiments to also probe such new physics. In spite of the present impressive technological progress, however, it is not conceivable now to build terrestrial particle accelerators to probe energies much above 10 TeV.

A possible way out is provided by high energy astrophysics observations [18]. It is well known for many decades that cosmic accelerators are able to power particles up to at least 10^{15} eV, and even higher in special cases, either through direct observation of very high energy particles (like Cosmic Rays) or because we detect high energy radiation produced by accelerated particles (essentially electrons/protons) propagating in regions filled by magnetic fields (synchrotron radiation) or by intense radiation fields (inverse Compton scattering).

Although the interpretation of astrophysical observations is subject to many uncertainties, because it is impossible to perform controlled astrophysical experiments, nevertheless valuable information about fundamental physics can be inferred from them, in some special cases. In particular, concerning LV physics, when the physical modeling of the source powering high energy particles is reliable and well assessed, it is indeed possible to make predictions for LV phenomena and place significant limits on LV theories. For example, the radiation spectra produced by synchrotron emission of spiralling charged particles can be strongly modified by LV effects in the source, or LV effects in particle propagation can affect the polarisation property of radiation, or introduce energy dependent time delays in the arrival of photons from distant sources.

The large amount of data available today allows also a different type of study, through the exploitation of multi-wavelength and multi-channel data. Indeed, one of the main results of this thesis is to show that combined analyses of many observables, and in general the exploitation of the largest possible amount of data, allow us to gather valuable information about theoretical models of LV, that would have been virtually impossible to infer with a less refined and thorough study.

A methodological remark is in order: conventional models of astrophysical sources are rather approximate. While to fit, e.g., the overall spectrum of the radiation produced by some astrophysical object is, to some extent, an easy task, which can be accomplished with rather simple assumptions, there might be small features that are not explicable within simple models, but need further assumptions and complications and detailed modeling.

Moreover, even within sophisticated models, these features may still be only approximately explained.

It is therefore possible that LV could help accounting for these detailed phenomena. Would this be an evidence for LV? We think the answer to this question should be no. The first reason is that LV naturally introduces more degrees of freedom in the astrophysical model, hence, if the model description of data is only rough, it is somewhat natural that LV improves the fit to data. Furthermore, due to their large uncertainties, astrophysical observations and models can hardly be used to make a *discovery* of such an exotic phenomenon like violation of Lorentz invariance, although they are certainly suited to place limits on it (i.e. to give negative answers to the question whether Lorentz violation exists in some form). In order to discover LV we would definitely need more direct evidence.

This thesis

This thesis is composed of four main chapters. In chapter 1 we introduce the reader into the field of research on Quantum Gravity, and in particular on possible violations of Lorentz invariance. We shall present both theoretical models accounting for LV and the most relevant and up-to-date terrestrial and astrophysical constraints.

Chapter 2 is devoted to the LV analysis of the Crab Nebula radiation. First of all we describe the most relevant observations and the current widely accepted model explaining the overall features of the radiation spectrum. Then we revisit and discuss in detail the main processes taking place in the Nebula, paying particular attention to possible modifications introduced by LV. The final part of chapter 2 contains results motivated by recent measurements of polarisation of hard X-rays from the Crab Nebula, obtained with a novel technique.

Chapter 3 contains a short introduction to the physics of cosmic rays, with particular emphasis on their energy spectrum, their composition and the problem concerning their sources. As an aside, we discuss also a new model for the propagation of galactic cosmic rays, proposed by the author of this thesis in collaboration with other colleagues.

The discussion in chapter 3 is preparatory for the constraints discussed in chapter 4, which is devoted to the study of the LV effects on the properties of cosmic rays with the highest energies.

This thesis presents original work of the author, which can be found in the papers listed here: [19, 20, 21, 22, 23, 24].

Chapter 1

Quantum Gravity phenomenology

> "Ma misi me per l'alto mare aperto"
>
> Dante Alighieri

Our understanding of the fundamental laws of Nature is based at present on two different theories: a relativistic quantum theory of particle interaction, the Standard Model (SM) of Fundamental Interactions, and classical General Relativity (GR).

The former is our best description to date of physics on microscopic, subnuclear scales and is the result of the connection between quantum mechanics and special relativity. It was found historically that a theory which combines consistently relativistic invariance with the quantum behaviour of matter is essentially a field theory, in which interactions are carried by fields and also particles are understood as excitations of fields above their ground state. As it is already evident from this simple description, an essential ingredient of any Quantum Field Theory (QFT), as we know it nowadays, is the presence of a given smooth structure, the space-time, in which fields are defined and can propagate.

Moreover, although it is possible to construct QFT in curved space-time, our fundamental theory of elementary particle interactions has been mostly studied and developed in a fixed flat background space-time, making it very hard to include a dynamical understanding of the generation of the space-time itself in the theory, i.e. to include gravity. There are many reasons for this, besides technical simplicity of the standard approach, as testified by the many unsuccessful attempts to go beyond it in a consistent way. One

reason is that gravitational interactions among elementary particles are very much weaker than others, hence they can be neglected and there is no need to include gravity into the SM. Another possible reason is that experiments aimed at testing the fundamental properties of particles and interactions are so small with respect to the typical radius of curvature of the gravitational field of Earth (accelerator rings have lengths of the order of tens of kilometres) that the effect of gravity on particle interactions is negligible.

GR is instead our best description of gravity, at a classical, non-quantum level. In GR, all quantum properties of particles are neglected. This theory is essential in understanding situations in which the role of gravity cannot be neglected: for example, it is important to describe to high accuracy the motion of planets in the Solar System, to understand astrophysical situations such as the formation of a neutron star, or some features of AGN emission, and also cosmology.

However, in spite of their phenomenological success, SM and GR leave many theoretical questions still unanswered. First of all, since we feel that our understanding of the fundamental laws of Nature is deeper (and more accomplished) if we are able to reduce the number of degrees of freedom and coupling constants we need to describe it, many physicists have been trying to construct unified theories in which not only sub-nuclear forces are seen as different aspects of a unique interaction, but also gravity is included in a consistent manner. At some extent, the theory should include a quantum description of gravity. In fact, by suitably combining the three fundamental constants $\hbar$, c and G_N (G_N is Newton's constant), it is possible to obtain an energy scale, the Planck mass $M_{\rm Pl} \equiv \sqrt{\hbar c/G_N} \simeq 1.22 \times 10^{19}$ GeV/c^2 at which the quantum behaviour of gravity might be relevant.

Another important reason why we seek for a new theory of gravity comes directly from the gravity side. We know that GR fails to be a predictive theory in some regimes. Indeed, some solutions of Einstein's equations are known to be singular in some points, meaning that in these points GR is not able to make any prediction. Moreover, there are apparently honest solutions of GR equations predicting the existence of time-like closed curves, which would imply the possibility of travelling back and forth in time. The problem of black-hole entropy is intimately linked to the issue of information loss in GR.

We just listed few of the many issues to be faced by a complete theory of gravity, but one can already get a feeling with the impressive difficulty of the problems we should face. However, these problems pertain essentially to a purely logical, or theoretical point of view. Rather surprisingly, there are at present no firm, undisputed experimental indications that a quantum version of a theory of gravity should be really needed to ultimately describe

Nature. Indeed, one of the most intriguing problems is the extreme difficulty of performing sensible observational tests of candidate QG models. Then, we expect QG effects at low energy (with respect to the Planck scale) to be extremely small, due to suppression by the Planck scale and only very high-precision (or very high-energy) tests to be in principle viable.

However, depending on the underlying model of QG, qualitatively new effects can arise and provide some intuition on Planck-scale physics. Some of these new phenomena, that can be found in the literature of QG phenomenology, are listed below.

- Quantum decoherence and state collapse [25]
- QG imprint on initial cosmological perturbations [26]
- Cosmological variation of couplings [27, 28]
- TeV Black Holes, related to extra-dimensions [29]
- Violation of discrete symmetries [30]
- Violation of Lorentz invariance [31]

Among them, we are mostly interested in the phenomenology of violation of fundamental symmetries, because a convenient way of performing high-precision tests is to look for experimental deviations from symmetries that are believed to hold *exactly* in nature and could be broken by QG.

An example of such a physics law is CPT invariance, that requires physics to be unchanged under the combination of charge conjugation (C), parity inversion (P) and time reversal (T). As usual, C connects particles and antiparticles, P represents a spatial reflection of physical quantities with respect to the coordinate origin, while T reverses in time a physics reaction.

Lorentz symmetry is intimately related to CPT symmetry, in Quantum Field Theory. Indeed one of the hypotheses of the well known "CPT theorem" is Lorentz invariance. If CPT is broken, then at least one of the hypotheses of the CPT theorem should also break down. It has been proven [32] that Lorentz symmetry is the failing assumption in the so called "anti-CPT theorem", stating that in any unitary, local, relativistic point-particle field theory CPT breaking implies Lorentz violation. Note however that the converse of this statement is not true: it is well possible to violate Lorentz invariance while keeping CPT exact, as it will be shown in sec. 1.3, where also the role played by SuperSymmetry (SUSY) is discussed. However, this theorem does not hold for theories which do not admit a field-theoretic description and can then have unexpected properties.

It seems then that, naively, violation of Lorentz symmetry is more general than violation of CPT. Lorentz invariance of physical laws only relies on few assumptions: the principle of relativity, stating the equivalence of physical laws for non-accelerated observers, isotropy (no preferred direction) and homogeneity (no preferred location) of space-time, and a notion of precausality, requiring that the time ordering of events in one reference frame is preserved [33]. Some of them could then be broken by Planck scale physics.

The Lorentz group includes rotations and boosts, and is a subset of the so called Poincaré group, which in addition includes translations. Being non-compact, the Lorentz group does not admit finite-dimensional, unitary representations, unlike the rotation group. This means, essentially, that in principle boosts span over the real semi-axis $[1, +\infty)$, or, in more physical terms, that, given a massive particle at rest in one reference frame (in QFT this frame exists by definition of a massive particle as a $0-$momentum representation of the Lorentz group), there are reference frames, related to the first one by a Lorentz rotation (a boost), in which the particle's energy E' is arbitrary large. In such a reference frame, our particle would probe tiny lengths λ, of the order of $1/E'$. If λ is comparable to the Planck length scale $l_{\rm Pl} \sim 1/M_{\rm Pl}$, then the particle will probe QG effects. Therefore, if $l_{\rm Pl}$ is a minimum length scale (which we do not know...), it is hard to imagine boost invariance to be preserved beyond $M_{\rm Pl}$.

Apart from this somewhat heuristic intuition of why Lorentz invariance might be broken in QG, it is possible to show more formally several ways in which it can be broken indirectly. As an example, suppose translation symmetry is broken [34]. Then, the generator of translations, the energy-momentum tensor $\theta^{\mu\nu}$, is no longer conserved. Consider now the generator of Lorentz transformations

$$J^{\mu\nu} = \int \mathrm{d}^3x(\theta^{0\mu}x^\nu - \theta^{0\nu}x^\mu) \ . \tag{1.1}$$

Since it contains the non-conserved energy-momentum tensor $\theta^{\mu\nu}$, in general $J^{\mu\nu}$ will have nontrivial dependence on time, hence the usual time-independent Lorenz transformation generators do not exist and Lorentz symmetry is no longer ensured. The same argument holds if rotations are broken instead of translations (but notice that violation of rotation invariance is strongly constrained, see sec. 1.4).

The above discussion shows that it is interesting to study both theory and phenomenology of Lorentz invariance violation (LV), as a possible first glimpse of Quantum Gravity. While from the theoretical point of view research has been very active since many years, the development of a phe-

nomenology of LV has started growing just in the last ten years or so. Before mid-90s only few works investigated the experimental consequences of LV, because new effects were expected only in particle interactions at energies of order the Planck mass $M_{\rm Pl}$. Afterwards, it was realised that there are special situation in which new effects could manifest also at lower energy. These situations were called "Windows on Quantum Gravity".

1.1 Windows on Quantum Gravity

In recent years, attempts to place constraints on high-energy deviations from LI have mainly focused on modified dispersion relations for elementary particles. Indeed, specific hints of Lorentz Violation arose from various approaches to Quantum Gravity. Among the many examples, string theory tensor VEVs [35], space-time foam [36], semiclassical spin-network calculations in Loop QG [37], non-commutative geometry [38, 39, 40], some brane-world backgrounds [41] and condensed matter analogues of "emergent gravity" [42].

In most of the above mentioned QG models, LV enters through dispersion relations which can be cast in the general form (it is assumed, for simplicity, that rotational invariance is preserved and only boost invariance is affected by Planck-scale corrections):

$$E^2 = p^2 + m^2 + f(E, p; \mu; M) \ , \tag{1.2}$$

where we set the low energy speed of light $c = 1$, E and p are the particle energy and momentum, μ is a particle-physics mass-scale (possibly associated with a symmetry breaking/emergence scale) and M denotes the relevant QG scale. Generally, it is assumed that M is of order the Planck mass: $M \sim M_{\rm Pl} \approx 1.22 \times 10^{19}$ GeV, corresponding to a quantum (or emergent) gravity effect. The function $f(E, p; \mu; M)$ can be expanded in powers of the momentum (energy and momentum are basically indistinguishable at high energies, although they are both taken to be smaller than the Planck scale), and the lowest order LV terms (p, p^2 and p^3) have been mainly considered [31].

At first sight, it appears hopeless to search for effects suppressed by the Planck scale. Even the most energetic particles ever detected (Ultra High Energy Cosmic Rays, see, e.g., [43, 44]) have $E \lesssim 10^{11}$ GeV $\sim 10^{-8} M_{\rm Pl}$. However, even tiny corrections can be magnified into a significant effect when dealing with high energies (but still well below the Planck scale), long distances of signal propagation, or peculiar reactions (see, e.g., [31]). A partial list of these *windows on quantum gravity* includes:

- sidereal variation of Lorentz violation (LV) couplings as the lab moves with respect to a preferred frame or direction
- cumulative effects: long baseline dispersion and vacuum birefringence (e.g. of signals from gamma ray bursts, active galactic nuclei, pulsars)
- anomalous (normally forbidden) threshold reactions allowed by LV terms (e.g. photon decay, vacuum Čerenkov effect)
- shifting of existing threshold reactions (e.g. photon annihilation from blazars, GZK reaction)
- LV induced decays not characterised by a threshold (e.g. decay of a particle from one helicity to the other or photon splitting)
- maximum velocity (e.g. synchrotron peak from supernova remnants)
- dynamical effects of LV background fields (e.g. gravitational coupling and additional wave modes)

However not all of these tests are in the same way robust against the underlying physical framework that one is choosing in order to justify the use of the modified dispersion relations of the form (1.2). In fact while the above cited cumulative effects use exclusively the form of the modified dispersion relations basically all the others are dependent on the underlying dynamics of interacting particles and on the fact that the standard energy-momentum conservation holds or not. Hence in order to cast most of the constrains on dispersion relations of the form (1.2) one needs to adopt a specific theoretical framework justifying the use of such deformed dispersion relations.

We will detail below the most important theoretical frameworks present in the literature, as well as the best constraints obtained by low energy, terrestrial experiments and by higher energy astrophysical probes.

1.2 Purely kinematic frameworks

In order to study phenomenological effects of LV induced by QG, it is crucial to have a theoretical framework as complete as possible. In this respect two different approaches have been proposed.

On the one hand, one can interpret the dispersion relation (1.2) as the Casimir invariant of some new relativity group (which would then incorporate two invariant scales, c and $M_{\rm Pl}$). This approach is usually referred to as "doubly (or deformed)-special relativity" (DSR) [45, 46].

On the other hand, the dispersion relation (1.2) can be thought of as a by-product of an Effective Field Theory characterised by Planck suppressed LV operators. EFT has proven very effective and flexible in the past. It produces local energy and momentum conservation laws, and seems to require for its applicability just locality and local space-time translation invariance above some length scale. It describes the Standard Model of particle interactions and general relativity, many condensed matter systems at appropriate length and energy scales, and even string theory. Furthermore, it is at the moment the only framework within which we can compute reaction rates and in general fully describe the particle dynamics.

However, the main difference between the two approaches resides in the fact that while in DSR-like theories the violation of Lorentz invariance is only apparent, because no preferred frame is actually introduced, in EFT there is an explicit breaking of Lorentz invariance through the existence of a preferred reference frame.

It is important to notice that while physics obviously requires dynamics, not all QG theories are at a stage of development which includes dynamics. For those theories (as, e.g. DSR) only purely kinematic tests are possible, until they become more mature. Due to their importance, we will review the main kinematical and dynamical frameworks proposed in the literature[1].

1.2.1 Systematic modified dispersion relations

A first, primitive way to violate Lorentz invariance in a particle physics framework is to phenomenologically modify particle dispersion relations, retaining energy-momentum conservation. In this context, it is assumed that the standard, Lorentz invariant dispersion relation $E^2 = m^2 + p^2$ is replaced, in a particular reference frame, by a more general $E^2 = F(p, m)$. The presence of such a particular frame introduces a "preferred reference frame", thereby explicitly violating Lorentz invariance. A usual choice for the preferred frame is that in which the Cosmic Microwave Background (CMB) radiation looks exactly isotropic (which is sometimes called the "rest frame" of CMB). Since our world is nearly Lorentz invariant and almost at rest with respect to CMB (the Earth velocity v_E with respect to CMB can be estimated by looking at the observed "dipole" anisotropy, which is of the order of $10^{-3} \equiv v_E/c$), in the preferred frame $F(p, m)$ must reduce to the Lorentz invariant dispersion relation at small momenta, hence it must admit a power

[1] Of course, in the absence of a complete and fully reliable theory of Quantum Gravity, the first attempts of description of Lorentz invariance violation did not include dynamics, but were essentially related to geometric properties of space and time. They are important for historical reasons.

series expansion around $p = 0$

$$E^2 = m^2 + p^2 + M_{\rm Pl} f_i^{(1)} p^i + f_{ij}^{(2)} p^i p^j + \frac{f_{ijk}^{(3)}}{M_{\rm Pl}} p^i p^j p^k + \dots \ , \qquad (1.3)$$

where the $f_{ij\dots}^{(n)}$ are dimensionless, arbitrary and (presumably) small coefficients and, in order to adjust dimensions, suitable powers of the high energy scale, which, being this construction motivated by QG, we assume to be of order of the Planck mass $M_{\rm Pl}$, are factored out. However, the fact that the correct mass factor is the Planck mass $M_{\rm Pl}$ is rather arbitrary, at least for linear and quadratic corrections, because we potentially miss huge suppression factors of the form $m/M_{\rm Pl}$. It is understood that the actual order n of the power expansion at which corrections in (1.3) start to be non-zero is set by the underlying physical model of QG.

A major simplification can be done assuming rotation invariance to be preserved. This procedure is somehow phenomenologically justified by the fact that it is virtually impossible to break rotations without having a corresponding break of boost invariance. For example, in field theory this is automatic, because if one breaks rotations by coupling matter with a non-zero space-like constant vector, then also boosts are broken [31]. Then, it is sound to consider first boost invariance breaking without violation of rotational symmetry. In this case, we have, with a slight abuse of notation,

$$E^2 = m^2 + p^2 + M_{\rm Pl} f^{(1)} |p| + f^{(2)} p^2 + \frac{f^{(3)}}{M_{\rm Pl}} |p^3| + \dots \ , \qquad (1.4)$$

where all the $f^{(n)}$ coefficients are in principle different from particle to particle. It is worth mentioning that this would lead also to a breaking of the equivalence principle.

1.2.2 Robertson-Mansouri-Sexl framework

This framework [47, 48, 49] is a kinematic test theory meant to parameterize departures from Lorentz invariance. The basic assumption of this model is that there exists a preferred frame in which the speed of light is isotropic. This corresponds to introducing the following new Lorentz transformations

$$t' = a^{-1}(t - \vec{\epsilon} \cdot \vec{x}) \qquad (1.5)$$

$$\vec{x} = d^{-1}\vec{x} - (d^{-1} - b^{-1})\frac{\vec{v}(\vec{v} \cdot \vec{x})}{v^2} + a^{-1}\vec{v}t \ , \qquad (1.6)$$

where a, b, d are functions of the relative velocity between frames.

It can be shown that the above transformations are the most general ones preserving rectilinear motion in absence of forces, and can be reduced to those of special relativity by setting $a = b^{-1} = \sqrt{1 - v^2}, d = 1$, assuming Einstein clock synchronisation. Actually, the vector $\vec{\epsilon}$ depends in general on the procedure adopted to synchronise clocks.

The main drawback of the RMS framework is its intrinsic incompleteness, evident in the lack of any dynamic prescription, in particular on how fundamental clocks and rods are related to the underlying fundamental physics. In particular, as the RMS transformation depends on the vector $\vec{\epsilon}$, which in turn is dependent on the synchronisation procedure adopted, it turns out that it is virtually impossible to compare tests on RMS frameworks based on different clocks and rods. However, this incompleteness can be attenuated, if not resolved, by noticing that it is possible to incorporate this framework in the Standard model extension [50], which will be discussed later.

1.2.3 Doubly special relativity

A radically different approach has been taken with the study of the so called "Doubly-special" relativity. Even though this theory is aimed also at including dynamics, we list it among the "kinematic theories" because, currently, it is not a complete theory and has major mathematical problems of internal consistency when considering dynamics. Hence, at present DSR is only a kinematic theory. Nevertheless, it is attractive because it does not postulate the existence of a preferred frame, but rather it deforms the usual concept of Lorentz invariance [51, 46, 45]. In fact, DSR theory postulates that the Lorentz group still generates space-time symmetries, but it acts in a non-linear way on the fields, such that not only the speed of light c is an invariant quantity, but also a new momentum scale $E_{\rm DSR}$ (hence the name of "doubly-special"), which is usually taken to be of the order of $M_{\rm Pl}$. It is interesting to notice that DSR-like features are found in models of non-commutative geometry, in particular in the κ-Minkowski framework [52, 53].

For what concerns phenomenology, it is important to have equations for the conservation of energy and momentum, as these can be used in deriving constraints on Lorentz invariance violation from particle physics phenomena. These equations are easily derived from the relations

$$E = \frac{\epsilon}{1 + \epsilon/E_{\rm DSR}} \tag{1.7}$$

$$p = \frac{\pi}{1 + \pi/E_{\rm DSR}} \,, \tag{1.8}$$

where E, p are the physical (i.e. actually measured) energy and momentum, while ϵ and π are the so called "pseudo-energy" and "pseudo-momentum" respectively. It was found in [54] that ϵ and π transform under the usual Lorentz transformations, thereby inducing the transformation laws for E, p. From these rules, it follows that particle interactions can be conveniently computed using the pseudo-variables, and then translated into the physical variables to obtain the new thresholds and kinematic conditions.

It is customary to see that the dispersion relation obtained from eq. (1.8) is of the form

$$E^2 - p^2 = m^2 \frac{1 - (E/E_{\mathrm{DSR}})^2}{1 - (m/E_{\mathrm{DSR}})^2} \tag{1.9}$$

However, some indication on DSR phenomenology can be obtained by considering that, as in Special Relativity, any phenomenon that would imply the existence of a preferred reference frame is forbidden. Hence, the detection of such a phenomenon would imply the falsification of both special and doubly-special relativity. An example of such a process is the decay of a massless particle.

1.3 Dynamic frameworks

Dynamically meaningful realisations of Lorentz invariance violation are more interesting from a phenomenological point of view, as they provide a more complete framework in which to compute reactions. An obvious property of any model aimed at representing our world is to agree with experimental observations. Hence, a convenient way to study Lorentz invariance violation is to embed it into an effective framework which also contains the Standard Model of particle interactions.

The approach of Effective Field Theory is a well established way of describing physics which could be used to our aim. Indeed, there are widely diffuse ideas that the Standard Model itself, though being able to describe at unprecedented precision, and also at the quantum level, particle interactions up to ~ 100 GeV, could be such an effective model. The reasons for that are both historical and theoretical.

From the historical point of view, physicists have learned over the years that every imagined high-energy physics model, although pretty well working up to some energy scale, was not able to give reliable predictions when applied to much larger energies, where it revealed itself as a part of a more complex and complete model. This is what happened, for example, with the Fermi model of weak interactions, which turned out to be a low energy, effective description of the weak interaction Standard Model sector. Actually, from

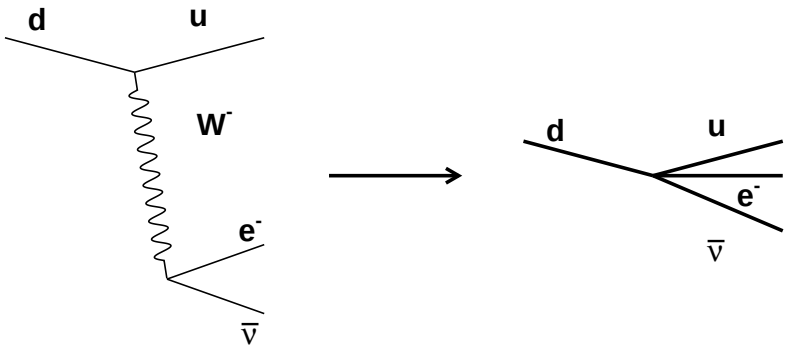

Figure 1.1: High energy degrees of freedom are integrated out at low energy, therefore the actual interaction becomes point-like. This is the basic interaction diagram for the neutron decay.

this story physicists learned even more, because it was realised that, within the SM, it was possible to give a unified description of electromagnetic and weak interactions.

On the other hand, the SM describes fundamental interactions (excluding gravity) as the manifestation of invariance under a symmetry group, identified as $SU(3) \times SU(2) \times U(1)$, which then contains 3 different interactions (expressed as 3 different coupling constants). The aim of theorists is now to describe the SM as the effective, low energy expression of some larger group, in which the 3 SM interactions can be unified, as it happened with electromagnetism and weak interactions, and, possibly, where also gravity could nicely fit.

One may wonder at this stage why is the SM so hard to embed into a more complete one, that more than 30 years after its discovery, this task has not been completed. A reason for this, among many others, is that, differently from the Fermi theory, whose coupling constant G_F has mass dimension -2, and is then non-renormalizable by power-counting, the SM is a renormalizable theory.

In EFT, the presence of non-renormalizable operators in the Lagrangian is a signal of the presence of new higher energy interactions. In particular, in the context of the Fermi interactions, high energy degrees of freedom, the $W^{\pm}$ bosons, whose mass is of the order of ~ 80 GeV, are too heavy to actually propagate, thereby inducing a point-like interaction, the so called $4-$fermion interaction, as exemplified in figure 1.1. On the contrary, for the SM this kind of reasoning cannot be applied, because its renormalizability does not allow to even guess at which scale new physics should appear.However, from a QG

point of view, this behaviour can be understood by simply admitting that the energy scale at which the full theory should be defined, i.e. the Planck scale $M_{\rm Pl}$, is so large that no effect can appear at ~ 100 GeV $\simeq 10^{-17} M_{\rm Pl}$. Nevertheless, it has been shown that, without some custodial symmetry protecting the SM from LV operators of dimension ≤ 4, Lorentz invariance violation can appear in the SM both in renormalizable extra operators and in non-renormalizable ones. Both possibilities have been explored in the so called Standard Model Extension (SME), which will be discussed below.

Albeit EFT is a natural framework in which to study LV, there are other possibilities, arising in some model of string theory, that deserve attention. Indeed, if in the high energy theory a hidden sector exists, which cannot be accessed because it lives, for example, on a different $D-$brane than us, there are LV effects that cannot be fit in an EFT description. Since the EFT approach is nothing more than a highly reasonable, but rather arbitrary "assumption", it is worth studying and constraining also these models.

1.3.1 Standard Model Extension with renormalizable operators

Concrete realisations of this framework can be divided in two main lines of research: EFT with only renormalizable (*i.e.* mass dimension 3 and 4) LV operators, or EFT with non-renormalizable (*i.e.* mass dimension 5 and higher) LV operators. We will deal here with SME with renormalizable operators, while the next section will be devoted to the study of SME with non-renormalizable operators, which is the proper subject of this thesis.

Most of the research along the first direction has been carried out within the so called (minimal) SME [35]. It consists of the standard model of particle physics plus all Lorentz violating renormalizable operators (*i.e.* of mass dimension ≤ 4) that can be written without changing the field content or violating gauge symmetry. The operators appearing in the SME can be conveniently classified according to their behaviour under CPT.

Gauge invariant form

We shall deal first with CPT odd terms. The additional LV operators of such form for the leptons are

$$-(a_L)_{\mu AB}\bar{L}_A\gamma^\mu L_B - (a_R)_{\mu AB}\bar{R}_A\gamma^\mu R_B \,, \tag{1.10}$$

where L_A is the left-handed fermion doublet, R_A is the right-handed lepton singlet and A, B are flavour indexes. The parameters $(a_{L,R})_{\mu AB}$ are constant

vectors that in principle can mix also flavour indexes. As a remark, we notice here that the $(a_{L,R})_{\mu AB}$ (as well as all other coefficients that will appear in the following) can be assumed to be constant because we only deal with flat-space models, whereas if we would have also diffeomorphism invariance they should have been promoted to dynamical fields.

For quarks, a similar equation holds

$$-(a_Q)_{\mu AB}\bar{Q}_A\gamma^\mu Q_B-(a_U)_{\mu AB}\bar{U}_A\gamma^\mu U_B-(a_D)_{\mu AB}\bar{D}_A\gamma^\mu D_B\ , \tag{1.11}$$

where now Q_A is the quark left-handed doublet, while U_A, D_A are the up and down quark right-handed singlets, respectively. For the gauge sector, instead, we have

$$\begin{aligned}&(k_0)_\kappa B^\kappa+(k_1)_\kappa\epsilon^{\kappa\lambda\mu\nu}B_\lambda B_{\mu\nu}\\&+(k_2)_\kappa\epsilon^{\kappa\lambda\mu\nu}\mathrm{Tr}(W_\lambda W_{\mu\nu}+\tfrac{2}{3}igW_\lambda W_\mu W_\nu)\\&+(k_3)_\kappa\epsilon^{\kappa\lambda\mu\nu}\mathrm{Tr}(G_\lambda G_{\mu\nu}+\tfrac{2}{3}ig_3G_\lambda G_\mu G_\nu)\ ,\end{aligned} \tag{1.12}$$

where B_μ, W_μ, G_μ are $U(1), SU(2), SU(3)$ gauge fields and $B_{\mu\nu}, W_{\mu\nu}, G_{\mu\nu}$ their respective field strengths. We notice that usually the $(k_0)_\kappa$ term is required to vanish, because it leads to instabilities in the theory, and that all the other terms have mass dimension 1.

Turning now to CPT even operators, for leptons we have

$$\frac{1}{2}i(c_L)_{\mu\nu AB}\bar{L}_A\gamma^\mu\overleftrightarrow{D^\nu}L_B+\frac{1}{2}i(c_R)_{\mu\nu AB}\bar{R}_A\gamma^\mu\overleftrightarrow{D^\nu}R_B\ , \tag{1.13}$$

while for quarks

$$\frac{1}{2}i(c_Q)_{\mu\nu AB}\bar{Q}_A\gamma^\mu\overleftrightarrow{D^\nu}Q_B+\frac{1}{2}i(c_U)_{\mu\nu AB}\bar{U}_A\gamma^\mu\overleftrightarrow{D^\nu}U_B+\frac{1}{2}i(c_D)_{\mu\nu AB}\bar{D}_A\gamma^\mu\overleftrightarrow{D^\nu}D_B \tag{1.14}$$

Furthermore, for gauge fields we have

$$-\frac{1}{4}(k_B)_{\kappa\lambda\mu\nu}B^{\kappa\lambda}B^{\mu\nu}+\frac{1}{2}(k_W)_{\kappa\lambda\mu\nu}\mathrm{Tr}(W^{\kappa\lambda}W^{\mu\nu})-\frac{1}{2}(k_G)_{\kappa\lambda\mu\nu}\mathrm{Tr}(G^{\kappa\lambda}G^{\mu\nu})\ . \tag{1.15}$$

These terms are all of mass dimension 0, but we should warn that the apparent correspondence between CPT parity and odd/even mass dimension is only accidental and will not hold for higher dimension operators.

We should also consider the Yukawa coupling between fermions and the

Higgs field. These are

$$-\tfrac{1}{2}\left[(H_L)_{\mu\nu AB}\bar{L}_A\phi\sigma^{\mu\nu}R_B + (H_U)_{\mu\nu AB}\bar{Q}_A\phi^*\sigma^{\mu\nu}U_B + (H_D)_{\mu\nu AB}\bar{Q}_A\phi\sigma^{\mu\nu}D_B\right] + h.c.\ , \tag{1.16}$$

while for the Higgs field alone one finds the CPT odd term

$$i(k_\phi)^\mu\phi^\dagger D_\mu\phi + h.c.\ , \tag{1.17}$$

while the CPT even terms are

$$\frac{1}{2}[(k_{\phi\phi})^{\mu\nu}(D_\mu\phi)^\dagger D_\nu\phi - (k_{\phi B})^{\mu\nu}\phi^\dagger\phi B_{\mu\nu} - (k_{\phi W})^{\mu\nu}\phi^\dagger W_{\mu\nu}\phi] + h.c. \tag{1.18}$$

Low energy form

Since tests on renormalizable LV operators are usually made at low energy, when the $SU(2)$ gauge symmetry has been broken, it may be useful to re-express the SME in an easier form to deal with. In particular, we can single out each individual fermion and identify its own coefficient.

After the gauge breaking, the CPT odd fermion LV terms become

$$-a_\mu\bar{\psi}\gamma^\mu\psi - b_\mu\bar{\psi}\gamma^5\gamma^\mu\psi\ , \tag{1.19}$$

while the CPT even terms are

$$-\frac{1}{2}H_{\mu\nu}\bar{\psi}\sigma^{\mu\nu}\psi + \frac{1}{2}ic_{\mu\nu}\bar{\psi}\gamma^\mu\overleftrightarrow{D^\nu}\psi + \frac{1}{2}id_{\mu\nu}\bar{\psi}\gamma_5\gamma^\mu\overleftrightarrow{D^\nu}\psi\ . \tag{1.20}$$

The symbol ψ represent the fermion spinor and it is understood that each fermion has its own set of LV parameters. It is customary to see that the constant a-term in equation (1.19) could be reabsorbed by spinor redefinition $\psi \to e^{-ia\cdot x}\psi$. However, in presence of theories with many interacting particles it is possible to remove only one a_μ, hence only differences between these parameters can be probed by multi-fermion tests.

At present, gauge boson LV is only probed in the electromagnetic sector. For this reason, we show here the LV operators for electromagnetism

$$-\frac{1}{4}(k_F)_{\kappa\lambda\mu\nu}F^{\kappa\lambda}F^{\mu\nu} + \frac{1}{2}(k_{AF})^\kappa\epsilon_{\kappa\lambda\mu\nu}A^\lambda F^{\mu\nu}\ , \tag{1.21}$$

where the (k_F) term is CPT even, while the (k_{AF}) one is CPT odd and, since it leads to instabilities in the theory, is assumed to vanish.

LV QED

Since the most common particles used to cast constraints on LV are photons and electrons, a prominent role is played by LV QED.

If we label by $\pm$ the two photon polarisations, we can write the photon dispersion relation, due to (1.21), as [50]

$$E = (1 + \rho \pm \sigma)|\vec{p}| \tag{1.22}$$

where $\rho = \tilde{k}^{\alpha}_{\alpha}/2$, $\sigma^2 = 1/2(\tilde{k}_{\alpha\beta})^2 - \rho^2$, $\tilde{k}_{\alpha\beta} = (k_F)_{\alpha\beta\gamma\delta}p^{\gamma}p^{\delta}/|\vec{p}|^2$.

The structure of the coefficients $(k_F)_{\alpha\beta}$ is in general quite complicated, and could make it very hard to obtain significant constraints. In particular, in general rotational invariance is not preserved. We already gave (see section 1) motivations for assuming rotation invariance to be preserved, at least in first approximation, in LV contexts. If we make this assumption here, we obtain a major simplification of our framework, because in this case all LV tensors must reduce to suitable products of a time-like vector field, which is usually called u^{α} and, in the preferred frame, is assumed to have components $(1, 0, 0, 0)$. Then, the rotational invariant LV operators are

$$-bu_{\mu}\bar{\psi}\gamma_5\gamma^{\mu}\psi + \frac{1}{2}icu_{\mu}u_{\nu}\bar{\psi}\gamma^{\mu}\overleftrightarrow{D^{\nu}}\psi + \frac{1}{2}idu_{\mu}u_{\nu}\bar{\psi}\gamma_5\gamma^{\mu}\overleftrightarrow{D^{\nu}}\psi \tag{1.23}$$

for electrons and

$$-\frac{1}{4}(k_F)u_{\kappa}\eta_{\lambda\mu}u_{\nu}F^{\kappa\lambda}F^{\mu\nu} \tag{1.24}$$

for photons. The high energy ($M_{\rm Pl} \gg E \gg m$) dispersion relations for the SME can be expressed as

$$E^2 = m^2 + p^2 + f_e^{(1)}p + f_e^{(2)}p^2 \tag{1.25}$$

$$E^2 = (1 + f_{\gamma}^{(2)})p^2 \tag{1.26}$$

where, if $s = \pm 1$ is the helicity state of the electron, $f_e^{(1)} = -2bs$, $f_e^{(2)} = -(c - ds)$, and $f_{\gamma}^{(2)} = k_F/2$. The positron dispersion relation is the same as (1.25) with the replacement $p \to -p$, which will change only the $f_e^{(1)}$ term.

We notice here that the typical energy at which a new phenomenology should start to appear is quite low. In fact, taking for example $f_e^{(2)} \sim O(1)$, one finds that the corresponding extra-term is comparable to the electron mass m precisely at $p \simeq m \simeq 511$ keV. Even worse for the linear modification to the dispersion relation, which in principle could be Planck-scale enhanced, rather than suppressed, leading to $p_{\rm th} \sim m^2/M_{\rm Pl} \sim 10^{-17}$ eV. (Notice that this energy corresponds by chance to the present upper limit on the photon

mass, $m_\gamma \lesssim 10^{-18}$ eV [55].)

However, it may well be that the natural values for the parameters $f_e^{(n)}$ are much less than $O(1)$. For example, they can be suppressed by ratios of $(m_e/M_{\rm Pl})^k$, with $k > 0$. If we take $k = 1$, than the suppression factor is $m_e/M_{\rm Pl} \simeq 4 \times 10^{-23}$, which is not too far from the limits that have been placed on dimension 4 LV parameters up to now.

1.3.2 SME with non-renormalizable operators

An alternative approach within EFT is to study non-renormalizable operators. Nowadays it is widely accepted that the SM could just be an effective field theory and in this sense its renormalizability is seen as a consequence of neglecting some higher order operators which are suppressed by some appropriate mass scale. It is a short deviation from orthodoxy to imagine that such non-renormalizable operators can be generated by quantum gravity effects (and hence be naturally suppressed by the Planck mass) and possibly associated to the violation of some fundamental space-time symmetry like local Lorentz invariance.

Myers & Pospelov [56] found that there are essentially only three operators of dimension five, quadratic in the fields, that can be added to the QED Lagrangian preserving rotation and gauge invariance, but breaking local LI. Actually these criteria allow the addition of other (CPT even) terms, but these would not lead to modified dispersion relations (they can be thought of as extra interaction terms) [57].

These extra-terms, which result in a contribution of $O(E/M_{\rm Pl})$ to the dispersion relation of the particles, are the following:

$$-\frac{\xi}{2M_{\rm Pl}} u^m F_{ma}(u\cdot\partial)(u_n \tilde{F}^{na}) + \frac{1}{2M_{\rm Pl}} u^m \bar{\psi}\gamma_m(\zeta_1 + \zeta_2\gamma_5)(u\cdot\partial)^2\psi\,, \quad (1.27)$$

where $\tilde{F}$ is the dual of F and ξ, $\zeta_{1,2}$ are dimensionless parameters. All these terms also violate the CPT symmetry.

More recently, this construction has been extended to the whole SM [57] and to extra interaction terms in QED.

Gauge sector of QED

In particular, regarding QED, which is the most important theory to be studied for placing constraints, it can be shown that no new pure gauge interactions arise due to LV. In fact, a generic content of a gauge invariant tensor has to be bilinear in the field strength $F_{\mu\nu}$ and contain one extra

derivative (which must be a covariant derivative in the case of a non-abelian field). The only non-vanishing terms satisfying these properties are

$$F_{\mu\nu}\partial^{\nu}\widetilde{F}^{\mu\rho}\ , \qquad F_{\mu\nu}\partial^{\nu}F^{\rho\sigma}\ , \qquad F_{\mu\lambda}\partial_{\nu}\widetilde{F}^{\rho\lambda} \qquad \text{and} \qquad F^{\mu\nu}\partial^{\lambda}F^{\rho\sigma}\ . \quad (1.28)$$

The first two terms are *reducible* on the equations of motion, hence must be ignored. Concerning the remaining two structures, $F_{\mu\lambda}\partial_{\nu}\widetilde{F}_{\rho}{}^{\lambda}$ and $F^{\mu\nu}\partial^{\lambda}F^{\rho\sigma}$, the first has been shown to modify the dispersion relations of the photon [56]. It was shown in particular that this operator has to be contracted with an irreducible absolutely symmetric tensor, in order to be protected from uncontrollable divergencies:

$$C^{\mu\nu\rho}\,F_{\mu\lambda}\partial_{\nu}\widetilde{F}_{\rho}{}^{\lambda}\ , \qquad C^{\mu}{}_{\mu}{}^{\rho}=0\ . \quad (1.29)$$

Moreover, the conditions of symmetry and irreducibility of the tensor $C^{\mu\nu\rho}$ follow from the requirement of independence of this operator of the lower-rank operators of (1.28), which is also a way of protection against the mixing with such operators at the loop level.

The last operator in (1.28), the five-index object $F^{\mu\nu}\partial^{\lambda}F^{\rho\sigma}$, can be shown to be irrelevant. In fact, one needs to separate it from all lower-rank interactions. In other words, one needs to subtract all possible $g^{\mu\nu}$ and $\epsilon^{\mu\nu\rho\sigma}$ traces of this term, before substituting it into the equation of motion to see if it brings nontrivial contributions. It turns out that this operator is completely expressible in terms of its $\epsilon^{\mu\nu\rho\sigma}$-trace, which coincides with the operator $C^{\mu\nu\rho}$. Then it is not possible to bring the rank five operator to an irreducible form, and consequently there is no dimension 5 LV interaction contracted with an irreducible rank five tensor.

Matter Sector of QED

In contrast to what happens in the gauge sector, the LV terms in the matter sector of QED have much wider variety than the set of structures presented in [56]. The reason is that the operators can be formed both by using covariant derivatives $\mathcal{D}_{\mu}$ and by inserting gamma matrices.

Using a Young tableaux technique, it can be shown that all the relevant

operators are the following [57]

$$
\begin{aligned}
&\mathcal{L}_{\rm QED}^{\rm matter} = \qquad (1.30)\\
&\quad \widetilde{c}_1^{\mu}\cdot\overline{\psi}\,\gamma^{\lambda}\widetilde{F}_{\mu\lambda}\psi^{+} + \widetilde{c}_2^{\mu}\cdot\overline{\psi}\,\gamma^{\lambda}\gamma^{5}\widetilde{F}_{\mu\lambda}\psi^{-} + f_1^{\mu\nu}\cdot\overline{\psi}\,F_{\mu\nu}\psi^{-} + f_2^{\mu\nu}\cdot\overline{\psi}\,F_{\mu\nu}\gamma^{5}\psi^{-}\\
&\quad + h_1^{\mu\nu}\cdot\overline{\psi}\,\mathcal{D}_{(\mu}\mathcal{D}_{\nu)}\psi^{+} + h_2^{\mu\nu}\cdot\overline{\psi}\,\mathcal{D}_{(\mu}\mathcal{D}_{\nu)}\gamma^{5}\psi^{+} + C_1^{\mu\nu\rho}\cdot\overline{\psi}\,\gamma_{(\mu}\mathcal{D}_{\nu}\mathcal{D}_{\rho)}\psi^{-}\\
&\quad + C_2^{\mu\nu\rho}\cdot\overline{\psi}\,\gamma_{(\mu}\gamma^{5}\mathcal{D}_{\nu}\mathcal{D}_{\rho)}\psi^{+} + D_1^{\mu\nu\rho}\cdot\overline{\psi}\,\gamma_{(\mu}F_{\rho)\nu}\psi^{+} + D_2^{\mu\nu\rho}\cdot\overline{\psi}\,\gamma_{(\mu}F_{\rho)\nu}\gamma^{5}\psi^{-}\\
&\quad + E_1^{\mu\nu\rho\lambda}\cdot\overline{\psi}\,\sigma_{\mu)\nu}\mathcal{D}_{(\rho}\mathcal{D}_{\lambda}\psi^{-} + E_2^{\mu\nu\rho\lambda}\cdot\overline{\psi}\,\sigma_{\mu)(\lambda}F_{\rho)(\nu}\psi^{+}\\
&\quad + E_3^{\mu\nu\rho\lambda}\cdot\overline{\psi}\,\sigma_{\mu)[\nu}F_{\rho](\lambda}\psi^{+}\\
&\quad + E_4^{\mu\nu\rho\lambda}\cdot\overline{\psi}\,\left(\sigma_{\mu)[\nu}\mathcal{D}_{\rho]}\mathcal{D}_{(\lambda} - \sigma_{\nu](\mu}\mathcal{D}_{\lambda)}\mathcal{D}_{[\rho} + 2\,\sigma_{\nu\rho}\mathcal{D}_{(\mu}\mathcal{D}_{\lambda)}\right)\psi^{-}\,.
\end{aligned}
$$

Here, + and − superscripts refer to the parity of the corresponding LV term under the charge conjugation C.

As it is customary to see, the C_1 and C_2 terms in (1.30) are those found in the first analysis by [56], while all the others are interaction terms that do not lead to modified dispersion relations. However, in order to detect these effects, we would need much more accurate experimental facilities than what are built or planned at present.

QED modified dispersion relations

From (1.27) the dispersion relations of the fields are modified as follows. For the photon

$$\omega_{\pm}^2 = k^2 \pm \frac{\xi}{M_{\rm Pl}}k^3\,, \qquad (1.31)$$

(the + and − signs denote right and left circular polarisation), while for the fermion (with the + and − signs now denoting positive and negative helicity states)

$$E_{\pm}^2 = p^2 + m^2 + \eta_{\pm}\frac{p^3}{M_{\rm Pl}}\,, \qquad (1.32)$$

with $\eta_{\pm} = 2(\zeta_1 \pm \zeta_2)$. For the antifermion, it can be shown by simple "hole interpretation" arguments that the same dispersion relation holds, with $\eta_{\pm}^{af} = -\eta_{\mp}^{f}$ where af and f superscripts denote respectively anti-fermion and fermion coefficients [58, 59].

Modified dispersion relations affect standard processes (such as threshold reactions) and permit new processes. Of course, this new physics will be visible only at sufficiently high energies, given that Planck suppression characterises the new relations. To estimate the energy scale, consider, for example, a threshold reaction involving photons and electrons such as photon-photon annihilation, leading to electron-positron pair creation. In such a case the

characteristic energy scale of the process – to which the LV term $\xi k^3/M_{\rm Pl}$ should be comparable – is the electron mass $m_{\rm e}$. Assuming a LV coefficient $O(1)$ the effect of LV should become visible around the critical energy $k_{\rm cr} \approx 10$ TeV (cfr. section 1.5.3). While prohibitive for laboratory experiments, this energy is within the range of the observed phenomena in high energy astrophysics.

1.3.3 Naturalness and the role of other symmetries

Observations involving very high energies can thus potentially cast an $O(1)$ constraint on the coefficients defined above. A natural question arises then: what is the theoretically expected value of the LV coefficients in the modified dispersion relations shown above?

This question is clearly intimately related to the meaning of any constraint procedure. Indeed, let us suppose that, for some reason we do not know, because we do not know the ultimate high energy theory, the dimensionless coefficients $\eta^{(n)}$, that in principle, according to the Dirac criterion, should be of order $O(1)$, are defined up to a dimensionless factor of $m_e/M_{\rm Pl} \sim 10^{-22}$. (This could well be as a result of the integration of high energy degrees of freedom.) Then, any constraint of order larger than 10^{-22} would be meaningless, if our aim is learning something about the underlying QG theory.

This problem could be further exacerbated by renormalization group effects, which could, in principle, strongly suppress the low-energy values of the LV coefficients even if they are $O(1)$ at high energies. Let us, therefore, consider the evolution of the LV parameters first.

Bolokhov & Pospelov [57] recently addressed the problem of calculating the renormalization group equations for QED and the Standard Model extended with dimension-five operators that violate Lorentz Symmetry. In the framework defined above, assuming that no extra physics enters between the low energies at which we have modified dispersion relations and the Planck scale at which the full theory is defined, the evolution equations for the LV terms in eq. (1.27) that produce modifications in the dispersion relations, can be inferred as

$$\frac{d\zeta_1}{dt} = \frac{25}{12}\frac{\alpha}{\pi}\zeta_1 \,, \quad \frac{d\zeta_2}{dt} = \frac{25}{12}\frac{\alpha}{\pi}\zeta_2 - \frac{5}{12}\frac{\alpha}{\pi}\xi \,, \quad \frac{d\xi}{dt} = \frac{1}{12}\frac{\alpha}{\pi}\zeta_2 - \frac{2}{3}\frac{\alpha}{\pi}\xi \,, \tag{1.33}$$

where $\alpha = e^2/4\pi \simeq 1/137$ ($\hbar = 1$) is the fine structure constant and $t = \ln(\mu^2/\mu_0^2)$ with μ and μ_0 two given energy scales. (Note that the above formulae are given to lowest order in powers of the electric charge, which

allows one to neglect the running of the fine structure constant.)

These equations show that the running is only logarithmic and therefore low energy constraints are robust: $O(1)$ parameters at the Planck scale are still $O(1)$ at lower energy. Moreover, they also show that η_+ and η_- cannot, in general, be equal at all scales.

However, this does not solve our problem of investigating what are the natural values of the LV parameters, mainly the ones corresponding to renormalizable operators.

In fact it is generic that even starting with an EFT with only Lorentz violations of mass dimension 5 for free particles, radiative corrections due to particle interactions will generate lower dimension Lorentz violating terms which will then be dominant [60]. Hence radiative corrections will not allow a dispersion relation of the form (1.31,1.32) but will automatically induce extra unsuppressed LV terms in p and p^2 which will be dominant on the p^3 one. Thus either there is a symmetry or some other mechanism protecting the lower dimension operators from large LV, or the suppression of the non-renormalizable operators will be indeed always greater than that of the renormalizable ones.

A possible solution to this problem is given by another symmetry, the so called Super Symmetry (SUSY), that has attracted much attention in the last 40 years [61, 62]. SUSY is by definition a symmetry relating fermions to bosons i.e. matter with interaction carriers. As a matter of fact, SUSY is intimately related to Lorentz invariance. Indeed, it can be shown that the composition of at least two SUSY transformations induces space-time translations. However, SUSY can still be an exact symmetry even in presence of LV and can actually serve as a custodial symmetry preventing certain operators to appear in LV field theories.

The effect of SUSY on LV is to prevent dimension ≤ 4, renormalizable LV operators to be present in the Lagrangian. Moreover, it has been demonstrated [61, 62] that the renormalization group equations for Supersymmetric QED plus the addition of dimension 5 LV operators à la Myers & Pospelov do not generate lower dimensional operators, if SUSY is unbroken. However, this is not the case for our low energy world, of which SUSY is definitely not a symmetry. The effect of soft breaking of SUSY was again investigated in [61, 62]. It was found there that, as expected, when SUSY is broken the renormalizable operators appear in the Lagrangian. In particular, dimension κ ones arise from the percolation of dimension $\kappa + 2$ LV operators[2]. The effect of SUSY soft-breaking is, however, to introduce a suppression of order $m_s^2/M_{\rm Pl}$ ($\kappa = 3$) or $(m_s/M_{\rm Pl})^2$ ($\kappa = 4$), where $m_s \simeq 1$ TeV is the scale of

[2]We consider here only $\kappa = 3, 4$, for which these relationships have been demonstrated.

SUSY soft breaking. Although, given present constraints, the theory with $\kappa = 3$ needs a lot of fine tuning to be viable, since the SUSY-breaking-induced suppression is not enough powerful to kill linear modifications in the dispersion relation of electrons, if $\kappa = 4$ then the induced dimension 4 terms are suppressed enough, provided $m_s < 100$ TeV.

Summarising, it seems that dimension 5 LV is unnatural, even considering the effects of SUSY, because the corresponding LV parameters have to be much less than their "natural" value $O(1)$ in order to fit current data, while dimension 6 LV does not suffer this problem. There is not a clear general argument as to why the dimension 5 operators should not appear in the high energy theory. However, it can be shown that if we assume CPT invariance for the Planck scale theory, then dimension 5, CPT odd LV operators are forbidden and only dimension 6 ones can appear.

Therefore, CPT and (soft broken) SUSY produce a viable LV theory, that will be studied afterwards.

This is encouraging enough for considering this theory as a serious candidate test theory for Lorentz violations, but at the moment no conclusive statements can be done.

1.3.4 Higher dimension contributions

For the reasons explained above, it is interesting to study theories with high dimension contributions. The candidate theory should preserve CPT and be supersymmetric. In absence of a dynamical model, we can proceed effectively by adding to the SM (actually, for simplicity, to the QED) all possible dimension 6, CPT even operators [63].

The complete dimension 6 SME, however, is not known. We still miss the LV induced interaction terms and the CPT odd kinetic ones. This is not a severe limitation, though. Indeed, LV induced interactions are expected to have a very suppressed rate, hence we do not expect them to be observable in elementary particle experiments, and, moreover, we are not aware of even planned experiments meant to look for LV using new interactions. On the other hand, we already explained that the major attraction of dimension 6 SME is essentially related to the assumption of CPT to be an exact symmetry, hence we neglect CPT odd terms because we assume CPT symmetry.

The CPT even dimension 6 LV terms have been computed only recently [63] adopting the same procedure also Myers & Pospelov used for dimension

5 LV. The known nonrenormalizable CPT even fermion operators are

$$\begin{aligned} &-\tfrac{1}{M_{\rm Pl}}\bar{\psi}(u\cdot D)^2(\alpha_L^{(5)}P_L+\alpha_R^{(5)}P_R)\psi \\ &-\tfrac{i}{M_{\rm Pl}^2}\bar{\psi}(u\cdot D)^3(u\cdot\gamma)(\alpha_L^{(6)}P_L+\alpha_R^{(6)}P_R)\psi \\ &-\tfrac{i}{M_{\rm Pl}^2}\bar{\psi}(u\cdot D)\Box(u\cdot\gamma)(\tilde{\alpha}_L^{(6)}P_L+\tilde{\alpha}_R^{(6)}P_R)\psi\ , \end{aligned} \tag{1.34}$$

where $P_{R,L}$ are the usual left and right spin projectors $P_{R,L}=(1\pm\gamma^5)/2$ and D is the usual QED covariant derivative. All coefficients α are dimensionless because, as usual, we factorize suitable powers of the Planck mass.

The known photon operator is

$$-\frac{1}{2M_{\rm Pl}^2}\beta_\gamma^{(6)}F^{\mu\nu}u_\mu u^\sigma(u\cdot\partial)F_{\sigma\nu}\ . \tag{1.35}$$

From these operators, the dispersion relations of electrons and photons can be computed, yielding to

$$\begin{aligned} E^2-p^2-m^2 &= \frac{m}{M_{\rm Pl}}(\alpha_R^{(5)}+\alpha_L^{(5)})E^2+\alpha_R^{(5)}\alpha_L^{(5)}\frac{E^4}{M_{\rm Pl}^2} \\ &\quad +\frac{\alpha_R^{(6)}E^3}{M_{\rm Pl}^2}(E+sp)+\frac{\alpha_L^{(6)}E^3}{M_{\rm Pl}^2}(E-sp) \\ \omega^2-k^2 &= \beta^{(6)}\frac{k^4}{M_{\rm Pl}^2}\ , \end{aligned} \tag{1.36}$$

where m is the electron mass and $s=\boldsymbol{\sigma}\cdot\mathbf{p}/|\mathbf{p}|$. Notice that also a term proportional to E^2 is generated. This term is however suppressed by the tiny ratio $m/M_{\rm Pl}\sim 10^{-22}$ and can be safely neglected provided $E>\sqrt{mM_{\rm Pl}}$.

Since the high energy fermion states are almost exactly chiral, we can further simplify the fermion dispersion relation in eq. (1.37) (we pose $R=+$, $L=-$)

$$E^2=p^2+m^2+f_\pm^{(4)}p^2+f_\pm^{(6)}\frac{p^4}{M_{\rm Pl}^2}\ . \tag{1.37}$$

Since it is suppressed by $m/M_{\rm Pl}$, we will drop in the following the quadratic contribution $f_\pm^{(4)}p^2$ [63].

It may seem puzzling that in a CPT invariant theory we distinguish between different fermion helicities. However, although being CPT invariant, some of the LV terms displayed in eq. (1.35) are odd under P and T. This effectively breaks the identity between fermions and antifermions. However, CPT invariance allows us to determine a relationship between the LV coef-

ficients of the electrons and those of the positrons. Indeed, to obtain it we have to consider that, by CPT, the dispersion relation of the positron is given by (1.37) with the replacements $s \to -s$ and $p \to -p$. This implies, in the end, that the relevant positron coefficients $f^{(6)}_{\text{positron}}$ are such that $f^{(6)}_{e^+_\pm} = f^{(6)}_{e^-_\mp}$, where $e^+_\pm$ indicates a positron of positive/negative helicity (and similarly for the $e^-_\pm$).

These dispersion relations will be considered and constrained in chapters 3 and 4, by exploiting observations in Ultra-High-Energy Cosmic Ray physics.

1.3.5 LV and gravity in EFT

So far, we have dealt only with LV in the matter sector. However, also gravity can be included and new phenomena may arise when introducing LV.

It can be shown that the best formalism to be used to include LV in gravity is that of vierbein, as it allows also to couple fermions to LV. In this formalism, which corresponds to Riemann-Cartan geometry, the gravitational degrees of freedom are represented by the vierbein itself and spin connection, which allow to construct and completely determine the Riemann and torsion tensor in space-time.

Setting torsion to zero for simplicity, the most general low energy action for gravity involving only second derivatives of the metric is

$$S = \frac{1}{16\pi G}\int d^4x\, e\, \left(R - 2\Lambda + s^{\alpha\beta}R_{\alpha\beta} + t^{\alpha\beta\gamma\delta}R_{\alpha\beta\gamma\delta}\right)\,, \tag{1.38}$$

where e is the determinant of the vierbein, R, $R_{\alpha\beta}$ and $R_{\alpha\beta\gamma\delta}$ are the Ricci scalar, tensor and Riemann tensor respectively and Λ is the cosmological constant. G is the gravitational coupling constant, which may be affected by LV as well. As a matter of fact, being translational invariance lost, the coupling tensors $s^{\alpha\beta}$ and $t^{\alpha\beta\gamma\delta}$ can be in general space-time dependent, acting effectively as space-time varying couplings.

However, this very straightforward approach suffers several problems: first of all it does not lead to energy-momentum conservation, unless very restrictive conditions on $s^{\alpha\beta}$ and $t^{\alpha\beta\gamma\delta}$ are imposed. Secondly, it constitutes prior geometry, whereas the ultimate theory should be also able to predict which geometry we live in.

A more flexible approach would be to assume the LV coefficients to be dynamical [64, 65, 66, 35, 67]. In this case, we obtain that the energy-momentum tensor is automatically conserved when all fields are on-shell, but we lose in simplicity, as the LV coefficients have to be promoted to dynamical fields, for which not only kinetic terms, but also potentials must

be introduced, in order to make them non-zero at low energy.

Although the complete theory for $s^{\alpha\beta}$ and $t^{\alpha\beta\gamma\delta}$ is not known, the simpler theory of a dynamical "aether" has been studied thoroughly [64, 65, 35, 68, 69].

In aether models it is assumed that the whole LV is carried by a vector field u^α, hence greatly simplifying the structure of $s^{\alpha\beta}$ and $t^{\alpha\beta\gamma\delta}$, which must be written in terms of u^α (in particular it can be shown that $t^{\alpha\beta\gamma\delta}$ can reduced to suitable combination of $s^{\alpha\beta}$ via the symmetries of the Riemann tensor).

The action for this model is, in $D-$dimensions,

$$S = -\frac{1}{16\pi G}\int d^D x\,\sqrt{-g}\left(R + K^{\alpha\beta}{}_{\mu\nu}\nabla_\alpha u^\mu \nabla_\beta u^\nu + V(u^\alpha u_\alpha)\right)\,, \qquad (1.39)$$

where $K^{\alpha\beta}{}_{\mu\nu} = c_1 g^{\alpha\beta}g_{\mu\nu} + c_2\delta^\alpha_\mu\delta^\beta_\nu + c_3\delta^\alpha_\nu\delta^\beta_\mu + c_4 u^\alpha u^\beta g_{\mu\nu}$. The c_i are dimensionless constants and the potential $V(u^\alpha u_\alpha)$ is introduced in order to force $u^\alpha \neq 0$ at low energy.

It can be shown [70] that this model suffers several problems of instability if the potential V is different from $V(u^\alpha u_\alpha) = \lambda(u^\alpha u_\alpha - 1)$, where λ is a lagrange multiplier, to enforce $|u|^2 = 1$. This means that the aether field is forced to be time-like and to have unit norm.

The aether specifies then a preferred reference frame, which is usually assumed to be aligned to that of the CMB. Consequences of the presence of a aether field can be re-expressed in terms of post-newtonian gravity parameters and can be constrained by looking at modifications of geodesian motion of particles, or of gravitational wave emission during collapse of SuperNovae or neutron stars mergers. A recent summary can be found in [71].

A similar way to introduce a preferred frame is to consider ghost condensates. In this setup, a scalar field ϕ has a Lagrangian of the form $P(X)$, where P is a polynomial in $X = \partial_\mu\phi\partial^\mu\phi$, with a minimum at some value $X = m$, at which ϕ has a constant velocity. If this field is effective in the Early Universe, then Hubble friction drives it to the minimum, thereby generating a preferred frame, defined by the field velocity m. This kind of model has the very same consequences as aether models, hence constraints on aether parameters also place limits on m.

1.3.6 Non EFT-motivated models

Although the EFT approach to LV seems quite reasonable from a low-energy point of view, as it describes fairly accurately particle interactions up to roughly 100 GeV, also non-EFT-motivated LV models have been studied. The most interesting phenomenological property of this kind of models is

that they may evade the majority of the constraints discussed in this thesis, in particular in sec. 1.4 and 1.5 and in chap. 2.

As an example of such models, let us consider the one presented in [72], where modified dispersion relations are found based on the Liouville string approach to quantum space-time [73]. Liouville-string models of space-time foam [73] motivate corrections to the usual relativistic dispersion relations that are first order in the particle energies, corresponding to a vacuum refractive index $\eta = 1 - (E/M_{\rm Pl})^{\alpha}$, with $\alpha = 1$. These effects are associated generically with deviations from conformal invariance in the effective theory of low-energy excitations interacting with singular or topologically non-trivial quantum-gravitational degrees of freedom, inaccessible to low-energy observers [73]. Models with quadratic dependences of the vacuum refractive index on energy: $\alpha = 2$ have also been considered [41].

Remarkably, this is exactly what is predicted by the Liouville string/D-particle model for space-time foam, according to which only gauge bosons such as photons might have QG-modified dispersion relations, and not charged matter particles such as electrons. This difference may be traced to a well known fact of D-brane physics, namely that [74] excitations which are charged under the gauge group are represented by open strings with their ends attached to the D-brane [75], and only neutral excitations are allowed to propagate in the bulk space transverse to the brane. Hence, if we consider photons and electrons, in this model the parameter η is forced to be null, while ξ is free to vary, and, even more important, the theory is CPT even, implying vacuum is not birefringent for photons ($\xi_+ = \xi_-$).

As we said, our interest in this kind of models is motivated by the fact that they can in principle evade most of the present constraints. For example, the electron and birefringence constraints discussed in chapter 2 do not apply to the Liouville-string-inspired model. On the other hand, time-of-flight constraints are viable for this model. Indeed, in [76] the best constraint on $\xi < 47$ using time-of-flight measurements is placed, as we also discuss in sec. 1.5.1. Moreover, the authors of [76] discuss LV as a possible explanation of the arrival time structure of TeV photons from Mkn 501, finding that the best-fit to data would be obtained by adopting $\xi \simeq 30$. If this is the case (which is not, as explained in the same paper [76], but let us assume it is for the moment), then we have to admit the remarkable fact that the EFT description of LV phenomena related to QG would be failing. In fact, the best-fit value $\xi \simeq 30$ would exceed by several orders of magnitude the best constraint on ξ in EFT [77].

This brief discussion shows, incidentally, that even though time-of-flight constraints are much weaker with respect to those exploiting other physical processes, it is nevertheless important to pursue them, because they have the

potentiality to reveal important features of the Planck-scale theory.

1.4 Terrestrial constraints on LV

In order to substantiate some of the statements made in the previous sections, and before to move to more recent results, it is unavoidable to discuss the current status of the constraints on LV. We will divide matter in two main branches: we first discuss constraints which can be posed with terrestrial experiments, then we will present those obtained using astrophysical observations.

1.4.1 Penning traps

A Penning trap is a combination of static magnetic and electric fields able to confine a particle in a finite region for long time [78]. There are essentially two trapped particle motions of great relevance for LV tests: they are cyclotron motion in the magnetic field and Larmor precession due to the spin. As it is customary to see (cfr. section 2.3.2), the ratio of the precession frequency ω_{pr} to the cyclotron one ω_{cy} is

$$\frac{\omega_{pr}}{\omega_{cy}} = \frac{g}{2} \,, \tag{1.40}$$

where g is the Landé factor of the trapped particle.

The energy levels for a spin-1/2 particle are $E_n^s = n\omega_{cy} + s\omega_{pr}$, where n is an integer and $s = \pm 1/2$. For electrons and positrons (for which $g = 2 + \bar{g}$, $\bar{g}$ being the anomalous magnetic moment), the states n, $s = -1/2$ and $n-1$, $s = +1/2$ are almost degenerate. The degeneracy is removed only by the anomalous magnetic moment $\bar{g}$ and the difference between frequencies is usually denoted as $\omega_a = \omega_{pr} - \omega_{cy}$. If an oscillating magnetic field is present in the trap, then it is possible to induce transitions between these almost degenerate states and determine the value of ω_a.

This procedure yields a very accurate measurement of ω_a (hence, of $g-2$) and can be used to test CPT and Lorentz invariance. In the SME, the magnetic moment of electrons and positrons does not have corrections at lowest order. However, both ω_a and ω_{cy} receive the following corrections [79] (assuming the trap's magnetic field is aligned in the z direction)

$$\begin{aligned} \omega_{cy}^{e^-} &\simeq (1 - c_{00}^e - c_{XX}^e - c_{YY}^e)\omega_{cy}^{e,0} \\ \omega_a^{e^\mp} &\simeq \omega_a^{e,0} \mp 2b_Z^e + 2d_{Z0}^e m_e + 2H_{XY}^e \,, \end{aligned} \tag{1.41}$$

as expressed in a non-rotating frame and the coefficients correspond to the notation we used for the SME (section 1.3.1).

Two kinds of constraint can be performed using equations (1.41). First of all, one can look at instantaneous CPT violation in the electron/positron system, by measuring the difference $|\omega_a^{e^-} - \omega_a^{e^+}|$, which is nonzero if b_Z^e is. Experimentally, $|\omega_a^{e^-} - \omega_a^{e^+}| = 4b_Z^e \lesssim 10^{-26}\, m_e$ [80].

On the other hand, one can track the sidereal variation of ω_{cy} and ω_a as the orientation of the experimental apparatus changes with respect to the background of the LV tensors. A bound on the diurnal variation of the anomaly frequency $\Delta\omega_a^{e^-} \leq 1.6 \cdot 10^{-21} m_e$ has been placed by [81] using this technique. However, this strategy only limits a particular combination of the SME coefficients. This technique has been used also to measure CPT violation in the proton/anti-proton system. Moreover, by measuring variations of ω_{cy}^p a limit of the order of 10^{-26} has been placed on some components of $c_{\mu\nu}^{p^-}$.

1.4.2 Clock comparison

Clock comparison experiments are well known tests of Lorentz invariance [82, 83]. In their basic setup, two "clocks", usually represented by two atomic transition frequencies, are located together at some point in space. As they move, the effect of different components of the SME LV parameters yields a sidereal drift between the two clocks. Since the difference between clock timings can be measured over long periods, this kind of constraints allows very strong bounds on LV. Of course, this measurement is possible only if the clocks are made of different materials or have different orientations in space, because otherwise the LV effect would be the same over both.

The best limit to date is placed in the neutron sector of the SME by a $^3He/^{129}Xe$ maser system [84]. In this experiment, both gases are placed into a state of inverted population, by the effect of collisions with a pumped vapor of rubidium. Both gases, if placed in a magnetic field of 1.5 G, act as a maser at frequencies of 4.9 kHz and 1.7 kHz for He and Xe respectively. While the Xe maser is used to calibrate the magnetic field, the emission of He is tracked over time, looking for sidereal variations. The leading order effect of LV is essentially on a valence neutron for both gases, so only the neutron parameters are probed by this kind of experiment. The magnitude of the frequency sidereal variation can be expressed, within SME, as

$$2\pi|\Delta f_J| = |-3.5\tilde{b}_J + 0.012(\tilde{d}_J - \tilde{g}_{D,J})|\,, \tag{1.42}$$

where J represents the X, Y components of the LV tensors, in a non-rotating frame, orthogonal to the Earth's rotation axis.

The relation between the above mentioned coefficients and the SME parameters is rather complicated. However, it turns out that the above mentioned coefficients can be constrained at the level of $\tilde{b}_\perp = \sqrt{\tilde{b}_X^2 + \tilde{b}_Y^2} = (6.5 \pm 5.4) \times 10^{-32}$ GeV, while the $\tilde{d}$ and $\tilde{g}$ parameters can be constrained to be about three orders of magnitude less. This means that some combination of the SME parameters can be constrained at a level of 10^{-28} GeV [31]. Other clock experiments [85] are able to cast constraints also on the following other neutron SME parameters

$$|\tilde{c}_{Q,J}| = |m(c_{JZ} + c_{ZJ})| < 10^{-25} \text{ GeV} \quad (1.43)$$

$$|\tilde{c}_{-}| = |m(c_{XX} - c_{YY})| < 10^{-27} \text{ GeV} \quad (1.44)$$

$$|\tilde{c}_{XY}| = |m(c_{XY} + c_{YX})| < 10^{-27} \text{ GeV} \quad (1.45)$$

Interestingly, a constraint on dimension 5 LV neutron operators can be placed using limits on the spatial variation of the hyperfine nuclear spin transition in Be^+ [86] as function of the angle between the spin axis and an external magnetic field. In fact, the LV terms introduce a small orientation dependent potential in the non-relativistic Schrödinger equation. This small potential leads to anisotropy of the hyperfine transition frequency, which can be probed experimentally. In the case of Be^+ the nuclear spin can be thought of as being carried by a single neutron. Experimental limits are $|\eta_1| < 6 \times 10^{-3}$, $|\eta_2| < 3$ if u^α is timelike, while if u^α is spacelike, then $|\eta_1| < 2 \times 10^{-8}$, $|\eta_2| < 10^{-8}$.

Other experimental setups can probe LV parameters in other particles' sectors. For example, for the proton sector one has roughly the same constraints as in the neutron one [87].

1.4.3 Cavity experiments

Also for historical reasons, interferometry is one of the best ways to study Lorentz invariance. Modern cavity experiments are able to provide very accurate tests and bounds on certain photon parameters. In a cavity experiment, one looks for a variation of the resonance frequency as the cavity changes its orientation with respect to a stationary frequency standard. This has indeed close relation with a clock comparison experiments, but since, in a sense, one of the clocks uses photons, it probes the photon sector of the SME.

Without entering in technical details of the theoretical background needed to approach this kind of study (electromagnetic field redefinition, dielectric theory, etc.), we list here the definitions and the meaning of the parameters that can be found in the specific literature. Constraints involve particular

combinations of the k_F SME coefficients. In particular

$$\tilde{\kappa}_{tr} = \frac{1}{3}(\kappa_{DE})^{ll} \tag{1.46}$$

$$(\tilde{\kappa}_{e+})^{jk} = \frac{1}{2}(\kappa_{DE}+\kappa_{HB})^{jk} \tag{1.47}$$

$$(\tilde{\kappa}_{e-})^{jk} = \frac{1}{2}(\kappa_{DE}-\kappa_{HB})^{jk} - \delta^{jk}\tilde{\kappa}_{tr} \tag{1.48}$$

$$(\tilde{\kappa}_{o+})^{jk} = \frac{1}{2}(\kappa_{DB}+\kappa_{HE})^{jk} \tag{1.49}$$

$$(\tilde{\kappa}_{o-})^{jk} = \frac{1}{2}(\kappa_{DB}-\kappa_{HE})^{jk}. \tag{1.50}$$

$\tilde{\kappa}_{tr}, \tilde{\kappa}_{e+}, \tilde{\kappa}_{e-}$ are all parity even while $\tilde{\kappa}_{o+}$ and $\tilde{\kappa}_{o-}$ are parity odd and the κ's on the right hand side are related to the k_F as

$$(\kappa_{DE})^{jk} = -2(k_F)^{0j0k} \tag{1.51}$$

$$(\kappa_{HB})^{jk} = \frac{1}{2}\epsilon^{jkq}\epsilon^{krs}(k_F)^{pqrs} \tag{1.52}$$

$$(\kappa_{DB})^{jk} = -(\kappa_{HE})^{jk} = \epsilon^{kpq}(k_F)^{0jpq}. \tag{1.53}$$

It can be shown [50] that $\tilde{\kappa}_{tr}$ induces a shift of the speed of light, as well as the $\tilde{\kappa}_{e-}$ and $\tilde{\kappa}_{o+}$, which act in an orientation dependent way. On the other hand, the parameters $\tilde{\kappa}_{e+}$ and $\tilde{\kappa}_{o-}$ generate birefringence effects.

These experiments are actually plagued by large systematics. It should be noted that many material dependent effects intervene to enhance or suppress the relative importance of different effects. Indeed, since the resonant frequency of a cavity is

$$f_r \equiv \frac{mc}{2nL}\,, \tag{1.54}$$

where m is the mode number, c is the speed of light, n is the index of refraction of the medium present in the cavity and L is the length of the cavity, the overall change on f_r is in general due to a combination of effects on c, n and L. Depending on the construction of the cavity, one of them can dominate over the others.

Overall, the photon SME parameters are constrained to be less than $O(10^{-15})$ [31]. Only the parameter $\tilde{\kappa}_{o+}$ is less constrained to $O(10^{-11})$, due to the relative boost of the Earth with respect to the solar system.

1.4.4 Spin polarised torsion balances

Spin polarised torsion balances place limits on the electron sector of the mSME [88]. The best limits on $\tilde{b}_i$ (i is the spatial direction, including the one parallel to the Earth's rotation axis) for the electron come from two balances, one in Washington [89, 90] and one in Taiwan [91].

In the Washington experiment (the Taiwan one is similar in its concept) two different types of magnets (SmCo and Alnico) are arranged in an octagonal shape, four SmCo magnets on one side of the octagon and four Alnico magnets on the other. The magnetisation of both types of magnets is tuned to be equal and in the angular direction around the octagon in order to minimise any magnetic interactions. However, the net electron spin of the SmCo and Alnico magnets differs because the SmCo magnets have a large contribution to their overall magnetisation from orbital angular momentum of Sm ions. Therefore the octagonal pattern of magnets has an overall spin polarisation in the octagon's plane.

A stack of four of these octagons are suspended from a torsion fibre in a vacuum chamber. The whole apparatus is mounted on a turntable. Lorentz violation in the SME introduces an extra interaction potential for non-relativistic electrons of the form $V = \tilde{b}_i \sigma^i$, where i stands for direction and σ^i is the electron magnetic moment. As the turntable rotates, since $\tilde{b}$ points in some fixed direction in space, the interaction produces a torque on the torsion balance. The magnet apparatus therefore twists on the torsion fibre by an amount proportional to the potential V, hence to the $\tilde{b}_i$. The absence of any extra twist limits all components of $|\tilde{b}|$ for the electron to be less than 10^{-28} GeV.

1.4.5 Neutral meson tests

Since CPT connects particles and antiparticles, tests of matter-antimatter correspondence are extremely sensitive to CPT. This implies, through the well known theorem [32] stating that CPT symmetry violation always comes together with Lorentz invariance violation in local field theories, that matter-antimatter tests are also a probe of LV.

This idea can be adopted for studies with mesons. In particular, neutral-meson oscillations (e.g. $K^0/\bar{K}^0$) are essentially controlled by the energy difference between the meson and its antimeson. Although the SME contains the same mass parameter for quarks and antiquarks, these particles are affected differently by the CPT- and Lorentz-violating background. This allows the dispersion relations for mesons and antimesons to differ, so that mesons and antimesons can have distinct energies.

In particular, if we specialise to the best studied oscillations in the $K^0/\bar{K}^0$ system, we are going to probe the parameters a_μ for the down and strange sector, since $K = d\bar{s}$. However, as we already noticed, since one of the a_μ can always be reabsorbed by field redefinition, only the difference $\Delta a_\mu = r_d a_\mu^d - r_s a_\mu^s$ controls CPT violation and can be therefore tested. The coefficients r_d and r_s allow for effects due to the fact we are probing a quark bound state [35].

A kaon state is in general the superposition of the strong eigenstates K^0 and $\bar{K}^0$. Adopting the two-component notation for the wave function Ψ_K, we can write the state evolution as

$$i\partial_t \begin{pmatrix} K^0 \\ \bar{K}^0 \end{pmatrix} = \Lambda \begin{pmatrix} K^0 \\ \bar{K}^0 \end{pmatrix} , \tag{1.55}$$

where the Hamiltonian Λ is a 2×2 complex matrix. Λ can be decomposed, in general, in its real and imaginary parts as $\Lambda = M - i\Gamma$, where M and Γ are hermitian matrices usually called the mass and the decay matrix respectively. The eigenvectors of Λ are the physically propagating states and are the well known K_S (the short living state) and K_L (the long living state). CPT violation only occurs if the two eigenvalues of Λ, Λ_{11} and Λ_{22} are not equal: $\Delta\Lambda \equiv \Lambda_{11} - \Lambda_{22} \neq 0$. The contribution of SME to $\Delta\Lambda$ can be determined as [92]

$$\Delta\Lambda \approx \beta^\mu \Delta a_\mu , \tag{1.56}$$

where $\beta^\mu = \gamma(1, \vec{\beta})$ is the four-velocity of the meson state in the observer frame. As a consequence of eq. (1.56), it can be seen that the size of the effect varies as the meson changes magnitude and orientation of its momentum. Moreover, since the laboratory frame is moving dragged by the Earth, one expects sidereal variation of $\Delta\Lambda$. This effect can be explicitly cast as [34]

$$\begin{aligned} \xi \;&\equiv\; \xi(\hat{t}, \vec{p}) \equiv \xi(\hat{t}, p, \theta, \phi) \\ &=\; \frac{\gamma(p)}{\Delta\lambda} \big\{ \Delta a_0 + \beta \Delta a_Z (\cos\theta\cos\chi - \sin\theta\cos\phi\sin\chi) \\ &\qquad + \beta \big[\Delta a_Y (\cos\theta\sin\chi + \sin\theta\cos\phi\cos\chi) \\ &\qquad\quad - \Delta a_X \sin\theta\sin\phi \big] \sin\Omega\hat{t} \\ &\qquad + \beta \big[\Delta a_X (\cos\theta\sin\chi + \sin\theta\cos\phi\cos\chi) \\ &\qquad\quad + \Delta a_Y \sin\theta\sin\phi \big] \cos\Omega\hat{t} \big\} , \end{aligned} \tag{1.57}$$

where $\hat{t}$ is the sidereal time, χ represents the co-latitude of the experimental setup, Ω is the Earth sidereal rotation frequency, $\vec{\beta} = \beta(\sin\theta\cos\phi, \sin\theta\sin\phi, \cos\theta)$ and $\gamma(p) = \sqrt{1 + p^2/m^2}$. $\Delta\lambda$ in (1.57) represents the difference be-

tween the eigenvalues of Λ.

The main experimental challenge of this kind of experiments is to be able to measure all the four components of a_μ. This result can be achieved by suitably combining measurements made with different setups of the experimental apparatus. Indeed, as the Earth, hence the laboratory, rotates with respect to the fixed background vector Δa_μ, the beam direction relative to it also changes. Then, in order to be sensitive to Δa_μ, the time stamp of each event must be recorded.

To look at sidereal variation of ξ yields information about $\Delta a_\perp$, i.e. the components of Δa_μ perpendicular to the Earth's spinning axis. More difficult is to have data on Δa_0 and $\Delta a_\parallel$, because they depend only on $|\vec{\beta}|$, which is only slowly varying with energy at high energy. However, the dependence on $\gamma(p)$ of ξ enhances the overall effect.

Experiments with K and D led to important constraints. For the K system, it has been found that a linear combination of Δa_0 and $\Delta a_\parallel$ is less than 10^{-20} GeV, while Δa_X and Δa_Y are less than 10^{-21} GeV [93, 92]. For the D meson system, the same parameters are constrained to be less than $O(10^{-16})$ GeV. We notice here that observations of the D system probe the quarks u and c, while other mesonic systems involve d, s and b.

Noticeably, different setups lead to other types of constraints. For example, measures of correlated systems (like quarkonium) in KLOE place a constraint $\Delta a_\parallel < 10^{-17}$ GeV [94].

Moreover, also the BaBar and BELLE experiments can place constraints of order 10^{-13} GeV on various combinations of the Δa_μ, by studying states involving the B_d meson.

1.4.6 Doppler shift of lithium

LV implies that the transformation laws for clocks in relative motion are different from the usual time dilation. The Doppler shift deviation from its standard relativistic form can be conveniently parameterized in the RMS framework. Comparisons of oscillator frequencies under boosts therefore can constrain the α_{RMS} parameter. The best test to date comes from spectroscopy of lithium ions in a storage ring [95]. In this experiment, $^7Li^+$ ions are trapped in a ring at a velocity of $0.064\,c$. The transition frequencies of the boosted ions are then measured and compared to the transition frequencies at rest. The resulting bound on the deviation from the special relativistic Doppler shift is $|\alpha_{RMS}| < 2 \cdot 10^{-7}$ in the RMS framework.

The results of [95] can be reinterpreted in the context of the mSME. For

the electron/proton sector the approximate bounds are [96]

$$\begin{aligned} |c^p_{XX} + c^p_{YY} - 2c^p_{ZZ}| &\leq 10^{-11} \\ |c^p_{TJ} + c^p_{JT}| &\leq 10^{-8} \\ |c^e_{XX} + c^e_{YY} - 2c^e_{ZZ}| &\leq 10^{-5} \\ |c^e_{TJ} + c^e_{JT}| &\leq 10^{-2} \end{aligned} \tag{1.58}$$

where $J = X, Y, Z$ in a heliocentric frame. In the photon sector, the limit $\tilde{\kappa}_{tr} \leq O(10^{-5})$ can also be set from this experiment [97].

1.5 Astrophysical constraints on LV

We have seen in the last sections what tests of CPT and Lorentz invariance can be done with terrestrial experiments. Being done on Earth, with an accurate control of the apparatus, these tests are extremely high precision probes of the fundamental symmetries. However, they have an important drawback: they are essentially low energy tests.

One of the main motivations of high energy tests of Lorentz invariance, is related to the intuition that Lorentz symmetry could be a very accurate low energy symmetry, but could be broken at high energies, where the structure of the space-time could be quite different from what we are used to. Hence, higher and higher energy tests are essential to understand until which energy scale we can trust Lorentz symmetry.

Astrophysical objects are suited to provide us with significant information in this respect. Indeed, it is well established that some objects in the Universe are able to accelerate particles at unattainable energies on Earth. Then, astrophysical tests of LV are important.

This section presents the most commonly used astrophysical tests. In Fig. 1.2 the status of the field when the author of this thesis started his work is shown. Each mentioned process is detailed in the next sections.

1.5.1 Photon time of flight

Although these kinds of constraint currently provide limits several orders of magnitude weaker than those we shall present, we briefly discuss them, because they are widely considered in the astrophysical community [36].

The dispersion relation (1.31) implies that photons of different colours (wave vectors k_1 and k_2) travel at slightly different speeds. The photon

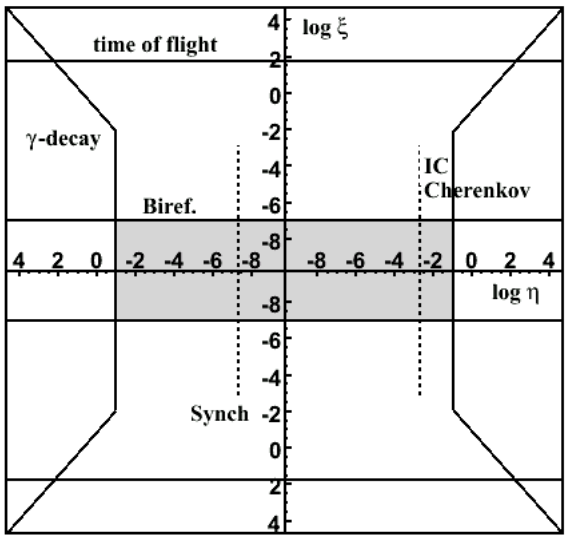

Figure 1.2: Present constraints on the LV coefficients for QED with dimension 5 Lorentz violation. The grey area is the allowed one and, within it, the region bounded by the two dashed vertical lines identifies the allowed range for at least one of the four lepton LV coefficients (albeit under some extra hypotheses).

group velocity can be computed, in general, as

$$v_g^{\pm} = \frac{\partial\omega}{\partial k} = \frac{k}{\omega}\left(1 \pm \frac{n}{2}\xi\left(\frac{k}{M}\right)^{n-2}\right) \approx 1 \pm \frac{n-1}{2}\xi\left(\frac{k}{M}\right)^{n-2} \tag{1.59}$$

When accumulated over a cosmological distance d, this effect naively produces a time delay

$$\Delta t^{(n)} = \frac{n-1}{2}\,\frac{k_2^{n-2} - k_1^{n-2}}{M_{\rm Pl}^{n-2}}\,\xi\, d\,, \tag{1.60}$$

which clearly increases with d and with the energy difference. The largest systematic error affecting this method is the uncertainty about whether photons of different energy are produced simultaneously in the source (e.g., a Gamma-Ray Burst, or an Active Galactic Nucleus).

So far, the most robust constraints on ξ for $n = 3$, derived from time of flight differences, have been obtained from a statistical analysis applied to the arrival times of sharp features in the intensity at different energies from a large sample of GRBs with known redshifts [98], leading to limits $\xi \leq O(10^3)$. Using single objects (generally Blazars or GRBs) it is possible to obtain a stronger, but less robust, constraint of order $|\xi| \leq O(10^2)$ [99]. A recent example of how important are systematic uncertainties can be found in [76], where the strongest, up to date, limit $\xi < 47$ is found by looking at a very strong flare in the TeV band of the AGN Markarian 501, but also a best fit of the flare time structure (of course readily explained by standard plasma physics) could be achieved with $\xi \sim O(1)$.

One way of alleviating systematic uncertainties, available only in the context of birefringent theories, like the one with $n = 3$, would be to measure the velocity difference of the two polarisation states at a single energy, corresponding to

$$\Delta t = 2|\xi| k\, d/M_{\rm Pl}\,. \tag{1.61}$$

However, this bound would require that both polarisations are observed and that no spurious helicity dependent mechanism (such as, for example, propagation through a birefringent medium) has affected the relative propagation of the two polarisation states.

As we said beforehand, this approach to time-of-flight constraints is rather naive, in particular when applied to birefringent theories. The reason is that astrophysical photon beams are not in general circularly polarized, hence they are a superposition of faster and slower modes, and therefore it is not straightforward to derive a prediction for the time delay in propagation due

to LV.

In order to assess this problem, let us describe a beam of light by means of the associated electric field, and let us assume that this beam has been generated with a gaussian width

$$\vec{E} = A\left(e^{i(\Omega_0 t - k^+(\Omega_0)z)}\, e^{-(z-v_g^+ t)^2\delta\Omega_0^2}\hat{e}_+ + e^{i(\Omega_0 t - k^-(\Omega_0)z)}\, e^{-(z-v_g^- t)^2\delta\Omega_0^2}\hat{e}_-\right) , \tag{1.62}$$

where Ω_0 is the wave frequency, $\delta\Omega_0$ is the gaussian width of the wave, $k^\pm(\Omega_0)$ is the "momentum" corresponding to the given frequency according to (1) and $\hat{e}_\pm \equiv (\hat{e}_1 \pm i\hat{e}_2)/\sqrt{2}$ are the helicity eigenstates. Notice that by complex conjugation $\hat{e}_+^* = \hat{e}_-$. Also, notice that $k^\pm(\omega) = \omega \mp \xi\omega/M$. Hence,

$$\vec{E} = A\, e^{i\Omega_0(t-z)}\left(e^{i\xi\Omega_0^2/Mz}\, e^{-(z-v_g^+ t)^2\delta\Omega_0^2}\hat{e}_+ + e^{-i\xi\Omega_0^2/Mz}\, e^{-(z-v_g^- t)^2\delta\Omega_0^2}\hat{e}_-\right) . \tag{1.63}$$

The intensity of the wave beam can be computed as

$$\vec{E}\cdot\vec{E}^* = |A|^2\left(e^{2i\xi\Omega_0^2/Mz} + e^{-2i\xi\Omega_0^2/Mz}\right) e^{-\delta\Omega_0^2\left((z-v_g^+ t)^2+(z-v_g^- t)^2\right)} \tag{1.64}$$

$$= 2|A|^2 e^{-2\delta\Omega_0^2(z-t)^2}\cos\left(2\xi\frac{\Omega_0}{M}\Omega_0 z\right) e^{-8\xi^2\frac{\Omega_0^2}{M^2}(\delta\Omega_0 t)^2} . \tag{1.65}$$

This shows that there is an effect even on a linearly-polarised beam. The effect is a modulation of the wave intensity which depends quadratically on the energy and linearly on the distance of propagation. In addition, for a gaussian wave packet, there is a shift of the packet centre, controlled by the square of ξ/M, hence strongly suppressed with respect to the cosinusoidal modulation.

1.5.2 Vacuum Birefringence

The fact that electromagnetic waves with opposite "helicity" have slightly different group velocities, in EFT LV with $n = 3$, implies that the polarisation vector of a linearly polarised plane wave with energy k rotates, during the wave propagation over a distance d, through an angle [37, 100, 59, 58]

$$\theta(d) = \frac{\omega_+(k) - \omega_-(k)}{2} d \simeq \xi\frac{k^2 d}{2\, M_{\rm Pl}} . \tag{1.66}$$

Note that for an object located at cosmological distance (let z be its redshift), the distance d will become

$$d(z) = \frac{1}{H_0}\int_0^z \frac{1+z'}{\sqrt{\Omega_\Lambda + \Omega_m(1+z')^3}}\, dz' \,, \tag{1.67}$$

where $d(z)$ is not exactly the distance of the object as it includes a $(1+z)^2$ factor in the integrand to take into account the redshift acting on the photon energies.

Observations of polarised light from a distant source can then lead to a constraint on $|\xi|$ that can be cast in essentially two different ways, depending on the amount of available information, both on the observational and on the theoretical (i.e. astrophysical source modelling) side.

Decrease in polarisation degree Since real detectors have a finite energy bandwidth, eq.(1.66) is never probed in real situations. Rather, if some net amount of polarisation is measured in the band $k_1 < E < k_2$, an order of magnitude constraint arises from the fact that if the angle of polarisation rotation (1.66) were to differ by more than $\pi/2$ over the energy range of interest, the detected polarisation would fluctuate sufficiently for the net polarisation of the signal to be suppressed [100, 59]. As the difference in the rotation angle over the band is

$$\Delta\theta \simeq \xi \frac{(k_2^2 - k_1^2)}{2\, M_{\rm Pl}} d(z) \,, \tag{1.68}$$

the constraint is obtained by imposing $\Delta\theta \leq \pi/2$. In this sense this procedure is independent of the amount of polarisation actually detected or expected and relies only on its detection.

A more refined limit could be obtained by calculating the polarisation degree Π weighted for the photon counts and polarisation efficiency of the instrument

$$\Pi(\xi) = \Pi(0)\sqrt{\langle\cos(2\theta)\rangle_{\mathcal{P}}^2 + \langle\sin(2\theta)\rangle_{\mathcal{P}}^2}, \tag{1.69}$$

where the average is over the source spectrum and instrumental efficiency, represented by the normalised weight function $\mathcal{P}(k)$ [100]. In this case one can in fact estimate how large ξ can be so not to lower Π below the observed value (starting from a conservative $\Pi(0) = 1$ or assuming an intrinsic value if argued on the basis of solid modelling of the emitting source).

Rotation of polarisation angle Let us suppose that some polarised light has been measured in a certain energy band with an angle $\theta_{\rm obs}$ with respect to a fixed direction. At fixed energy, the polarisation vector rotates by the angle (1.66)[3], and if the position angle is measured by averaging over a certain energy range, the final rotation will be given by the superposition of the polarisation vectors of all the photons in that range. Thus, if $\theta_{\rm f}$ is the position angle after propagation, referred to the position angle at emission $\theta_{\rm i}$, the following relation holds

$$\tan(2\theta_{\rm f}) = \frac{\int \sin(2\theta(k))\mathcal{P}(k)\,dk}{\int \cos(2\theta(k))\mathcal{P}(k)\,dk}\ , \tag{1.70}$$

where $\theta(k) = \xi(d/2M)k^2$ is the angle of rotation for a photon of energy k with respect to $\theta_{\rm i}$.

If $\theta_{\rm theo}$ in the same energy band can be determined by theoretical model of the emitting source, a constraint can be made by imposing

$$\tan(2\theta_{\rm f}) < \tan(2\theta_{\rm obs} - 2\theta_{\rm theo})\ . \tag{1.71}$$

While this will be tighter than those obtainable with the previous method, it clearly relies on assumptions on the process of emission of polarised light that may be affected by significant uncertainties.

The fact that polarised photon beams are indeed observed from distant objects imposes constraints on ξ. A strong constraint, $\xi \lesssim 2 \times 10^{-4}$, has been obtained by looking at UV radiation from distant galaxies [100]. Recently, a claim of $|\xi| \lesssim 2\times10^{-7}$ has been made using UV/optical polarisation measures from GRBs [77].

1.5.3 Threshold reactions

A very interesting phenomenology of threshold reactions is introduced by LV in EFT. Indeed, not only the LV corrections can shift the threshold energy of known reactions, but also new, normally forbidden reactions can be introduced. The reason why LV corrections are so surprisingly important in threshold reactions is that in this case the LV term (which as a first approximation can be considered as an additional mass term) has not to be compared to the momentum of the involved particles, but rather to the (invariant) mass of the particles produced in the final state. Hence, an estimate

[3] We are neglecting here Faraday rotation, which is irrelevant at such energies.

Table 1.1: Values of $p_{\rm th}$, according to eq.(1.72), for different particles involved in the reaction: neutrinos, electrons and proton. Here we assume $\eta_n \simeq 1$.

	$m_\nu \simeq 0.1$ eV	$m_e \simeq 0.5$ MeV	$m_p \simeq 1$ GeV
$n = 4$	0.1 eV	0.5 MeV	1 GeV
$n = 5$	500 MeV	14 TeV	2 PeV
$n = 6$	33 TeV	74 PeV	3 EeV

for the threshold energy can be given as

$$p_{\rm th} \simeq \left(\frac{m^2 M_{\rm Pl}^{\kappa-2}}{\eta_\kappa}\right)^{1/\kappa} , \tag{1.72}$$

where η_n is the generic LV parameter competing to the particles involved in the reaction and m is the particle mass.

Interesting values for $p_{\rm th}$ are given in table 1.1, from which it can be seen that reactions involving neutrinos would be the best candidate for observation of LV effects, while electrons/positrons are able to provide results for $n = 5$ theories[4], but very hardly can be accelerated by astrophysical objects up to the required energy for $n = 6$. In this last case reactions of protons can be very effective, because Cosmic Rays are known to have energies well above 3 EeV.

However, the phenomenology of thresholds is not exhausted in this brief discussion. Indeed, a completely new phenomenology of thresholds is possible in presence of LV. In [101, 102] it was found that in some cases not only standard, so called lower thresholds are affected by LV, but also upper thresholds are introduced, above which the reaction is no more allowed. The reason for this is that at high enough momentum, there is not enough energy to produce particles in the final state. Examples of the use of this phenomenology to cast constraints on LV will be shown in the following.

Photon decay

The decay of a photon into an electron/positron pair is made possible by LV because either the photon 4-vector is not null or the electron-positron total 4-momentum is null.

This process has a threshold which, if $\xi \simeq 0$ and $n = 3$, is set by the

[4]This n is related to the κ in eq. (1.72) as $n = \kappa + 2$.

condition

$$k_{th} = (6\sqrt{3}m_e^2 M/|\eta_\pm|)^{1/3} \,, \tag{1.73}$$

where η is the LV parameter for either an electron or a positron. Since, from birefringence $\xi \lesssim 10^{-7}$, the above expression for the photon decay can be used to constrain the electron/positron parameters. In [58] $|\eta_\pm| \lesssim 0.2$ was derived using the fact that 50 TeV γ-rays were measured from the Crab Nebula. This constraint has been tightened to $|\eta_\pm| \lesssim 0.05$, thanks to observations of 80 TeV photons by HEGRA [1].

Vacuum Čerenkov – IC electrons

In the presence of LV the process of Vacuum Čerenkov (VC) radiation $e \to e\gamma$ can occur. Taking again $\xi \simeq 0$ and $n = 3$, the threshold energy is given by

$$p_{\rm VC} = (m_e^2 M/2\eta)^{1/3} \simeq 11 \text{ TeV } \eta^{-1/3} \,. \tag{1.74}$$

Moreover, just above threshold this process is extremely efficient, having a time scale of order $\tau_{\rm VC} \sim 10^{-9}$ s [58]. TeV emission from the CN is usually attributed to the Inverse Compton scattering (IC) of electrons/positrons on background photons (mainly those from synchrotron radiation). These leptons would not be able to produce the observed IC radiation if they were above the VC threshold, because above $p_{\rm VC}$ the VC rate is much higher than the IC scattering rate in the CN.

The observation of 50 TeV photons from the CN implies (by energy conservation) the presence of at least 50 TeV leptons. This leads to the bound $\eta \lesssim 10^{-2}$ for at least one of the four fermion parameters [58]. With the observation of 80 TeV photons by HEGRA [1] the constraint can be strengthened to $\eta \lesssim 3 \times 10^{-3}$ as shown in fig. 1.2 (dashed vertical line in the positive η range).

1.5.4 Synchrotron radiation

Rather surprisingly, the synchrotron radiation emitted by electrons and positrons spiralling in a magnetic field is strongly affected by LV. In the LI case, as well as in the LV one [58, 103, 104], most of the radiation from an electron of energy E is emitted around a critical frequency

$$\omega_c = \frac{3}{2} eB \frac{\gamma^3(E)}{E} \tag{1.75}$$

where $\gamma(E) = (1 - v^2(E))^{-1/2}$, and $v(E)$ is the electron group velocity. However, in the LV case, and assuming again $n = 3$, the electron group velocity

is given by

$$v(E) = \frac{\partial E}{\partial p} = \frac{p}{E}\left(1 + \frac{3}{2}\eta\frac{p}{M}\right) . \tag{1.76}$$

Therefore, $v(E)$ can exceed 1 if $\eta > 0$ or can be strictly less than the low energy speed of light if $\eta < 0$, resulting in $\gamma(E) \lesseqgtr E/m_e$ for $\eta \lesseqgtr 0$. Moreover, if $\eta > 0$, $\gamma(E)$ grows without bound until it diverges at the soft VC threshold (1.74), which is well below the Planck scale for any $\eta \gg (m_e/M)^2 \approx 10^{-44}$. On the other hand, for any $\eta < 0$, $\gamma(E)$ has a maximum and, hence, the critical frequency has an upper bound, $\omega_c^{\max}$.[5] Then, if synchrotron emission up to some maximal frequency $\omega_{\rm obs}$ is observed, one can deduce that the LV coefficient for the corresponding leptons cannot be more negative than the value for which $\omega_c^{\max} = \omega_{\rm obs}$. This leads to the bound [58, 103]

$$\eta > -\frac{M}{m_e}\left(\frac{0.34\, eB}{m_e\, \omega_{\rm obs}}\right)^{3/2} , \tag{1.77}$$

which is strongest when the empirical ratio $B/\omega_{\rm obs}$ is minimised. Once again, the CN is the plerion for which the best constraint can be cast.

Making the conservative assumption that the 100 MeV photons detected by γ-ray experiments [109] are produced by synchrotron emission, a lower bound $\eta > -8 \times 10^{-7}$, for at least one η, has been set [58]. For the case of positive η, similar reasoning cannot be applied, because for any positive η a particle can emit all synchrotron frequencies (up to infinity, in principle). Hence, a detailed reconstruction of the emitted spectrum is needed in this case.

1.5.5 Helicity decay

Although it is not represented in Fig. 1.2, this reaction is relevant to our investigation. In the presence of LV, high energy electrons and positrons can flip their helicity with the emission of a suitably polarised photon (Helicity Decay, HD). This reaction does not have a real threshold, but rather an effective one [58]:

$$p_{\rm HD} = (m_e^2 M/\Delta\eta)^{1/3} , \tag{1.78}$$

[5] Notice that in EFT framework the sign of $\eta_\pm$ is undetermined. Conversely, in DSR-like scenarios only superluminal parametrisation (i.e. $\eta > 0$) is allowed [105] while in the string-inspired Liouville model of space-time foam [106, 107] such coefficients are exactly zero and only the photon dispersion relation acquires a LV modification. This stresses the importance of a clear choice of framework when discussing this sort of phenomenological constraints (see e.g. [108, 72, 58]).

where $\Delta\eta = |\eta_+ - \eta_-|$, at which the decay lifetime τ_{HD} is minimised. For $\Delta\eta \approx O(1)$ this effective threshold is around 10 TeV. For our purposes it is interesting to note that below threshold

$$\tau_{\rm HD} > \Delta\eta^{-3}(p/10\ {\rm TeV})^{-8}\, 10^{-9}{\rm s}, \tag{1.79}$$

while above threshold $\tau_{\rm HD}$ becomes independent of $\Delta\eta$ [58]. A constraint of $\Delta\eta < 0.4$ has been indirectly inferred in [58] from the photon decay bound (see Fig. 1.2) $|\eta_\pm| < 0.2$, by looking at the maximal difference of η allowed by the γ-decay bound.

1.5.6 Ultra-High-Energy Cosmic Rays and Neutrinos

Being the most energetic particles ever experienced on Earth, Ultra-High-Energy Cosmic Rays (UHECRs) have long been thought of as generic probes for physics beyond the SM. The spectrum of CRs is known to span several decades in energy with impressive regularity. Its shape is an almost featureless power-law, with only few breaks corresponding to still debated physical effects.

A more thorough discussion on CR physics, also in view of placing constraints on LV, will be done in chapter 3.

One of the most impressive facts about the UHECR spectrum is that its end-point historically increased as the experiments were able to probe higher and higher energies. This is puzzling, because we expect astrophysical accelerators to have a finite power, hence to be able to accelerate particles only up to some fixed energy.

However, it was realised in the 1960s that a cut off of the UHECR spectrum should exist, even if UHECRs are accelerated well above it. In fact, UHECR with energy larger than few 10^{19} eV are expected to lose energy by pion production induced by interactions with the Cosmic Microwave Background (CMB), through the resonant process $p + \gamma \to \Delta^+ \to p + \pi^0 (n + \pi^+)$ [110, 111]. Being a threshold process, this can be heavily affected by LV. Using this fact, constraints of order 10^{-24} on renormalizable operators have been obtained [112], while on non-renormalizable $O(E/M_{\rm Pl})$-suppressed operators constraints of order 10^{-10} have been obtained in two simplified cases [113, 114, 102, 63].

For what concerns neutrinos, they are thought of as the best candidates for observation of LV effects. Indeed, due to their mass they are already thought to be carriers of significant information on physics beyond the SM, which, in its original formulation, imposes zero mass for them, but since, in addition, their mass is now known to be rather small (best estimates are now

for $m_\nu \sim 0.1$ eV), the threshold energy for LV to be effective in the neutrino system is estimated to be of order 1 GeV for dimension 5 LV operators and 100 TeV for dimension 6 ones (see tab. 1.1). We notice that few GeV is the typical energy of atmospheric neutrinos produced by interactions of primary cosmic rays on the top of the terrestrial atmosphere, while 100 TeV is well within reach of planned or operating high energy Neutrino Telescopes.

However, the extreme difficulty of detecting extra-terrestrial high-energy neutrinos makes it very hard to propose now studies on LV in the neutrino sector.

Rather recently, however, the possibility of placing constraints on neutrino LV using Kamiokande detection of MeV neutrinos from the explosion of SN1987a and he OPERA neutrino beam [115] was explored. However, even after a thorough time-delay analysis, the LV parameters η_ν are found to be $\eta_\nu \lesssim O(10^9)$ for dimension 5 LV, and $\eta_\nu \lesssim O(10^{15})$ for dimension 6. These are very poor constraints, witnessing the extreme difficulty of gathering information on LV in the neutrino sector.

Chapter 2

Crab Nebula and LIV

"Les étoiles sont belles à cause
d'une fleur que l'on ne voit pas."

Antoine de Saint-Exupéry

2.1 An unfinished job

While the natural magnitude of the photon and electron coefficients $\xi, \eta_\pm$ would be $O(1)$ if there were one power of suppression by the inverse Planck mass in EFT with dimension 5 LV operators, the coefficients are currently restricted to the region $|\xi| \lesssim 10^{-7}$ by birefringence and $|\eta_\pm| \lesssim 10^{-1}$ by photon decay.

Thus, whereas the constraint on the photon coefficient is remarkably strong, the same cannot be said about the LV coefficients of leptons. A constraint on the lepton coefficients of comparable strength is given by the synchrotron limit, but this is not double sided and implies only that the LV coefficient of the population responsible for the CN synchrotron emission cannot be smaller than -8×10^{-7}. Similarly the VC-IC bound $\eta < +3 \times 10^{-3}$ constrains only one lepton population. These statements, although not void of physical significance, cannot be considered constraints on $\eta_\pm$, since for each of them one of the two parameters $\pm\eta_+$ (and $\pm\eta_-$) will always satisfy the bound.

More can be said by using information obtained from current models of the CN emission, in particular the fact that the CN emission is well fitted by assuming that a single lepton population accounts for both the synchrotron and IC radiation [58]. This implies that at least one of the four pairs $(\pm\eta_\pm, \xi)$ must lie in the narrow region bounded horizontally by the dashed lines of the

synchrotron and IC bounds and vertically by the birefringence constraint (see figure 1). However, the dashed region limits apply at most to one of the four pairs $(\pm\eta_{\pm}, \xi)$ as we cannot *a priori* exclude that only one out of four populations is responsible for both the synchrotron and IC emission (see again [58] for further details).

It is clear that these simple arguments do not fully exploit the available astrophysical information. A detailed comparison of the observations with the reconstructed spectrum in the LV case, where all reactions and modifications of classical processes are considered, can provide us with constraints on both positive and negative η for the four lepton populations, at levels comparable to those already obtained for the photon LV coefficient. Let us then move to reconsider such information concerning the astrophysical object that so far has proven most effective in casting constraints on the electron/positrons LV coefficients: the Crab Nebula (CN).

2.2 The Crab Nebula

The CN is a source of diffuse radio, optical and X-ray radiation associated with a Supernova explosion observed in 1054 A.D., at a distance from Earth of about 1.9 kpc. A pulsar, presumably the neutron star remnant of the explosion, is located at the centre of the Nebula, and is believed to supply both the radiating particles (mostly electrons and positrons) and magnetic fields, as well as the required power, which is somewhat less than the rotational energy loss-rate of the star (the "spin-down luminosity"), of roughly 5×10^{38} erg/s (for a recent review see [116]).

2.2.1 Observations

The Nebula emits an extremely broad-band spectrum (covering 21 decades in frequency), produced by relativistic leptons via two major radiation mechanisms: synchrotron radiation from radio to low energy γ-rays ($E < 1$ GeV), and IC scattering for the higher energy γ-rays. The clear synchrotron nature of the radiation below ~ 1 GeV, combined with a magnetic field strength of the order of $B \approx 100$ μG implies, when exact LI is assumed, the presence of relativistic leptons with energies up to 10^{16} eV. Their gyro period is comparable to the synchrotron cooling timescale, implying an acceleration rate close to the maximum estimated for shock-based mechanisms (e.g. [117]).

The appearance of the CN depends on the observational wavelength: in X-rays it is ellipsoidal, with angular dimensions $2' \times 3'$ (corresponding to

$\sim 1.2 \times 1.8\,$pc at the Crab distance). In the centre it displays a jet-torus structure in the X-ray and optical bands. In the radio, this feature is less apparent, and the Nebula is more extended, with a dimension of about $6'$ [118]. Low frequency (radio) observations allowed also the discovery of a number of structures on subarcsecond scale, such as wisps, ripples, jets and arcs. Interestingly, most of these substructures are seen also in the optical [118] and X-rays [119]. Deep optical observations by the Hubble Space Telescope (HST), in fact, revealed the presence of rich and complex structures, at scales of $0.2''$(corresponding to ~ 0.2 pc), such as wisps, jets, knots. Also the observations in the X-rays carried by Chandra (with subarcsecond resolution) confirmed the presence of such structures and the cylindrical, rather than spherical, symmetry of the whole complex.

In the frequency band ranging from radio to optical, the overall emission spectrum of the CN has an extremely regular power-law shape, with spectral index $\alpha_s = -0.27 \pm 0.04$ ($F \propto E^{\alpha_s}$).

The spectrum of the whole nebula in X-rays is found to be a power-law with spectral index $\alpha_s \approx -1.1$ in the energy range 1-20 keV [120]. The nebular spectrum becomes softer and softer (with the spectral index passing from 0.9 in the inner region to about 2.0 in the outer), in the 0.5-8 keV band, as the distance from the shock position in the Nebula increases [120]. This result is confirmed also by the findings of the XMM-Newton Experiment [121], though with less spatial precision. This spectral index variation and spectral softening on arcsecond scale is consistent with overall expectations from the magneto-hydro-dynamic model by [122]: in fact, with increasing time (and hence distance from the acceleration region) the spectrum of the diffusing particles becomes softer because of the shorter synchrotron lifetime of higher energy particles. Furthermore, in standard electrodynamics, the lifetime of an electron undergoing synchrotron energy losses can be estimated as

$$\tau \propto \nu_c^{-1/2} B^{-3/2} \,, \tag{2.1}$$

where ν_c is the characteristic emitted frequency and B is the magnetic field in which the electron is spiralling. According to eq. (2.1), electrons emitting at lower frequency have longer lifetime, being able to diffuse further away from the shock. This is confirmed by the measured extension of the Crab Nebula at different wavelengths: as we already noticed, while in X-rays the nebula angular extension is $2'$(corresponding to ~ 1.2 pc at the Crab distance), in radio its length is about $6'$[118].

In the γ-ray domain, the Energetic Gamma-Ray Experiment Telescope (EGRET) on the *Compton Gamma-Ray Observatory (CGRO)* observed the Crab Nebula and pulsar in the energy range from 50 MeV to 5 GeV [109]

with an angular resolution of several degrees. This poor angular resolution did not allow the separation between the emission from the pulsar and the one from the nebula. However, the flux in the off-pulse phase was measured to be

$$\frac{dF}{dE} = (9.1 \pm 0.8) \times 10^{-9} \left(\frac{E}{118 \text{ MeV}} \right)^{-2.93 \pm 0.15} \text{cm}^2\text{s}^{-1}\text{MeV}^{-1} \,. \quad (2.2)$$

This flux matches well the extrapolation of that reported by [123] in the 50–500 MeV range, which as been interpreted [124] as an extension of the synchrotron spectrum well established at lower energies. Moreover, in [124] it was shown that the low energy unpulsed emission cannot be accounted for by inverse Compton scattering, and under reasonable hypotheses about the magnetic field present in the emission region (close to the equipartition value of few 100 μG) it has been inferred the presence of electrons with energy of the order of 10^{16} eV. Also the hardening of the spectrum above 500 MeV was predicted by [124], as the IC becomes more important.

Information about very high energy emission from the Crab Nebula has been collected starting from the pioneering observations by Whipple [125], and since then by several Imaging Atmospheric Cherenkov Telescopes (IACT) (see e.g. [126, 127, 1, 128]) and Extensive Air Shower (EAS) detectors.

The TIBET [129] and MILAGRO [130] detectors observed the Crab nebula with an angular resolution of $1.5 - 2^\circ$. The reported flux by TIBET [129] was

$$\frac{dF}{dE} = (4.61 \pm 0.90) \times 10^{-12} (E/3 \text{ TeV})^{-2.62 \pm 0.17} \text{ cm}^{-2}\text{s}^{-1}\text{TeV}^{-1} \,, \quad (2.3)$$

where the errors are only statistical and the energy range is between 3 and 15 TeV. MILAGRO also reported [130] the detection of γ-rays from the Crab nebula direction, but did not reconstruct the spectrum, due to its poor energy resolution. However, they fitted the data points using the functional forms provided by other groups' measurements, finding results compatible, within errors, with those of other experiments.

The HEGRA stereoscopic IACTs observed the Crab Nebula between 500 GeV and 80 TeV [1]. The energy spectrum (with an overall uncertainty of $\sim$15%) is well approximated by a pure power-law

$$\frac{dF}{dE} = (2.83 \pm 0.04 \pm 0.6) \times 10^{-11} \left(\frac{E}{1 \text{ TeV}} \right)^{-2.62 \pm 0.02 \pm 0.05} \text{cm}^{-2}\text{s}^{-1}\text{TeV}^{-1} \,. \quad (2.4)$$

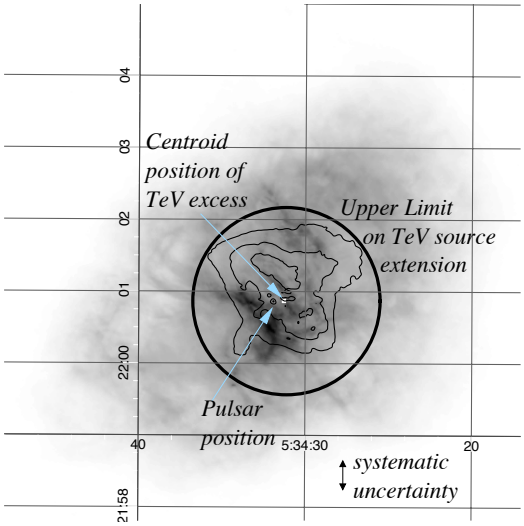

Figure 2.1: In gray scale the radio map of the Crab nebula with X-ray contours. The solid line circle indicates the upper limit on the TeV source size and as a white square the position of the TeV centroid (the sidelength indicate the 3″statistical error). Figure taken from [1].

Remarkably, the data show a 2.7σ excess even at 86 TeV. The position of the excess was determined to be shifted by about 12″(though with a systematic uncertainty of 25″) angular distance to the west of the nominal position of the pulsar, consistent with the centroid position of the X-ray emitting nebula.

The extension of the TeV excess (less than 3′at 10 TeV) excludes a strong contribution from the still undetected outer shock of the expanding supernova remnant and is compatible with the electrons being accelerated in the proximity of the termination shock and then cooled by synchrotron/IC process.

The data by HEGRA are also compatible with the expected softening of the spectrum at high energies (namely $E \geq 70$ TeV). This behaviour is confirmed by more recent HESS observations of the Crab nebula [128]. In fact, the combined data sets for the differential spectrum are best fitted by a power-law with slope $\Gamma = 2.39 \pm 0.03 \pm 0.09$ with exponential cut-off at $14.3 \pm 2.1 \pm 2.8$ TeV, rather than a pure power-law.

Though the maximum energy of the electrons is model dependent, the fact that photons with $E \gtrsim 10$ TeV have been detected from the Crab Nebula is an unambiguous evidence of effective acceleration of particles beyond 100 TeV. Let us stress that this statement has to be considered robust also in our test theory, in which energy–momentum conservation still holds.

2.2.2 Theoretical model

From the theoretical point of view, the CN is one of the most studied objects in astrophysics. However, in spite of more than 30 years of theoretical efforts, important details of the interactions between the pulsar wind and the synchrotron nebula are still missing. The current understanding is based on a spherically symmetric magneto-hydrodynamic (MHD) model presented in two seminal papers by Kennel & Coroniti [122, 131], that accounts for the general features seen in the spectrum. In their model, the synchrotron nebula is powered by the relativistic wind of cold electrons generated by the pulsar and terminated by a standing reverse shock wave at $r_S \simeq 0.1$ pc [132], due to the balance of the ram pressure of the flow with the pressure of the outer nebula.

Assuming, for simplicity, spherical symmetry, they divided the Crab complex in 6 regions.

1. The region in which electron-positron pairs are produced by the Goldreich & Julian [133] potential inside the pulsar magnetosphere.

2. The region where a highly relativistic wind of monoenergetic electron positron pairs and a toroidal magnetic field flows towards the nebula. The characteristic Lorentz factor of the wind is $\gamma \sim 10^6 - 10^7$. Both particles and the magnetic field are carried by the wind, but no synchrotron radiation is produced at this stage, since they are comoving.

3. The nebula, where the positronic flow has been decelerated and heated by a standing reverse shock at $r_S \simeq 0.1$ pc and extends to the outer nebula at $r_N \approx 2$ pc.

4. Three outer regions, which we group here, where the remnant of the Supernova explosion lies and a blast wave is likely to propagate and collect interstellar material.

Kennel & Coroniti found a stationary solution in which the particle flow evolves adiabatically in the magnetised nebula. The magnetisation of the flow is parametrised by $\sigma = B^2/4\pi\gamma\rho$, which is the ratio between the magnetic and the kinetic energy density in the flow (ρ being the density). The value of σ is determined by the conditions at the outer boundary of the Nebula. In fact, since the postshock flow has to match the velocity of the material at the interface between the Nebula and the remnant, which is non-relativistic, and a lower bound to the flow speed is given by $v \gtrsim \sigma/(1+\sigma)$ [122], it turns out that σ has to be small, of order 10^{-3} [134]. However, the magnetic field is clearly dynamically important in the Nebula, because it is responsible for its

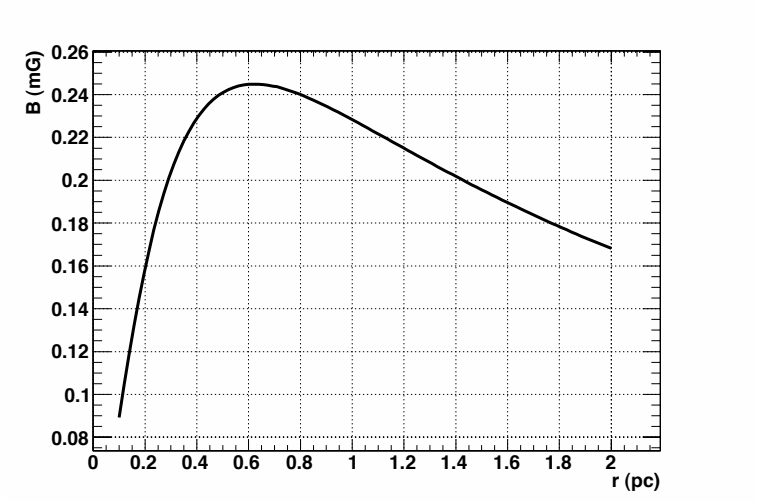

Figure 2.2: Magnetic field profile following Kennel & Coroniti, assuming the best fit value $\sigma = 0.003$ and the reverse shock wave position $r_{\rm S} \approx 0.1$ pc.

ellipsoidal shape [135, 136]. Therefore, the value of σ cannot be substantially less than 10^{-3}.

Observations of the radio and optical brightness distributions confirm that the magnetic field, which is to a good approximation toroidal, is not constant in the CN, but increases in the central region ($r \leq 0.5$ pc) with distance from the pulsar. Its behaviour as a function of radius downstream of the shock front (shown in fig. 2.2) is determined initially by the gas pressure, which remains almost constant. Because the gas behaves almost adiabatically, the density is also initially constant, and the radial velocity decreases as $1/r^2$, leading to an increase in the frozen-in toroidal magnetic field $B(r)$. When $B(r)$ approaches the equipartition value of 0.3 mG [137] and starts to play a role in the dynamics of the flow, it ceases to grow and then falls off with increasing distance.

The particle distribution all around the nebula and the energy spectrum evolution is calculated using flux conservation at the shock interface. Due to synchrotron and adiabatic energy losses, the energy of a particle, which at the termination shock position r_S was ϵ_2, will evolve as

$$\epsilon(z) = \frac{\epsilon_2 (v z^2)^{-1/3}}{1 + (\epsilon_2/\epsilon_c) I_1} \,, \tag{2.5}$$

where ϵ_c is an energy scale related to the synchrotron burn-off, $z = r/r_S$ and

$$I_1(z) = \int_1^z dx \frac{x^4}{(vx^2)^{10/3}} \ . \tag{2.6}$$

The conservation of the spectral number flux then reads

$$vz^2 n_{nebula}(E)dE = n_s(E')dE' \ . \tag{2.7}$$

Hence, the resulting particle spectrum, assuming an injection spectrum $n_s(E)$ in the termination shock, is

$$n_{nebula} = \frac{1}{(vz^2)^{4/3}} \left(\frac{\epsilon_2}{\epsilon}\right)^2 n_s(\epsilon_2) \ , \tag{2.8}$$

where $\epsilon_2(\epsilon)$ is found by inverting eq. (2.5).

At least two relativistic electron populations are needed to explain the broad band spectrum of the Crab nebula [138]:

- A population of high energy electrons (usually called the *wind electrons*) freshly accelerated.
- A population of low energy particles (the *radio electrons*) needed to reproduce the radio spectrum of the nebula.

Since the time scale for synchrotron energy losses is

$$t_{sync} \simeq 2.8 \times 10^8 \left(\frac{B}{0.3 \text{ mG}}\right)^{-2} \gamma^{-1} \text{ yr} \tag{2.9}$$

and the age of the nebula is about 1000 yr, the relativistic electrons can be cooled only down to a critical energy $E_{cr} \sim 200$ GeV. Therefore, the existing population of radio electrons, with $E \lesssim E_{cr}$, can be only the 'relic' of the history of the pulsar and the nebula. Moreover, in the frequency band ranging from radio to optical the overall emission spectrum of the Crab Nebula has an extremely regular power-law shape. The spectral index has been determined as $\alpha_{\text{radio}} = -0.27 \pm 0.04$ [118] in the radio and the extrapolation of this spectrum to IR and optical frequencies reproduces well the existing data. The continuity of the emission spectrum confirms that it is due to only one population of radio electrons homogeneously distributed in the nebula.

The characteristic frequency of synchrotron radiation, for isotropic pitch angle, is

$$\nu_{sync} \simeq 7 \times 10^2 \gamma^2 \left(\frac{B}{0.3 \text{ mG}}\right) \text{ Hz} \ . \tag{2.10}$$

Thus, the power-law radiation at long wavelengths is produced by electrons with $E \lesssim 150$ GeV. The best fit is achieved [138] assuming an energy spectrum for the radio electrons as

$$n_{re}(E) = A_{re} E^{-p_r} e^{-E/E_*} \,, \tag{2.11}$$

with $p_r \simeq 2\alpha_{\rm radio} - 1 \approx 1.5$, $E_* = 150$ GeV and A_{re} fixed according to the normalisation of the radio flux at GeV frequencies.

The wind electrons, on the other hand, have $E \gg E_{cr}$ and are continuously injected downstream of the termination shock. In order to fit the measured X-ray spectrum, a distribution of injected wind electrons as

$$n_s(E) = A_{we}(E_0 + E)^{-p_w} e^{-E/E_c} \tag{2.12}$$

with $p_w \gtrsim 2$ is needed. $E_0 \simeq 250$ GeV is a phenomenological parameter that accounts for the spectral softening required by observations at low energy, where the radio electron population dominates, while $E_c \simeq 3.5$ PeV is related to the maximum energy at which the shock can accelerate the electrons. The wind injection spectrum is propagated in the nebula according to eq. (2.8).

2.3 Modified Lagrangian and interactions

Due to the presence, in the LV Lagrangian, of a term proportional to γ_5, the dispersion relations of all the particles depend on their helicity state (or polarisation). However, one may wonder if they produce observable effects in the radiation of γ-rays of leptonic origin from the Crab Nebula. In order to answer that question, we have to compare the typical time scales of all the processes involving, at some extent, the helicity of the particles. While helicity dependence of the LV is expected also in the photon sector, we are going to neglect it, due to the strong limits imposed on ξ by vacuum birefringence constraints. We shall hence focus here on leptons.

However, we must notice that modifications in the Lagrangian could also affect our understanding of normal processes, since non-trivial terms are added. Hence, we are going in this rather technical section to first re-derive the Hamiltonian for an electron minimally coupled to the photon field, and show that new interactions may arise when preserving gauge invariance. We are also going to show that modifications in the structure of spinors due to the new LV terms do not affect the interacting part of the Hamiltonian by explicit calculations. Then, we will study the possible interference between standard spin precession effect, occurring when a charged particle is spiralling in a magnetic field, and the effect of helicity decay induced by LV.

Finally, we will compare the time-scales of the difference processes to deduce information on the helicity state of leptons radiating in the Crab Nebula.

2.3.1 Hamiltonian

Free theory

We consider now the full Lagrangian for free fermions including the LV terms [56]

$$L = \bar{\psi}(i\gamma^\mu\partial_\mu - m)\psi + \frac{1}{2M}u^\mu\bar{\psi}\gamma_\mu(\zeta_1 + \zeta_2\gamma_5)(u\cdot\partial)^2\psi \ . \tag{2.13}$$

The corresponding equation of motion for ψ is

$$(i\gamma^\mu\partial_\mu - m + \frac{1}{2M}u^\mu\gamma_\mu(\zeta_1 + \zeta_2\gamma_5)(u\cdot\partial)^2)\psi = 0 \ , \tag{2.14}$$

from which we can derive the well-known dispersion relation for the fermions

$$E^2 = p^2 + m^2 + \frac{\eta_+}{2M}E^2(E + sp) + \frac{\eta_-}{2M}E^2(E - sp) - \frac{\eta_+\eta_-}{4M^2}E^4 \ , \tag{2.15}$$

where $s = \boldsymbol{\sigma}\cdot\boldsymbol{p}/|\boldsymbol{p}|$ and $\eta_\pm = 2(\zeta_1 \pm \zeta_2)$. Notice that in principle, since the Lagrangian contains second order time derivative, it is not possible to use the standard QFT procedure to obtain the dispersion relation. However, it can be shown [139] by a careful mathematical analysis that the dispersion relation (2.15) is correct up to order $O(E/M_{\rm Pl})$, as we need.

The eigenspinors for the electron are

$$u_s(p) = \begin{pmatrix} \sqrt{E - sp - \frac{\eta_+E^2}{2M}}\chi_s(p) \\ \sqrt{E + sp - \frac{\eta_-E^2}{2M}}\chi_s(p) \end{pmatrix} . \tag{2.16}$$

However, since the factor $E^2/2M$ is suppressed with respect to the others if $E \ll M$, we are going to drop it.

It can be seen from eq. (2.15) that in the ultra-relativistic approximation in which $E \approx p$ the LV parameters $\eta_\pm$ depend on the helicity s. If for some reason s averages to 0, then only an "effective" $\langle\eta\rangle = (\eta_+ + \eta_-)/2$ (corresponding to $\langle\zeta\rangle = 0$) is left.

Interacting theory

Let us now minimally couple the fermions to the electromagnetic field by the usual replacement $\partial_\mu \to D_\mu = \partial_\mu + i\,e\,A_\mu$ where A_μ is the well-known electromagnetic potential. Since we know that the LV parameter for the photon is of the order of 10^{-4} or even smaller (see e.g. [58] and [77]), we are going to neglect it. The fermion Lagrangian is thus

$$L = \bar{\psi}(i\gamma^\mu\partial_\mu - e\gamma^\mu A_\mu - m + \frac{1}{2M}u_\mu\gamma^\mu(\zeta_1 + \zeta_2\gamma_5)(u\cdot(\partial + i\,e\,A))^2)\psi\ . \quad (2.17)$$

The Hamiltonian associated to this Lagrangian reads

$$H = i\vec{\alpha}\cdot(\vec{\nabla} - i\,e\,\vec{A}) + \beta m + eA^0 - \frac{1}{2M}\gamma^\mu u_\mu(\zeta_1 + \zeta_2\gamma_5)(u\cdot(\partial + i\,e\,A))^2\ , \quad (2.18)$$

where $\vec{\alpha} = \gamma^0\vec{\gamma}$ and $\beta = \gamma^0$. It is interesting to notice here that since the 4-vector u is timelike, in the preferred frame where $u = (1, \vec{0})$ the last term contains only an extra-interaction with A^0. Thus, the interaction Hamiltonian is

$$H_{int} = -ie\int d^3x\bar{\psi}\gamma^\mu\psi A_\mu\ , \quad (2.19)$$

as usual[1].

Since we are interested mainly in the interaction of particles with magnetic fields, let us suppose that we are in presence of only a static magnetic field. Then, we can pose $A^0 = 0$ and make the gauge choice $\partial_\mu A^\mu = 0$ (this can be realised for example by choosing $\vec{A} = 1/2\,\vec{B}\times\vec{r}$) and the last LV term does not produce any extra interaction with the magnetic field. Moreover, the last term does not affect the evolution of the others, since $[\gamma_5, \gamma^\mu] = 0 \quad \forall\mu$.

For a static magnetic field the potential can be calculated in the standard way taking H_{int} and the spinor fields in the interaction representation. We have seen and justified the fact that the extra terms depending on the ζs do not affect neither the evolution of H_{int} (exactly!) nor the form of the spinors (approximately well, within a factor 10^{-16}, in the energy range around the TeV).

Hence, the result for the potential of interaction of electrons with a static magnetic field is

$$V_{int} = -g\,\frac{e}{2}\,\frac{\sigma^{\mu\nu}}{2}F_{\mu\nu}\mid_{magn} = -g\,\frac{e}{2}\,\vec{\sigma}\cdot\vec{B}\ , \quad (2.20)$$

[1]Note that we have dropped here the extra term depending on A^0. However this is suppressed with respect to the (2.19) by a factor of M.

where $F_{\mu\nu}$ is the usual electromagnetic field strength and $\sigma^{\mu\nu} = \frac{i}{2}[\gamma^\mu, \gamma^\nu]$.

2.3.2 Spin rotation and Helicity Decay

Once we have demonstrated that in the modified non Lorentz Invariant theory we recover, at low energy, all the known processes, we can study how the new processes opened by the modified dispersion relations affect the usual ones. Namely, we want to study simultaneously the magnetic field interactions with the Helicity Decay (or rotation) process.

As a preliminary consideration, let us notice that the total amplitude for the 2 processes is barely the sum of the two individual amplitudes, whose square moduli have been computed in the literature (see for instance [58] for the HD and [140] for the Spin Precession). We are, in fact, asking whether the interference term produces new effects. However, it should be noted that if the magnetic field is static, then the electron just undergoes elastic scattering, so that its energy is conserved[2].

On the other hand, the HD effect requires that a photon is effectively emitted, with non-zero energy. Thus, the two amplitudes have different support and cannot produce, at least at tree level, interference.

Spin rotation in external magnetic field

We will base the following discussion on [140]. The interaction of a non-relativistic spin-1/2 particle can be described by the hamiltonian:

$$H = H' - \mu\vec{\sigma}\cdot\vec{B}\,, \tag{2.22}$$

where we put in H' all the terms not containing the spin and we indicated by $\vec{B}$ the magnetic field and by $\vec{\sigma} = \{\sigma_1, \sigma_2, \sigma_3\}$ the Pauli matrices. The magnetic moment intensity is μ which, for the electron, can be written as

$$\mu = g\frac{e}{2\,m}\frac{1}{2}\,, \tag{2.23}$$

[2]This can be also seen formally, going in the Fourier space. In fact, if A^μ is independent of time and $q = p' - p$,

$$\tilde{A}^\mu(q) = \int d^4x\, A^\mu(x)\, e^{iq\cdot x} = 2\,\pi\,\delta(q^0)\int d^3x\, A^\mu(\vec{x})\, e^{-i\vec{q}\cdot\vec{x}}\,, \tag{2.21}$$

thus the interaction with the static magnetic field produces no change in the electron energy ($q^0 = 0 \Rightarrow p'^0 = p^0$).

where g accounts for all the possible deviation for the non-anomalous value $g = 2$. We will in fact denote as μ' the anomalous part of the magnetic moment $\mu - \frac{e}{2\,m}$.

The equation of motion for the spin $\vec{s} = \vec{\sigma}/2$ is

$$\dot{\vec{s}} = \frac{i}{2}[H, \vec{\sigma}]\,. \tag{2.24}$$

Substituting in (2.24) we find

$$\dot{\vec{s}} = 2\,\mu \vec{s} \times \vec{B}\,. \tag{2.25}$$

Averaging over a semi-classical wave-packet, and denoting by $\zeta/2$ the average spin $\langle \vec{s} \rangle$, we have

$$\dot{\vec{\zeta}} = 2\,\mu\,\vec{\zeta} \times \vec{B}(t)\,. \tag{2.26}$$

From eq. (2.26) we deduce that the magnetic moment is in precession around the direction of the magnetic field, without changing his magnitude, with an angular velocity of $-2\mu\vec{H}/\hbar$. In the same non-relativistic case the velocity of the particle, due to the Lorentz force, obeys the following equation of motion

$$\frac{\mathrm{d}\vec{v}}{\mathrm{d}t} = \frac{e}{2\,m}\vec{v} \times \vec{B}\,. \tag{2.27}$$

Comparing the two equations we find that if $g = 2$ the magnetic moment and the velocity rotate around the magnetic field at the same rate, i.e. the angle between the polarisation and the direction of motion is **constant**.

The same result holds in the relativistic case. We are not going to re-derive the equation of motion for the polarisation vector in this case. We barely quote it as

$$\begin{aligned}\frac{\mathrm{d}\vec{\zeta}}{\mathrm{d}t} =& \frac{e}{2\,m}\left(g - 2 + 2\,\frac{m}{\epsilon}\right)\vec{\zeta} \times \vec{B} + \\ & \frac{e}{2\,m}(g-2)\frac{\epsilon}{\epsilon + m}(\vec{v}\cdot\vec{B})\vec{v} \times \vec{\zeta} + \frac{e}{2\,m}\left(g - \frac{2\,\epsilon}{\epsilon + m}\right)\vec{\zeta} \times (\vec{E} \times \vec{v})\,,\end{aligned} \tag{2.28}$$

where ϵ is the energy of the particle and $\vec{E}$ is the electric field. From eq. (2.28) is clear that the motion of the polarisation of a particle moving in presence of only a magnetic field $\vec{B}$ in a plane perpendicular to it is

$$\frac{\mathrm{d}\vec{\zeta}}{\mathrm{d}t} = \frac{e}{2\,m}\left(g - 2 + 2\,\frac{m}{\epsilon}\right)\vec{\zeta} \times \vec{B}\,. \tag{2.29}$$

Since the corresponding equation for the velocity in presence of a pure magnetic field is

$$\frac{\mathrm{d}\vec{p}}{\mathrm{d}t} = e\,\vec{v}\times\vec{B}\,, \tag{2.30}$$

the polarisation vector is in precession with respect to the velocity if $g \neq 2$. The precession velocity is then

$$\frac{\mathrm{d}\vec{\zeta_{pr}}}{\mathrm{d}t} = -\frac{e}{m}\,\frac{g-2}{2}\,\vec{B}\,. \tag{2.31}$$

One may be interested in the motion of the actual angle between the polarisation vector and the velocity, namely $\vec{\zeta}\cdot\vec{v} = \cos(\theta)$. This is found to obey the following equation

$$\frac{\mathrm{d}\cos(\theta)}{\mathrm{d}t} = \frac{e}{m}\frac{g-2}{2}B\sin(\theta)\,. \tag{2.32}$$

Let us suppose now that an electron is spiralling at ultra-relativistic velocity $v \simeq c$ in a constant magnetic field. The gyration radius is then $R = \epsilon/(e\,B)$. The variation of the polarisation angle during one cycle is, from (2.32),

$$\Delta\alpha = \frac{e}{m}\,\frac{g-2}{2}\,B\times\frac{2\,\pi\,\epsilon}{e\,B\,c} = 2\,\pi\,\frac{g-2}{2}\frac{\epsilon}{m}\,. \tag{2.33}$$

The time needed for the precession to reverse the electron polarisation is

$$\Delta t_{\mathrm{rev}} = \frac{\pi}{2\,\mu'\,B}\,. \tag{2.34}$$

2.3.3 Helicity dependence and the Crab Nebula

We are now going to compare the time-scales of the relevant processes taking place in the Crab Nebula.

One can distinguish three classes of time scales: one class, which is typically longer than few years, is that of the energy gain/loss processes, responsible for the observed radiation, while the second is mainly related to the behaviour of the internal degrees of freedom of the particles (namely the spin) and is shorter than a year. The Vacuum Čerenkov scale, finally, is so short that it introduces a sharp cut-off in the particle acceleration spectrum[3].

[3]The question whether the Čerenkov radiation is observable or not could be made. Since the VC time scale is so short, this process is effective as soon as the particle is above threshold. Thus, the amount of energy that goes into emitted radiation is so tiny that it is practically impossible to detect it.

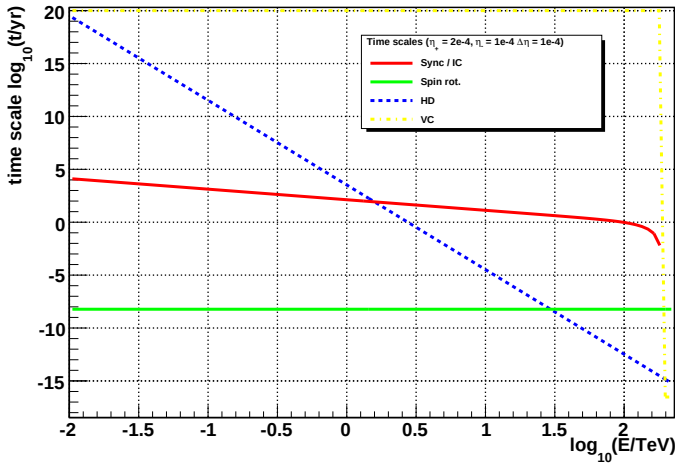

Figure 2.3: Comparison of different time scales for $\eta_+ = 2 \times 10^{-4}$ and $\eta_- = 10^{-4}$.

Let us deal for simplicity just with the electrons (similar considerations can be made for the positrons). Our initial assumption is that the acceleration mechanism is at low energies independent on the LV. More specifically, as long as the electron energy is below few TeV, we can safely assume that the positive and negative helicity populations are equal, because both the acceleration and the energy loss processes do not care about the spin (the spin orientation does not modify the acceleration and energy loss rates) and also any initial asymmetry between the two populations would be spoiled by the spin rotation effect. These helicities, as we said, will have different LV coefficients and we will assume for simplicity that $\eta_+ > \eta_-$. Obviously for our analysis the relative strength of η and $\Delta\eta$ is important as these quantities determine the rapidity of the VC and HD processes. Let us first consider the case $\Delta\eta \sim \eta$.

$\Delta\eta \sim \eta$

Let us suppose for concreteness that $\eta_+ = 2 \times 10^{-4}$ and $\eta_- = 10^{-4}$. In order to have a quantitative overview let us show in fig. 2.3 the relevant time-scales for LV parameters in the interesting range of values.

We see that in this case, as soon as $E \gtrsim 30$ TeV the time scale for helicity decay becomes much shorter than that of the spin rotation.

From the above values we can infer that in this case all the positive helicity electrons are converted into negative helicity ones above ~ 30 TeV, given that the spin rotation becomes, above this energy, ineffective against

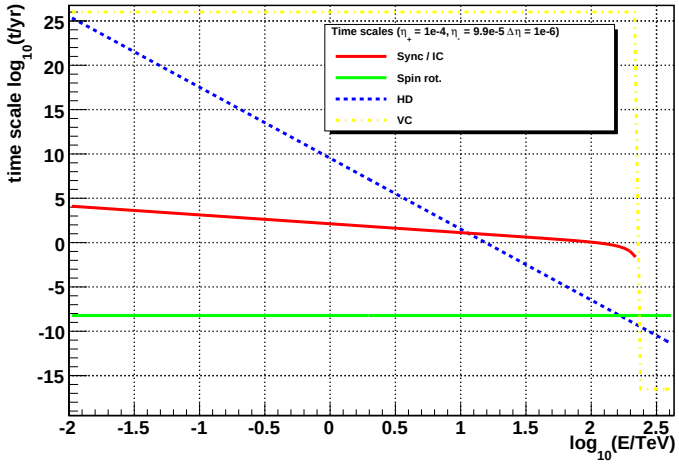

Figure 2.4: Comparison between different time scales $\eta_+ = 10^{-4}$ and $\eta_- = 9.9 \times 10^{-5}$.

helicity decay. Therefore, while the initial population was equally divided into positive and negative helicity electrons below 30 TeV, the population at $E \gtrsim$ tenths TeV is composed by only negative helicity particles. Note that in this case the cut-off of the electron flux due to the Vacuum Čerenkov effect will occur at $E \simeq 11 \times (\eta_-)^{-1/3}$ TeV $\simeq 240$ TeV, hence there is a broad region dominated by just one helicity type.

$\Delta\eta \ll \eta$

One might wonder if one might get a different result by considering LV parameters which are very similar i.e. $\Delta\eta \ll \eta$. Let us suppose for example that $\eta_+ = 10^{-4}$ and $\eta_- = 9.9 \times 10^{-5}$, so that $\Delta\eta \simeq 10^{-6} \ll \eta$. The time scales are compared in fig. 2.4.

We see that also in this case the helicity decay will become faster than the spin flipping well before reaching the Vacuum Čerenkov limit. Hence we expect again that all the positive helicity electrons above a certain energy (around 200 TeV) will be converted into negative helicity electrons until they reach the threshold for the VC emission to be effective.

Is there a regime in which at least one of the VC energy thresholds is below the effective threshold (i.e. where it becomes faster than the spin flipping) for the HD? In fact, if this case occurs we have that above the energy threshold $11 \cdot \eta_+^{-1/3}$ TeV apparently only the negative helicity electrons are left. These particles, still being below threshold for VC emission (because they have a

slightly lower LV coefficient), will be further accelerated. It then seems that only half of the initial population survives above the lower VC threshold.

However, in this case the effect of the spin flipping has to be taken into account. If the survivor negative helicity electrons do live long enough before reaching their VC threshold, then there will be time for many, if not all, of them to flip their spin and hence immediately be pushed below the lower (positive helicity) VC threshold. In the alternative scenario, in which the spin flipping is too slow to change sensibly the population of the negative helicity "survivor" electrons, then the latter will have time to reach their intrinsic cut-off represented by their (higher energy) VC threshold. However in this case this high energy tail of negative helicity electrons will just "sit there" a little bit below their threshold and sooner or later flip spin and then immediately drop at energies just below the lower VC threshold. So it seems that in both cases the negative helicity electron population will be sooner or later reconverted to positive helicity one and then pushed back below the lowest VC threshold energy.

However the spin flipping also affects the positive helicity electrons (both those left just below their VC energy threshold and those coming from the recycling of the negative helicity ones above it). So, after enough time, their helicity will be reversed by spin flip and they will become negative helicity electrons. Thus, they are able to be accelerated further above the lower VC threshold. After a while, they can possibly flip again the helicity, becoming positive helicity electrons, and then, being above threshold, emit VC radiation. Note: we are assuming that the VC emission process is much faster than helicity decay and any other process in the game (as it should be expected given that we are in a regime in which $\eta \gg \Delta\eta$).

So in the end this case looks, in some sense, like a loop chain in which all particles, no matter what their helicity is, spend some time in the energy range between the lower and the higher VC thresholds. Hence, in this case we have that all particles can fill, for some time, all the allowed energy range.

Numerical example for $\eta \gg \Delta\eta$ We put here a numerical example of the above situation. This shows that, in order to push the effective threshold of the helicity decay above the lowest Cherenkov threshold, one needs $\Delta\eta$ so small that any difference between the two populations is practically erased.

Let us suppose $\eta_+ \simeq 10^{-4}$. The VC threshold for the positive helicity electrons is at $E \simeq 237$ TeV. Requiring that the time scale for the HD is longer than the spin flipping one at energies above 237 TeV implies that $\Delta\eta \lesssim 4 \times 10^{-7}$. However this also implies that the negative helicity electrons will experience VC emission practically at the same energy of 237 TeV! In fact,

one can show that the difference between the VC threshold for positive and negative helicity electrons is just 300 GeV. The time required to accelerate particles by 300 GeV is around[4] 10^{-3} yr, which is higher than the spin flipping time. Thus, the negative helicity electrons have in this case, on average, enough time to reverse their polarization and decay by VC emission until they reach energies just below the lower VC threshold. The Čerenkov radiation, emitted in soft regime, should be hardly detectable.

Final remarks

In presence of LV effects it is not possible to average the electron and positron polarisations above an energy that depends on the actual value of the LV parameters. For parameters in the range of our interest, this energy can be estimated as being above few $\times 10$ TeV. Once the HD becomes faster than the spin flipping its effect consist in converting all the population with the highest η in that with the lowest one. Therefore, once the HD process is effective, all other processes involving the spin are frozen-out and it is in the end the VC emission that produces a sharp cut-off in the particles' energy distribution. Hence, above few $\times 10$ TeV we do get a single helicity population which at some energy is bounded by its VC threshold energy. Noticeably in this scenario the effect of the HD could perhaps be seen if we could reliably measure the polarisation of the γ-rays from the Crab Nebula. Perhaps this "helicity selection" might be used to pose a constraints on $\Delta\eta/\eta$.

The case in which the HD becomes effective after one population has undergone VC emission would instead correspond to a case in which a sort of recycling mechanism allows all the electrons to reach the higher of the VC thresholds. However this case requires so tiny difference between the LV coefficients that, as matter of fact, the region between the lower and the higher VC threshold could not be resolved. It is however true that in this case both positive and negative helicity electrons could be found up to the Čerenkov cut-off.

2.3.4 More on Helicity Decay

Since from the above analysis HD seems to be very important in a LV picture of the Crab Nebula, one may wonder whether direct observable conse-

[4]The typical acceleration time in shock acceleration scenarios is in fact $t_{acc} = \alpha\, r_L\, c/v^2$, where r_L is the Larmor radius, v the shock velocity (around 1000 km/s in the Crab) and α an order 1 parameter. Putting numbers, it can be shown that $t_{acc} \simeq \alpha \times 0.1$ yr $(E/10$ TeV), and recalling the definition of $t_{acc} = E/\dot{E}$ we find $\dot{E} \simeq 200/\alpha$ TeV/yr. Then, the result follows.

quences of the effectiveness of this process can be found. Indeed, HD implies the emission of a soft photon, whose energy should be of the order of the energy saved in "decelerating" the electron by simply lowering its effective mass (recall that HD acts in the sense of reducing the value of the LV parameter η competing to the particle, which, in the model of Myers & Pospelov, can be accomplished by simply changing its helicity). The soft photons produced by HD could be in principle detected.

In order to understand what is the typical energy of the photon emitted during the HD, we sketch here an estimate. An incoming electron with 4-momentum p^μ and LV parameter η_1 decays into another electron with 4-momentum q^μ and LV coefficient η_2 plus a photon of 4-momentum k^μ, whose angle with respect to the direction of motion of the primary electron is θ. Since $\xi < 10^{-7}$ we set $\xi = 0$.

Therefore, the dispersion relations for the particles involved are

$$E_p^2 = m^2 + p^2 + \eta_1 \frac{p^3}{M} \ , \quad E_q^2 = m^2 + q^2 + \eta_2 \frac{q^3}{M} \ , \quad \omega^2 = k^2 \ . \tag{2.35}$$

The conservation of energy-momentum $p^\mu = q^\mu + k^\mu$ implies, when the ultra relativistic approximation is made for $E_q/q \approx 1 + m^2/(2q^2) + \eta_2\, q/(2M)$, that

$$\eta_1 \frac{p}{M} = \tag{2.36}$$
$$\eta_2 \frac{p}{M} \alpha(z,\theta)^3 + 2z \left(\alpha(z,\theta) + \frac{m^2}{2p^2 \alpha(z,\theta)} + \eta_2 \frac{p}{2\,M} \alpha(z,\theta)^2 - \cos\theta + z \right)$$

where $z = \omega/p$ and $\alpha(z,\theta) = \sqrt{1 - 2z\cos\theta + z^2}$. If $z \ll 1$ (we will see that this assumption is justified *a posteriori*),

$$\Delta\eta \frac{p}{M} \approx z \left(\frac{m^2}{p^2} + 2(1 - \cos\theta) - 3\eta_2 \frac{p}{M} \cos\theta \right) \ , \tag{2.37}$$

where $\Delta\eta \equiv \eta_1 - \eta_2$ and whose solution is

$$z(\theta, p) = \frac{\Delta\eta \ p^3/M}{m^2 + 2p^2(1 - \cos\theta) - 3\eta_2 \, p^3/M \cos\theta} \, . \tag{2.38}$$

If far from the VC threshold (1.74) one can safely neglect the last term in the denominator of (2.38), finding

$$z(\theta, p) = \frac{\Delta\eta \ p^3/M}{m^2 + 2p^2(1 - \cos\theta)} \, . \tag{2.39}$$

From an experimental point of view, the angle θ is unobservable. Hence, (2.39) has to be averaged over the angular distribution of the emitted photons. According to [58], we assume that, at lowest order, the matrix element governing this process is angle independent. Therefore, the mean photon energy is ($x \equiv \cos\theta$ and redefine $z(\theta, p) \to z(\cos\theta, p)$)

$$\bar{z}(p) = \frac{\int_{-1}^{1} \mathrm{d}x \; z(x,p)}{\int_{-1}^{1} \mathrm{d}x} = \Delta\eta \frac{p}{2\ M} \ln\left(2\frac{p}{m}\right) \ . \tag{2.40}$$

Assuming a typical value $\Delta\eta = 10^{-6}$, from (2.43) $p_{\mathrm{HD}}^{(\mathrm{eff})} = 160$ TeV. Equation (2.40) then implies that $\bar{z}\left(p_{\mathrm{HD}}^{(\mathrm{eff})}\right) = 1.7 \times 10^{-19}$, *i.e.* $\bar{\omega} \simeq 2.8 \times 10^{-5}$ eV, well within the radio band.

2.4 The Crab model revisited

Because we consider a LV version of electrodynamics, we must check whether this introduces modifications into the model of the CN and, if so, what effects it produces.

The observed spectrum of the CN is the composite result of several processes, as sketched in sec. 2.2. The way LV affects the physics of the CN is basically twofold. On the one hand, classical processes, such as acceleration, synchrotron emission and IC scattering, can be modified. On the other hand, new processes (such as VC or HD) come into play. On general grounds, we expect both the modifications and the new processes to be important at energies above $(m_e^2 M/\eta)^{1/3} \approx 10\ \mathrm{TeV}\eta^{-1/3}$, which is the typical scale of threshold for almost all LV features. We now investigate how the processes at work in the CN would appear in a LV framework.

2.4.1 Acceleration

Several mechanisms have been suggested for the formation of the spectrum of energetic leptons in the CN. The spectrum is unusual in the sense that most of the leptons are concentrated at low energy, $E \sim 100\,\mathrm{MeV}$, whereas the energy density contained in each decade of particle energy peaks at about 1 TeV. Above this energy, the spectrum appears to fall off roughly as $E^{-2.2}$. Most of the uncertainty concerning the acceleration mechanism refers to the low energy part of this distribution, $E \leq 1\,\mathrm{TeV}$. The power-law spectrum of high energy particles is usually interpreted in terms of the first order Fermi mechanism operating at the ultra-relativistic termination

shock front of the pulsar wind, since, in the simplest kinematic picture, this mechanism predicts a power law index of just the right value [116].

In this picture, electrons and positrons acquire energy by crossing and recrossing a shock front that propagates in a magnetised medium. In between crossings, they are continually deflected by the random magnetic field present in the medium, and may, therefore, reverse their direction of travel. The magnetic deflections do not change the particle energy as seen from a reference frame travelling with the plasma. However, when a particle crosses a shock, it is exposed to magnetic fluctuations embedded in an approaching plasma flow. These increase the particle energy whenever it is deflected back to the shock front.

The cycle of shock crossing and recrossing can be accomplished many times, and each time the particle has a finite probability of escaping from the vicinity of the shock front into the downstream medium, never to return. The competition between energy gain and escape leads to a scale-free power-law spectrum of accelerated particles. The power-law index depends on the shock compression ratio, and, in the relativistic case, on the angular dependence of the deflection process. In the ultra-relativistic case, a variety of scattering laws have been tested by different methods [141, 142], all of which appear to give an index in the range -2 to -2.3, close to the asymptotic value of -2.23, which can be derived semi-analytically for isotropic diffusion in angle [143].

The Fermi mechanism in the LV scenario.

From the LV point of view, the important issue about the Fermi mechanism is that its scale-free nature rests purely on the angular distribution of the particles at the shock front. This determines both the escape probability $P_{\rm esc}$ of a particle that crosses from upstream to downstream, as well as the average change in particle Lorentz factor $\langle \Delta\gamma \rangle$. The latter is found by convolving the Lorentz boost into the upstream plasma frame with the return boost, averaged in each case over the angular distribution function. Both $P_{\rm esc}$ and $\langle \Delta\gamma \rangle$ are independent of the length scale associated with the scattering process – an increase in the scattering mean free path simply produces a longer time interval between crossings, and a slower fall-off of the particle distribution with distance from the shock, but changes neither the angular distribution at the shock front, nor the escape probability.

In the LV picture, both the particle energy and Lorentz factor enter into the computation of the trajectory. But, given that the angular distribution is not a function of either of these, the spectrum produced by the first order Fermi mechanism depends on the Lorentz factor alone, through the quantity

$\langle \Delta\gamma \rangle$. On the other hand, the maximum energy E_c to which the process can accelerate particles may depend on loss processes as well as on the time interval between shock crossings, which controls the acceleration rate. In the standard LI case, E_c is essentially determined either by setting the particle gyro radius to equal the size of the system, or the acceleration rate (which scales with the gyro frequency) to equal the loss rate. In each case, a condition on the particle energy rather than the particle Lorentz factor results. In the CN, if we phenomenologically model the cut-off at E_c as an exponential, we expect a particle spectrum in the high energy region, $E > 1\,\mathrm{TeV}$, of the form

$$n(E) \quad \propto \quad \gamma(E)^{-p} \mathrm{e}^{-E/E_c} \tag{2.41}$$

with $p \approx 2.4$ and $E_c \approx 2.5 \times 10^{15}\,\mathrm{eV}$.[5]

Then, we can safely deal with the electron/positron distributions inferred by [131, 138], paying attention to replace the energy with the Lorentz boost factor in the expressions given by [138]. Of course, as we mentioned, the cut-off of the spectrum results in a condition on the particle energy rather than its boost.

The role of Vacuum Čerenkov emission.

However, in the LV theory there are additional mechanisms that can influence E_c because the modified dispersion relations that we consider allow processes that are otherwise forbidden. In particular, the VC emission, due to its extreme rate above threshold, can produce a sharp cut-off in the acceleration spectrum (let us remind that above threshold $\tau_{VC} \sim 10^{-9}$ s, to be compared with the acceleration time scale $\tau_{acc} > 10^3$ s).[6]

One might expect that the VC radiation emitted by particles above threshold should produce some modification in the spectrum. However, since the photon LV parameter ξ has been independently constrained to be very small, the VC process occurs in the soft regime [58]. In this regime the emitted photon carries away a small fraction of the electron energy, being at most

[5] Super-exponential cut-off spectral shapes do not lead to significant differences in the output spectrum. For this reason we considered a simple exponential cut-off, which also gives the best fit to the data.

[6] An order of magnitude estimate of a lower limit to the acceleration timescale can be obtained by assuming the particle doubles its energy whenever it completes a cycle of crossing and recrossing the shock front. Since magnetic fields bend the particle trajectory to make it do this, a lower limit to the cycle time is given by the gyro period (magnetic turbulence may make the particle diffuse, enhancing the time needed to complete a cycle). The acceleration timescale is, therefore, $\tau_a > \gamma m_e/eB \approx 1.1 \times 10^3$ s $(E/1\ \mathrm{TeV})\,(B/100\ \mu\mathrm{G})^{-1}$.

in the optical/UV range. Moreover, the emitting leptons are just in the high energy tail of the spectrum, so that they are few in number, compared to the optical/UV emitting ones. Therefore, the contribution of VC to the CN spectrum in the optical/UV range should be negligible.

The role of Helicity Decay and spin precession.

A more subtle effect in the determination of the emitting particle spectrum is given by the HD process. At high energies, the electron and positron states have well-defined helicity and the LV coefficients $\eta_\pm$ are different depending on the particle helicity.

As discussed, the HD rate peaks at energies around $p_{\rm HD}$ (see (1.78)). Below $p_{\rm HD}$ the rate increases with energy and depends on $\Delta\eta$, while above $p_{\rm HD}$ it decreases independently of η [58]. The expressions (1.74) and (1.78) for $p_{\rm VC}$ and $p_{\rm HD}$, respectively, show that at most $p_{\rm HD} \gtrsim p_{\rm VC}$ for $\Delta\eta \lesssim \eta$ (otherwise $\Delta\eta \ll \eta$ and $p_{\rm HD} \gg p_{\rm VC}$). Since the VC emission acts as a hard cut-off on the accelerated particles, in our scheme the HD process will occur only in the regime $p \lesssim p_{\rm HD}$, where the (not yet maximised) rate grows with energy.

However, in order to understand whether the HD is effective, one has to compare its typical time scale $\tau_{\rm HD}$, as given in eq. (1.79), with the other relevant ones. In particular, a competitive process is the precession of the spin of a particle moving in a magnetic field. According to [140] (see also section 2.3.2 for a more thorough discussion) in the LI case (it can be checked that this is still valid in the LV case, without any modification, to within 10^{-14}) the rate of change of the spin orientation with respect to the instantaneous direction of motion of the lepton in the laboratory frame is [7]

$$\frac{{\rm d}\theta}{{\rm d}t} \equiv \omega_{\rm SR} = \frac{e}{m_e}\frac{g-2}{2}B \ , \tag{2.42}$$

where $(g-2) = \alpha/\pi$ represents the anomalous magnetic moment of the lepton and a constant magnetic field B is assumed. (Indeed it is expected that the magnetic field in the CN is constant only over some typical correlation length

[7] A comment is in order here as, in principle, there could be interference between spin precession and HD. However, assuming a static magnetic field, during spin precession the electron energy is constant while HD implies the emission of a photon, leading to non conservation of the electron energy. Therefore they cannot interfere. Moreover, if a constant timelike vector u^μ is used to "parametrise" Lorentz symmetry violation, a term like $\bar\psi\gamma_\mu u^\mu\psi$ can appear in the Lagrangian, which mimics the usual electromagnetic interaction term. However, as long as u^μ is constant, it cannot give rise to magnetic-like interactions.

after which it reverses sign. For our purposes, however, it is the rate of spin-rotation that is relevant, rather than its direction.)

The spin rotation will effectively prevent helicity decay if the spin precession rate is faster than the time needed for LV induced effect. Therefore, the HD will play a role in spite of the spin precession whenever the condition $\omega_{\rm SR}\tau_{\rm HD} \ll 1$ is met.

According to (1.79) and (2.42) this condition translates into

$$p_{\rm HD}^{(\rm eff)} \gtrsim 930 \text{ GeV} \left(\frac{B}{0.3 \text{ mG}}\right)^{1/8} |\Delta\eta|^{-3/8} . \tag{2.43}$$

Electrons and positrons with $E > p_{\rm HD}^{(\rm eff)}$, can therefore be found only in the helicity state that corresponds to the lowest value of $\eta_\pm$. Correspondingly, the population of greater η will be sharply cut off above $p_{\rm HD}^{(\rm eff)}$ while the other will increase.

Finally, the HD process implies the emission of a suitably polarised photon. However, this has no consequences for the observed spectrum, since the mean photon energy (for $\Delta\eta \sim 10^{-6}$) is well within the radio band, where the synchrotron spectrum, emitted by an overwhelmingly large number of low energy electrons, is dominant. We refer the reader to the previous section 2.3.4 for a detailed discussion.

2.4.2 More on synchrotron radiation

The main modifications of the synchrotron emission process in presence of LV have already been presented in Section 1.5.4. Let us however consider them in more detail.

There is a fundamental difference between particles with positive or negative LV coefficient η. If η is negative the group velocity of the electrons is strictly lower than the (low energy) speed of light. This implies that, at sufficiently high energy, $\gamma(E)_- < E/m_e$ for all E. As a consequence, the critical frequency $\omega_c^-(\gamma, E)$ is always lower than the LI one, and so the exponential cut-off of the LV synchrotron spectrum will be at lower frequencies than in the LI case, as illustrated in fig. 2.5.

On the other hand, particles with a positive LV coefficient can be superluminal and, therefore, $\gamma(E)$ increases more rapidly than E/m_e, reaching infinity at a finite energy, which corresponds to the threshold for soft VC emission.[8] Therefore, the critical frequency is also larger than that found in

[8]Of course such an infinity will be automatically "regulated" by the fact that, as the electron approaches the threshold, its energy loss rate will at some point exceed its rate

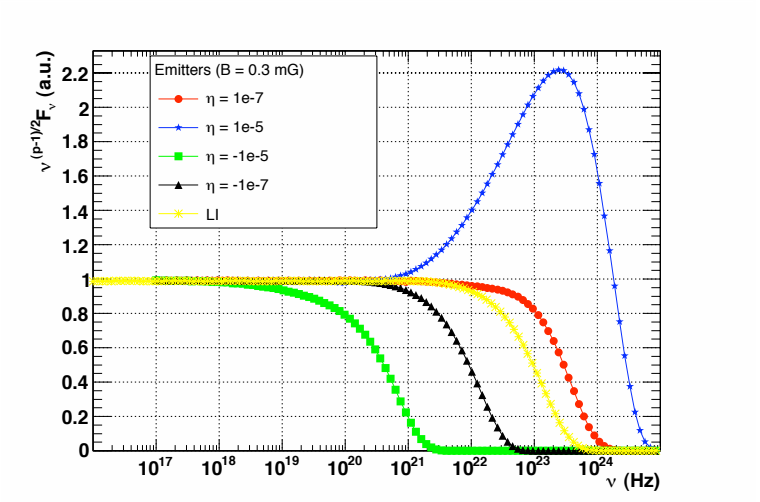

Figure 2.5: Modifications occurring due to LV in the synchrotron spectrum produced by a power-law distribution of leptons. The spectrum is normalised to a LI one without cut-off.

the LI case, and the spectrum will show a characteristic hump due to the enhanced ω_c (see fig. 2.5).

The final remark concerns the characteristic synchrotron loss timescale, defined as $\tau_{cool} = E/(dE/dt)$. The classical result for an electron spiralling in a given magnetic field is

$$\frac{dE}{dt} = -\frac{2\,e^4}{3\,m_e^2}\gamma^2\,B^2 v^2 \sin^2\phi\,, \tag{2.44}$$

where ϕ is the pitch angle and $\gamma = E/m_e$. As the electron loses most of its energy at frequencies around the critical one, a comparable expression for the LV case can be written as

$$\frac{dE}{dt} \sim \frac{\omega_c}{\Delta\, t} \sim \frac{\gamma^4}{E^2}\,, \tag{2.45}$$

where we have used eq. (1.75) and the fact that the typical emission time at ultra-relativistic energy is $\Delta t = 2\pi R(E)/\gamma$, with $R(E) = E/eB$. The numerical factor in front of expression (21) can be fixed by fitting the energy loss rate at low energies, where $\gamma = E/m_e$.

One might wonder if this modified rate could alter the effectiveness of the acceleration mechanism in producing the highest energy leptons. In fact,

of energy gain, thus preventing further acceleration.

while for $\eta < 0$ this is not an issue, for $\eta > 0$ one expects the rate to grow much faster than the LI one for sufficiently high energies. Nonetheless it is easy to see that appreciable deviations from the LI rate (2.44) occur at energies $E \gtrsim 8\ \mathrm{TeV}/\eta^{1/3}$, i.e. in the proximity of the VC threshold. Therefore the effective cut-off on the spectrum of the injected particles is not significantly lowered by the synchrotron cooling in the LV case.

2.4.3 IC radiation

The IC process is not strongly affected by LV. At the kinematic level all LV terms intervene at a level of $< 10^{-11}$ at $E \lesssim 1$ PeV, whereas the cross section should be corrected by adding factors proportional to p^3/M_{Pl} and, therefore, the LV contribution is again suppressed at the same level. Since the IC and synchrotron emission mechanisms can be thought as being due to the scattering of a lepton off a real or a virtual photon respectively [144], one may wonder why the synchrotron is much affected by LV while the IC is not.

The main difference between the two processes is that IC scattering involves the interaction between a real lepton and a real photon, whereas the synchrotron process involves a virtual photon of the magnetic field in which the lepton is spiralling. In the former case, the interaction is effective no matter what the photon energy is. In the latter case, however, the reaction is more subtle. An electron spiralling in a static magnetic field can exchange momentum but not energy with the field, since it is static. Moreover, the exchanged momentum is such that the electron accelerates and describes a spiral trajectory. Therefore, a synchrotron emitting electron does not interact with all possible virtual photons, but only with those that provide it with the required momentum transfer. In a sense, this is a sort of a resonant process, where the resonance is dependent not only on the electron energy, but also on its velocity.

Therefore, the admixture of dynamical and kinematic variables in the synchrotron emission process makes it much more sensitive to LV compared IC scattering, where only energetic considerations matter: this is another example of the fact that, in LV reasoning, velocity (or boost in γ) and energy are not quite the same concept.

2.5 Results

In order to constrain our test theory by exploiting the information contained in broad band observations of the CN, we adopt the following strategy.

First of all we construct a numerical algorithm[9] that calculates in full generality, for any set of LV parameters, the synchrotron emission from a distribution of leptons, according to the model of the CN presented in sec. 2.2 and taking into account all the processes discussed in sec. 2.4. Of course, the LI model is recovered by simply setting $(\eta_+, \eta_-) = (0, 0)$. Then, we fix most of the model parameters (magnetic field strength and particle energy density) so as to match observations from radio to soft X-rays, i.e. in a regime where the LV terms here considered are not expected to produce significant effects.

This procedure leads to model parameters (and a LI spectrum) which are in agreement with those providing the best fit to the data in [138]. We report here the most relevant parameters, namely $p = 2.4$ as the spectral index and $E_c = 2.5$ PeV as the high energy cut-off of the freshly accelerated wind leptons.[10] The same parameters are known to be able to reproduce the IC part of the CN spectrum in the LI case [138]. Given that the IC reaction is basically unaffected by LV, agreement with the high energy data will hold also for non zero LV coefficients. Of course this also implies that, at least with current data accuracy, the IC cannot be used to improve on the constraints obtainable from the synchrotron part of the spectrum.

2.5.1 Spectra

The general features of the spectra produced by our numerical computation are illustrated in fig. 2.6 for $\eta_+ \cdot \eta_- > 0$ (left panel) and $\eta_+ \cdot \eta_- < 0$ (right panel) with η_+ assumed to be positive for definiteness. It is clear that only these two cases are really different: in fact, the one with both $\eta_\pm$ negative is the same as the $(\eta_+ \cdot \eta_- > 0,\ \eta_+ > 0)$ case, while that with the signs scrambled is equivalent to the case $(\eta_+ \cdot \eta_- < 0,\ \eta_+ > 0)$. This is simply due to the fact that positron coefficients are related to electron coefficients through $\eta^{af}_\pm = -\eta^f_\mp$ (see section 1.5.4).

One can easily see that in the LI case the data are reasonably fitted (as in [138]) and that the LV effects indeed appear at the expected energy scales. Hence the procedure of fixing the free (LI) parameters from the low energy observations is well defined.

The main difference between the left and right panels of fig. 2.6 consists in the fact that in the first case $(\eta_+ \cdot \eta_- > 0)$ only a population with positive η survives to the HD, while in the opposite case $(\eta_+ \cdot \eta_- < 0)$ only a

[9] The code is written in C++ and takes great advantage of many tools provided by the ROOT package, see http://root.cern.ch

[10] Note however, that in the LV case the cut-off energy of the injected particles can be lowered by the VC process.

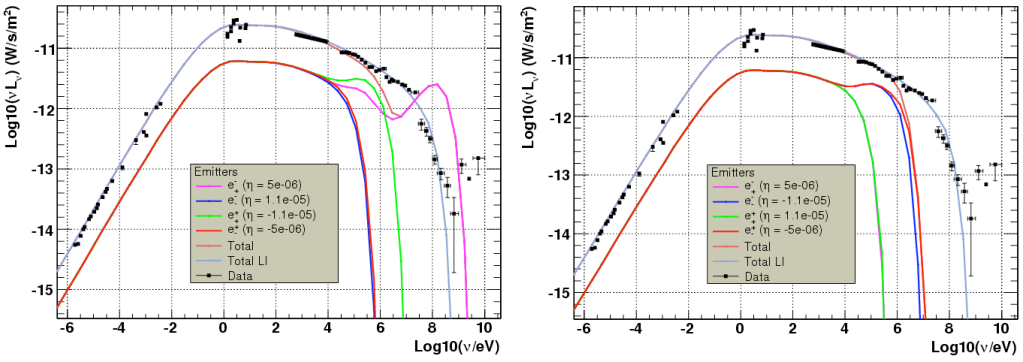

Figure 2.6: Comparison between observational data, the LI model and a LV one with $\eta_+ \cdot \eta_- > 0$ (left) and $\eta_+ \cdot \eta_- < 0$ (right). The values of the LV coefficients are reported in the inserted panels and are chosen in order to show the salient features of the LV modified spectra. The leptons are injected according to the best fit values $p = 2.4$, $E_c = 2.5$ PeV. The individual contribution of each lepton population is shown.

population with negative η does. This has consequences for the total synchrotron spectrum. In particular, the right panel of fig. 2.6 shows a sharp cut-off since the high energy emission in this case is produced by a population with negative η which, as discussed, has an upper bounded ω_c. On the other hand, for $\eta_+ \cdot \eta_- > 0$ (left panel of fig. 2.6) a pronounced feature appears with a dip followed by a hump. The dip is due to the combination of two effects: the population is decaying with increasing energy, while the critical frequency ω_c is growing faster than "usual" with energy. Hence, at some point the spectrum has a minimum and then starts growing. Since, however, the population of the highest energy leptons (responsible for the γ-ray part of the synchrotron spectrum) is decaying very rapidly, the flux does, in the end, also decay. This effect is responsible for the hump.

Finally, one might wonder if in this last case it is possible to reproduce the high energy synchrotron emission even with $E_c \lesssim 1$ PeV. However, this would require so high values of the LV parameters (of order $10^{-4} \div 10^{-3}$) that the resulting spectrum would show a feature in hard-X/soft γ-rays incompatible with the observations.

2.5.2 Constraints

In order to evaluate the constraints in an objective and quantitative manner, we present a χ^2 analysis of the agreement between models and data. Figure 2.7 and fig. 2.8 show the contour levels of the reduced χ^2 for the

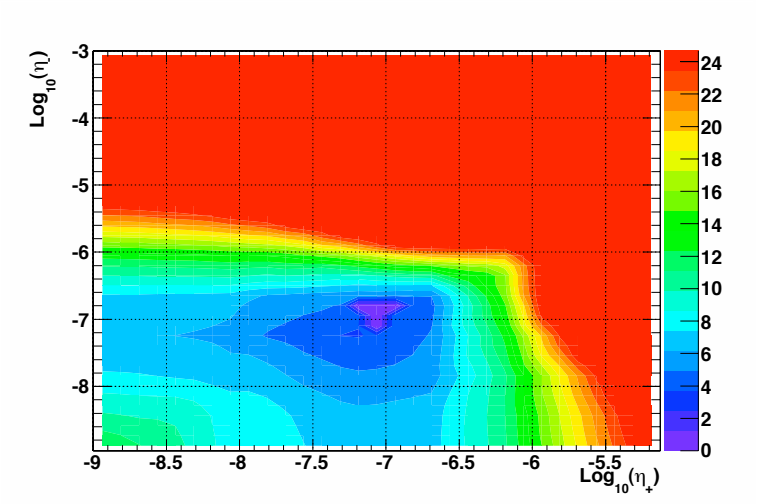

Figure 2.7: Contour plot of the reduced χ^2 versus η_+ and η_-, in the case $\eta_+ \cdot \eta_- > 0$.

two cases $\eta_+ \cdot \eta_- > 0$ and $\eta_+ \cdot \eta_- < 0$, respectively. Constraints at 90%, 95% and 99% Confidence Level (CL) correspond, respectively, to $\chi^2 > 8$, $\chi^2 > 10$, $\chi^2 > 13.5$. The minimum value of χ^2 we obtain is ~ 3.6 (see [55] for more complete information). From fig. 2.7 and fig. 2.8 we conclude that the LV parameters for the leptons are both constrained, at 95% CL, to be $|\eta_\pm| < 10^{-5}$.

Our statistical analysis shows that there are values of the pair (η_+, η_-) that provide a better fit of the CN data than the LI model. In particular, for $(\eta_+, \eta_-) \sim (5.2 \times 10^{-8}, 5.7 \times 10^{-8})$ it is possible to reproduce (see fig. 2.9) some features in the MeV range that are not found in the standard model. Of course, while it is possible to explain these features by introducing new components into the LI model, at the moment it seems that such alternatives would imply some sort of departure from the standard model of the CN emission (for example, [138] postulate the existence of an additional population of emitting particles, with a Maxwellian distribution).

Putting aside for the moment alternative (Lorentz invariant) models, something more can be said about the above result by further investigating its statistical significance. This can be accomplished by assessing the significance of the difference between the χ^2 values of the best fit (LV) model and the standard LI one given that the extra two degrees of freedom characterising the LV case obviously allow for better fits. (Unfortunately, it is not possible to assess the probability to find the best fit value of the LV parameter η given our ignorance of its theoretical expected magnitude or prior

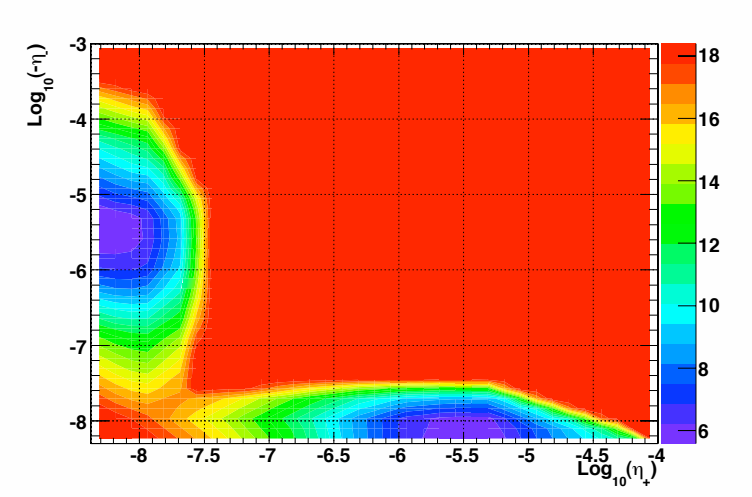

Figure 2.8: Contour plot of the reduced χ^2 versus η_+ and η_-, in the case $\eta_+ \cdot \eta_- < 0$.

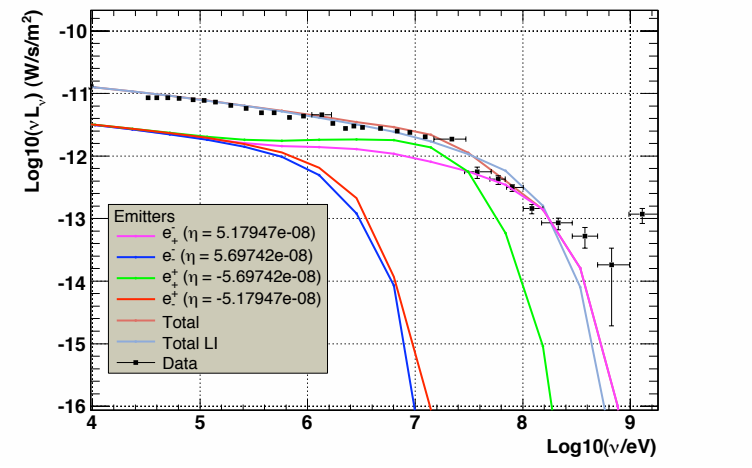

Figure 2.9: Best fit LV spectrum compared to the LI one.

distribution.) This can be accomplished using the so called F-test [145]. We find a value of 1.11 for the F-variable, from which we conclude that the LI model and the best fit LV model are statistically indistinguishable at 95% CL. The critical value of the F-variable, for which the models would indeed be distinguishable, is 1.67, and the significant improvements in the $40 - 250$ MeV data expected from the up-coming GLAST experiment may enable this value to be reached.

2.6 Remarks

We have studied how relaxing the assumption of exact Lorentz invariance (within the framework set up in [56]) influences the electromagnetic output of astrophysical source models. In general, the most important effects are those related to modifications of the particle dispersion relations, which affect their propagation and their interactions.

Starting from the most accurate theoretical model of the CN [131, 138], and taking into account the LV contributions of *all* the electron/positron populations, we reproduce the observed synchrotron spectrum. To do this, one must reconsider LI "biases". Concerning the acceleration process, we give arguments according to which the particle Lorentz boost, rather than energy, enters in the acceleration spectrum. Moreover, we study the effect of VC emission and HD on the emitting particle distribution.

The synchrotron, as well as the IC, processes are discussed and the spectrum emitted by an arbitrary distribution of leptons, taking into account all the subtleties occurring in LV reasoning, is calculated numerically. In this way *both* $\eta_{\pm}$ can be constrained by comparing the simulated spectra to the observational data. The χ^2 statistics sets 90% and 95% CL exclusion limits at $|\eta_{\pm}| < 10^{-6}$ and $|\eta_{\pm}| < 10^{-5}$, respectively. The resulting state-of-the-art constraints are shown in fig. 2.10.

The GLAST observatory is likely to achieve a significant step forward. An order of magnitude estimate of the improvement can be obtained by considering its sensitivity, which is ~ 30 times better than that of EGRET in the relevant energy range. Assuming that GLAST will observe the CN at least as long as EGRET did (a very conservative assumption), measurement errors in the 10 MeV-500 MeV band will be statistically reduced by roughly a factor of ~ 5. A constraint of order 10^{-6} at 99% CL (10^{-7} at 95% CL) would thus be within reach.

As a final remark, we would like to stress that the very tight constraints achieved here on our test theory [56, 59] show the remarkable potential of this approach and suggest that similar studies should be undertaken for other

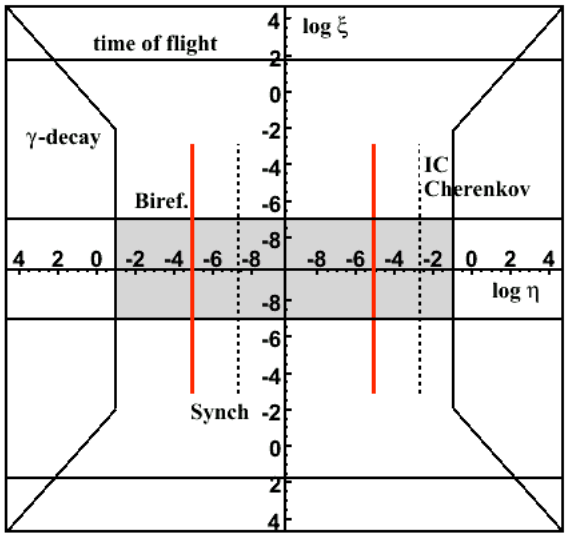

Figure 2.10: Updated overview of the constraints. The new allowed region of the parameter space is now the grey region bounded vertically by the birefringence constraint $\xi < O(10^{-7})$ and horizontally by the red lines representing the synchrotron constraint, $|\eta_{\pm}| < O(10^{-5})$, discussed here.

plausible theoretical frameworks. For example, if one is not willing to accept CPT violation in quantum gravity, then the QED dimension 5 LV operators considered here would be forbidden and dimension 6 operators (corresponding to $O(E^2/M_{\rm Pl}^2)$ suppressed terms in the dispersion relations) should be considered. In this direction, on the one hand a theoretical development of the theory is much needed as we still lack a formalisation of the QED extension in this case (including the consideration of possible effects on lower dimensional operators which could play a crucial role in casting constraints). On the other hand, more accurate, higher energy and possible new observations will be needed in order to overcome the larger suppression of such higher order LV terms.

2.7 Crab Nebula polarisation further limits LIV

Observations of the CN allow further improvements. The main result presented in this section is to further strengthen the limits on LV of order $E/M_{\rm Pl}$ by more than three orders of magnitude for photons, by looking at vacuum birefringence effects. We use for the first time the very recent observations [146] of polarised hard X-rays from the Crab system. While the most robust against astrophysical systematic uncertainties, but less tight constraint is obtained following the arguments by [100, 59], we show that this can be further improved by another two orders of magnitude when considering the astrophysical model of the Crab nebula and pulsar.

We exploit here the procedures described in section 1.5.2 in the Introduction.

2.7.1 Constraints

Recently the analysis of data from the CN by the INTEGRAL mission [147] has provided [146] (see also [148]) the measurement of $(40 \pm 3)\%$ linear polarisation in the 100 keV $-$ 1 MeV band. While the polarisation has been estimated by considering all photons within the SPI instrument energy band, the convolution of the sensitivity of the instrument to polarisation with the number counts as a function of energy, $P(k)$, is maximised (and happens to be approximately constant) within a narrower energy band, between 150 and 300 keV, and fall steeply outside this range [149]. For this reason most of the polarised photon are concentrated in this range which we shall, conservatively, adopt in order to cast our constraint.

Decrease in polarisation degree

Given that $d_{\rm Crab} = 1.9$ kpc, $k_2 = 300$ keV and $k_1 = 150$ keV, by requiring $\Delta\theta < \pi/2$, eq.(1.68) gives

$$|\xi| \lesssim 2 \times 10^{-9} \, . \tag{2.46}$$

A more accurate limit follows from eq. (1.69).

In the case of the CN there is a robust understanding that photons in the range of interest are produced via the synchrotron process, for which the maximum degree of intrinsic linear polarisation is about 70% (see e.g. [150]). Figure 2.11 illustrates the dependence of Π on ξ for the distance of the CN and for $\Pi(0) = 70\%$. The requirement $\Pi(\xi) > 16\%$ (taking account of a 3σ

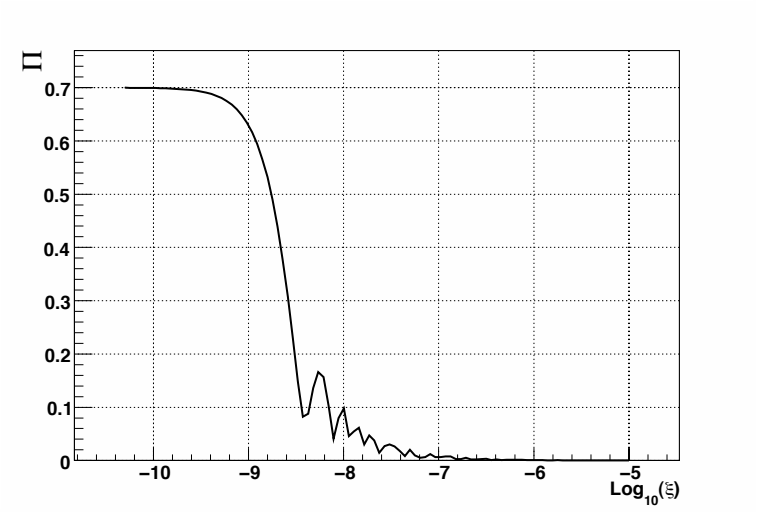

Figure 2.11: Constraint for the polarisation degree. Dependence of Π on ξ for the distance of the CN in the 150–300 keV range, for a constant $\mathcal{P}(k)$.

offset from the best fit value 46%) leads to the constraint (at 99% CL)

$$|\xi| \lesssim 6 \times 10^{-9} \, . \tag{2.47}$$

It is interesting to notice that X-ray polarisation measurements of the CN already available in 1978 [151], set a constraint $|\xi| \lesssim 5.4 \times 10^{-6}$, only one order of magnitude less stringent than that reported in [77].

Rotation of polarisation angle

Constraint (2.47) can be tightened by exploiting the current astrophysical understanding of the source. The CN is a cloud of relativistic particles and fields powered by a rapidly rotating, strongly magnetised neutron star. Both the *Hubble Space Telescope* and the *Chandra* X-ray satellite have imaged the system, revealing a jet and torus that clearly identify the neutron star rotation axis [152]. The projection of this axis on the sky lies at a position angle of $124.0^\circ \pm 0.1^\circ$ (measured from North in anti-clockwise). The neutron star itself emits pulsed radiation at its rotation frequency of 30 Hz. In the optical band these pulses are superimposed on a fainter steady component with a linear polarisation degree of 30% and direction precisely aligned with that of the rotation axis [153]. The direction of polarisation measured by INTEGRAL-SPI in the γ-rays is $\theta_{\rm obs} = 123^\circ \pm 11^\circ$ (1σ error) from the North, thus also closely aligned with the jet direction and remarkably consistent with

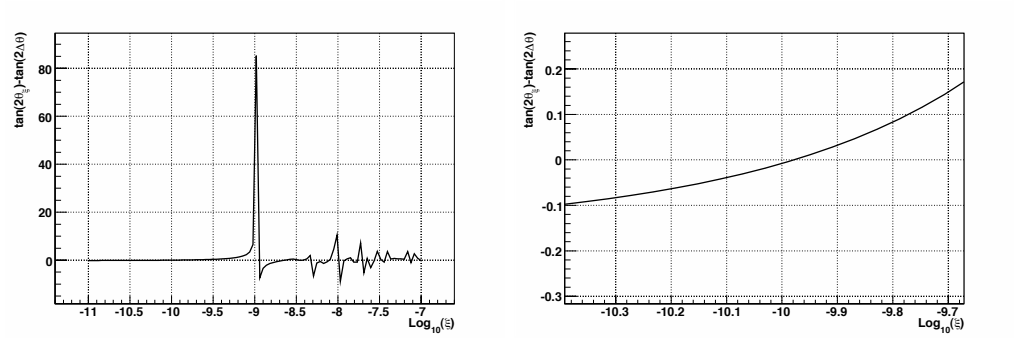

Figure 2.12: Constraint for the polarisation rotation case. Upper panel: dependence of $\tan(2\theta_{\rm f})$ on ξ, the spikes correspond to rotations by $\pi/4$. The lower panel is a zoom in on the interesting range of values. The constraint is cast according to eq.(1.70).

the optical observations.

This compelling (theoretical and observational) evidence allows us to use eq. (1.71). Conservatively assuming $\theta_{\rm i} - \theta_{\rm obs} = 33^\circ$ (i.e. 3σ from $\theta_{\rm i}$, 99% CL), this translates into the limit

$$|\xi| \lesssim 9 \times 10^{-10} \,, \tag{2.48}$$

and $|\xi| \lesssim 6 \times 10^{-10}$ for a 2σ deviation (95% CL). Figure 2.12 shows $\tan(2\theta_{\rm f})$ as function of ξ. The left–hand panel reports the global dependence (the spikes correspond to rotations by $\pi/4$), while the right–hand panel focuses on the interesting range of values[11].

2.7.2 Discussion

The constraints presented in (2.47) and (2.48) are remarkably strong. Although based on a cumulative effect, they are achieved using a local (Galactic) object. The reason lies, on the one hand, in the quadratic dependence of θ on the photon energy, in contrast with the linear gain given by distance (see e.g. eq. (1.66)). On the other hand, the robust theoretical understanding of the CN has enabled us to strengthen the constraints significantly.

Further improvements on LV constraints via birefringence are expected thanks to the forthcoming high-energy polarimeters, such as XEUS [2], PoGo-Lite [154], Polar-X [155] and Gamma Ray Imager [156] which will provide

[11]Note that the constraint (2.47) rules out the possibility that the polarisation angle is close to the expected one after rotating by some multiple of π (the polarisation angle is defined on the interval $[0, \pi]$).

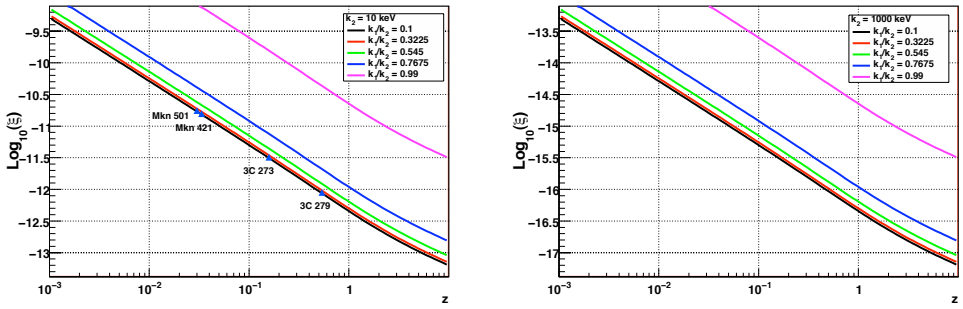

Figure 2.13: Expected constraints from medium X- and soft γ-ray polarimetry of extra-galactic sources. High energy scale $k_2 = 10$ keV (upper panel) and 1 MeV (lower panel), with κ from 0.1 to 0.99. Points in the upper panel refer to the characteristics of a new generation X-ray polarimeter [2] assuming that polarisation is detected from the mentioned objects. The constraints are derived as in case of eq.(1.68) for a concordance cosmology ($\Omega_m = 0.28$, $\Omega_\Lambda = 0.72$ and $H_0 = 73\ \mathrm{km\,s^{-1}Mpc^{-1}}$).

an unprecedented sensitivity, sufficient to detect polarised light at a few % levels also in extra-galactic sources. The LV limits will be optimised by balancing between source distance and observational energy range depending on the detector sensitivity. This is illustrated in fig. 2.13, where the strength of the possible constraints (cast with the first, most general method described above) is plotted versus the distance of sources (in red-shift z) and for different energy bands (medium X- and γ-rays). Remarkably, constraints of order $|\xi| < O(10^{-16})$ could be placed if some polarised distant sources ($z \sim 1$) will be observed by such instruments at 1 MeV.

Chapter 3

A bottom-up introduction to Cosmic Ray physics

"Cosmic Ray puzzle due to be solved"

New York Times,
December 29th, 1932

Cosmic Rays (CR) are among the most puzzling astrophysical phenomena we experience on Earth. Their discovery dates back to 1912 with the pioneering observations of Victor Hess, who found that the ionisation rate in air was increasing with its height above the Earth surface, after an initial decrease (explained by the decrease of Earth radioactivity effects as the instrumentation departs from the Earth surface). This simple observation could be explained with the hypothesis that there were cosmic particles impinging on the top of the atmosphere able to produce the secondary ones detected by Hess. This triggered the beginning of studies on Cosmic Rays. Initially they were thought of as highly energetic photons, rather than charged particles, but, after the geomagnetic effect (the intensity of radiation was fading according to the Earth magnetic field) was discovered in 1927, it became clear that CRs were charged particles.

After Hess' discovery, the existence of ionising radiation was observed in cloud chambers and Pierre Auger [157] observed coincident hits over a wide area with his detectors, showing that the primary cosmic rays induce a cascade of particles, known as an extensive air shower (EAS), when they encounter the atmosphere. From the numbers of particles involved in these showers, Auger was able to estimate the energy of some showers, and show that some must be very energetic. The phenomenology of EAS was worked

out by Heitler [158] and others.

Many experiments were designed and run over the years to better understand the characteristics of these particles. Their findings were surprising indeed. The CR energy spectrum displayed an almost exact power-law shape above energies of about 1 GeV. Below this threshold, spectral modulation, fading according to solar activity, due to solar winds, was found, confirming CRs to be charged particles rather than photons. Moreover, it was understood that CRs are mostly protons, with a small amount of heavier nuclei and a fraction of electrons/positrons not larger than $\sim 1\%$.

Several mysteries are associated with Cosmic Rays: for example we do not know what are their sources, how do they propagate from sources to us, whether there is an end point of their spectrum. But also, being the most energetic particles we observe on Earth, we expect to gather from them relevant information on physics beyond the Standard Model (as an example, the highest energy points of the total proton-proton cross section have been inferred from EAS measurements [55]), and also on Quantum Gravity [159].

3.1 Spectrum of Cosmic Rays

The CR spectrum is known to span more than ten decades in energy (from < 100 MeV to $> 10^{19}$ eV) with a power-law shape of impressive regularity ($F(E) \propto E^{-p}$) as shown in fig. 3.1. The spectral slope p of the differential spectrum above few GeV has been measured as $p \simeq 2.7$ for $E \lesssim 10^{15.5}$ eV, followed by a softening (the so called "knee") to $p \simeq 3.0$ for $10^{15.5}$ eV $\lesssim E \lesssim 10^{17.5}$ eV, a further steepening to $p \simeq 3.2$ (the "second knee") up to $E \simeq 10^{18.5}$ eV and a subsequent hardening (the so called "ankle") to again $p \simeq 2.7$ at $E \gtrsim 10^{18.5}$ eV [160, 161].

While lower energy CRs are believed to be of galactic origin, CRs with energy $\gtrsim 10^{18}$ eV are thought to be extra-galactic. In fact, being charged particles, CRs are deflected by magnetic field on a curve trajectory of radius the Larmor radius

$$r_L \simeq 1 \text{ kpc} \frac{E[\text{EeV}]}{Ze\, B[\mu\text{G}]} \,. \tag{3.1}$$

Since the typical galactic dimension is few kpc, and the typical galactic magnetic field strength is of order of few μG, it follows that the Milky Way is able to confine particles up to the EeV[1].

[1]It should be noticed, however, that the thickness of the most dense region of the Galaxy (the disk) is roughly $h_d \simeq 100$ pc. The energy corresponding to $r_L \sim 100$ pc is $E \sim 10^{15}$ eV, which corresponds to that of the knee in the CR spectrum.

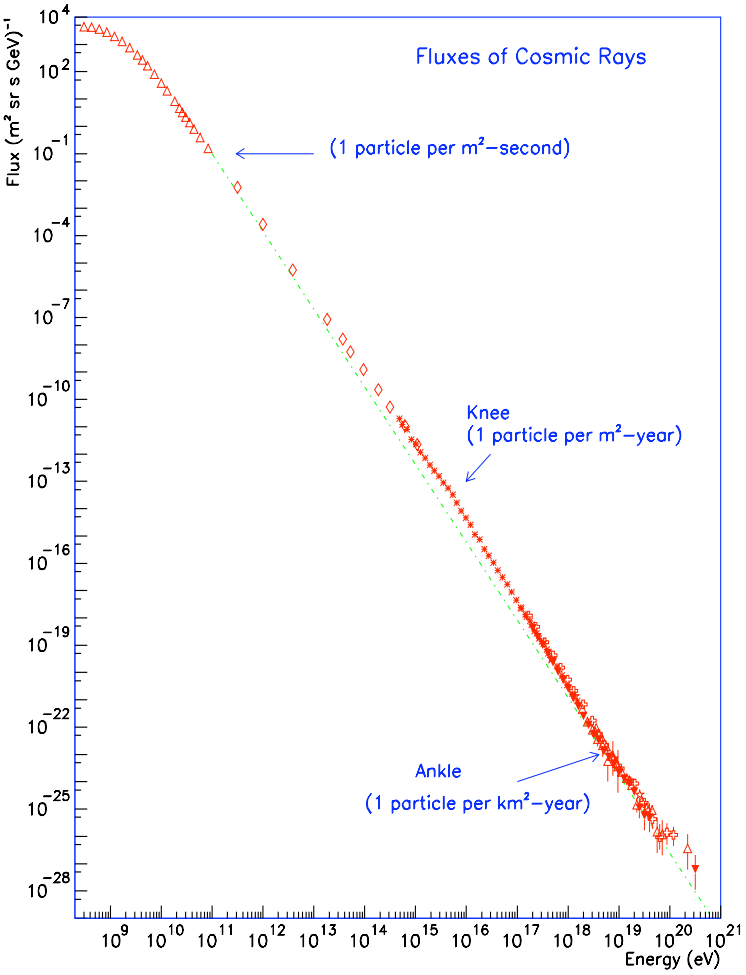

Figure 3.1: CR spectrum, from [3].

Many questions arise when considering these simple observational results. First of all, we do not know which astrophysical objects are able to power particles up to more than 10^{19} eV, giving them a macroscopic energy density. Moreover, the physical mechanism producing such a regular power-law spectrum has been unknown for long time, while is now believed to be the first order Fermi shock acceleration [162, 163], which possesses at least two important properties: it very efficiently produces a power-law spectrum of particles with a slope which, in the most common case of strong astrophysical shocks, is close to $p \sim 2$, and is easily realised in many astrophysical situations.

This leads to the important question of how CRs propagate to the Earth. Since the observed spectrum has a spectral slope close to 2.7, while the source spectrum should have $p \simeq 2$, propagation effects should be able to change it. In most simplified models of low energy CR propagation, the observed primary spectrum $\phi(E)$ and the source spectrum $Q(E)$ are connected by a relation of the form

$$\phi(E) \propto Q(E)\tau_{\rm esc}(E) \ , \tag{3.2}$$

where $\tau_{\rm esc}(E)$ represents an energy dependent escape time from the Galaxy, which, as it will be shown later in this chapter, is estimated of the order of 10 Myr at few GeV. It is clear that a simple profile $\tau_{\rm esc}(E) \propto E^{-\delta}$ with $\delta \approx 0.6$ gives a good fit to data[2].

Another big question is instead whether there is an end-point of the CR spectrum. Historically, the end-point has moved together with the maximal reachable energy of CR experiments.

Much interest about the physics of the UHECRs is related to this question. A high-energy cut off is theoretically expected, because the interactions of UHECRs with the Cosmic Microwave Background (CMB) lead to the production of neutral pions, thus effectively dumping the particle spectrum[3]. Pion production occurs only if the energy of the interacting UHECR is above $E_{\rm th} \simeq 5 \times 10^{19}\ (\omega_0/1.3\ {\rm meV})^{-1}$ eV (ω_0 is the target photon energy), with a mean-free-path of the order of few Mpc. Hence, it has long been thought to be responsible for a cut off in the UHECR spectrum, the Greisen-Zatsepin-

[2]It should be noted, however, that this relation cannot hold over a large energy range without coming in conflict with the observed isotropy of high-energy CRs. For example, extrapolating eq. (3.2) to 10^{15} eV would lead to a value of $\tau_{\rm esc}$ of the order of the light travel time across the Galaxy, implying a larger anisotropy than is observed. A possible solution to this problem is to take into account the change in propagation regime occurring at energies $E \sim 10^{15}$ eV [164].

[3]Although a similar process is possible for heavy nuclei, we are not going to consider it because they are effectively photo-disintegrated by resonant interactions with ambient photons, whose threshold is well below the pion photo-production one.

Kuzmin (GZK) cut-off [110, 111]. Moreover, trans-GZK particles arriving at Earth must be accelerated within the so called GZK sphere, whose radius is expected to be of the order of 100 Mpc at $\sim 10^{20}$ eV and to shrink down at larger energies. A simple analytic description of the GZK sphere can be given. In fact, assuming that the $p\gamma$ interaction occurs only at the onset of the Δ-resonance ($p\gamma \to \Delta^+ \to p\pi^0$), whose width is assumed to be $\Delta_{p,\gamma}$, we can write

$$ct_{p,\gamma}^{-1} = \sigma_{p,\gamma} \int_{\frac{E_{p,\gamma}-\Delta_{p,\gamma}}{2\Gamma}}^{\frac{E_{p,\gamma}+\Delta_{p,\gamma}}{2\Gamma}} n(E)dE \ , \tag{3.3}$$

where $E_{p,\gamma} = 310$ MeV is the photon threshold energy in the proton rest frame corresponding to the $\Delta-$resonance, $\Delta_{p,\gamma} = 100$ MeV, $n(E)$ is the angle averaged incident photon spectrum and $\sigma_{p,\gamma} \simeq 0.5$ mb is the interaction cross section. Assuming that $n(E)$ corresponds to the CMB spectrum, at a temperature $T = 2.73$ K, eq.(3.3) can be re-written as,

$$ct_{p,\gamma}^{-1} = \sigma_{p,\gamma} n_\gamma \int_{x_0}^{x_1} f(x)dx \tag{3.4}$$

where $f(x) = x^2/(e^x - 1)$, $x_0 = E_{p,0}/(3E_p)$, $x_1 = 2E_{p,0}/(3E_p) = 2x_0$, and $E_{p,0} = m_p E_{p,\gamma}/kT = 10^{20.6}$ eV. Since at threshold $E_{p,th} \sim m_p m_\pi/2E_\gamma = 10^{20}$ eV, at threshold the integral probes the $x \approx 10$ region, hence

$$l_{\text{horiz.}} = \frac{l_0}{[e^{-x}(1 - e^{-x})]} \tag{3.5}$$

where $l_0 = 5$ Mpc, $x = E_{p,0}/3E_p$ and $E_{p,0}/3 = 10^{20.53}$ eV. Equation (3.5) is represented in fig. 3.2, where it can be compared to the results of a full numerical computation of the GZK horizon. Experimentally, the presence of a suppression of the UHECR spectrum has been confirmed only recently with the observations by the HiReS detector [44] and the Pierre Auger Observatory (PAO) [43]. Although the cut off could be also due to the finite acceleration power of the UHECR sources, the fact that it occurs at the expected energy favours the GZK explanation. The results shown in [165] further strengthen this hypothesis.

3.2 Cosmic Ray composition

Other questions arise when considering more detailed properties of CRs. In particular, composition measurements are very interesting.

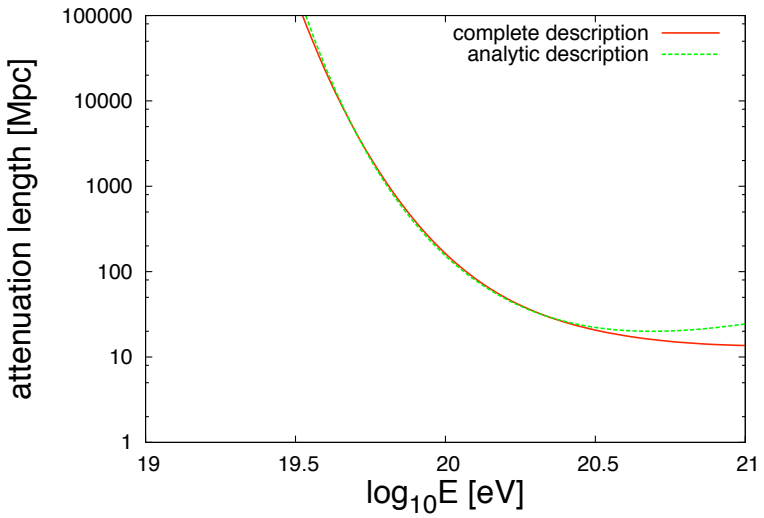

Figure 3.2: The proton attenuation length as a function of proton energy demonstrating the effectiveness of the analytic description

The CR composition can be measured directly via spectroscopy in the low energy region ($E < 1$ TeV), by satellite or balloon experiments. At higher energy only indirect measurements are possible, through the analysis of the profile and the content of the particle shower produced by CRs interacting with Earth atmosphere. These measurements are achieved both by fluorescence and by ground array detectors. Although shower physics is very complicated and suffers of many sources of systematic errors, it is nevertheless possible to relate the number of electrons and muons arriving on the Earth surface to the mass number A of the primary CR [166]. Moreover, without entering in any detail, also the lateral distribution of the shower, orthogonal to the main propagation direction, and the depth of the maximum shower development $X_{\max}$ (usually called elongation rate) are observables that allow discriminating the species of the primary CR that initiated the shower.

Low energy measurements revealed that the CR composition is very similar, within uncertainties, to that of the interstellar medium (ISM). However, there are important differences. Figure 3.3 shows a comparison between CR and ISM abundances. While the overall agreement between the two distributions is evident, major differences can be found at a closer look: the Boron is almost absent in the ISM, while is present, with comparable abundance to

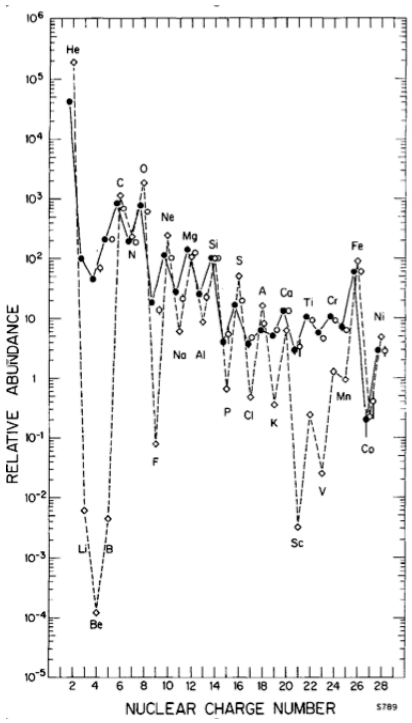

Figure 3.3: Comparison between CR and ISM abundances, from [4].

ISM nuclei like C, N, O, in CRs, as well as the radioactive nuclei ^{10}Be, ^{26}Al, ^{36}Cl and ^{54}Mn, and also some sub-Iron species like Sc, V and Ti.

These observations revealed that CRs spend in the Galaxy more time than what is expected by ballistic propagation $\tau \simeq L/c \simeq 20\,\mathrm{kpc}/(3{\times}10^{10}\,\mathrm{cm/s}) \sim 4 \times 10^3$ yr. In fact, as firstly pointed out by [167], the anomalous abundances of light nuclei (Li, Be, B) could only be explained by assuming that they are produced as secondary particles in hadronic interactions (spallation) of primary CRs with the gas in the ISM. Given the spallation cross section, of the order of $\sigma \simeq 10^{-26}$ cm^2, it was possible to infer that CRs should have passed through an equivalent layer of 5 g/cm^2 of material in order to produce the observed amount of secondaries before escaping from the Galaxy[4]. This implies, assuming as typical number density of protons in the ISM $n_{\mathrm{gas}} \sim 1$ cm^{-3}, that CRs should have propagated for million years, instead of thousands, leading to $\tau_{\mathrm{esc}} \approx$ few 10^6 Myr.

This conclusion is also supported by study of the abundances of radioac-

[4]The most important observable in this physics is the B/C ratio, as the Boron is essentially completely secondary. It is noticeable that also the energy behaviour of this ratio gives important information on CR propagation properties [163], as will be detailed in sec. 3.4.

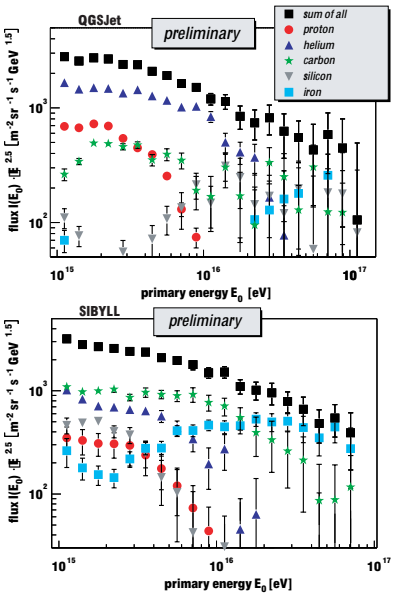

Figure 3.4: Change in composition at the knee, measured by KASKADE [5]. Uncertainties produced by different hadronic models are evident from a comparison of the upper and lower plot.

tive nuclei, compared to those of their stable isotopes. The most relevant observable in this case is the ratio $R_{10} = {}^{10}\mathrm{Be}/{}^{9}\mathrm{Be}$. Both isotopes are produced in comparable amounts by spallation of heavier nuclei, but the ^{10}Be is unstable to β-decay with a lifetime of order $\tau_{Be} \sim 2.2$ Myr $\times E/M_{^{10}\mathrm{Be}}$. It is clear that if the measured R_{10} is comparable to the production ratio then $\tau_{\mathrm{esc}} \ll \tau_{Be}$, while if $R_{10} \sim 0$ then $\tau_{\mathrm{esc}} \gg \tau_{Be}$. Data indicate $\tau_{\mathrm{esc}} \sim 10^7$ Myr.

Composition measurements in the knee region are shown in fig. 3.4. A change in composition is observed by KASKADE [5]. As it is evident, the composition changes from a light one, dominated essentially by protons and helium, to a heavier one, dominated by C, Si and Fe. This is consistent with expectations from magnetised shock acceleration models, because the relevant dynamical quantity is the rigidity $\rho \equiv E/Z$, hence if all nuclei are accelerated at a maximal ρ their maximum energy will increase with the atomic number Z, as it is observed[5].

Higher energy composition measurements suffer of major uncertainties due to the hadronic interaction models used in the data analysis. However, observations by HiRes [168] and AUGER [169] show a proton dominated

[5]Actually, while this is the standard expectation, the experimental situation is not so clear, because experimental uncertainties do not allow to disentangle a Z (i.e. ρ) dependent from a A (i.e. total energy) dependent composition yet.

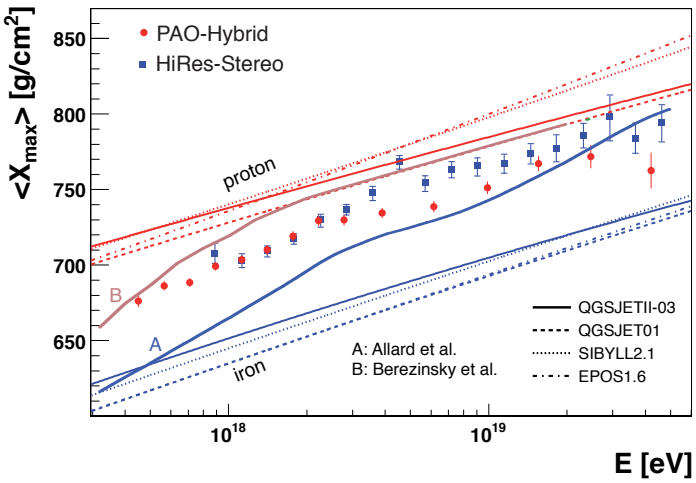

Figure 3.5: Model uncertainties on composition of UHECRs and measurements, from [6].

composition in the region up to the ankle, strengthening the ankle scenario envisaged in [170], while there is an apparent changeover to a heavier composition slightly above it, as shown in fig. 3.5.

3.3 CR sources

One of the most puzzling problems in CR physics concerns their origin. Being charged particles, CRs are deflected by intergalactic and (mostly) galactic magnetic fields as they propagate, hence information about the source direction is spoiled and their arrival directions are observationally almost isotropically distributed. Only CRs with $E \gtrsim 10^{19}$ eV are not strongly deflected and may show some anisotropy. In fact, the expected angle δ of deflection due to, e.g., galactic magnetic fields, is (we assume 1 kpc as the typical coherence length of the GMFs and a mean field strength of 3 μG) [165]

$$\delta = 2.7^\circ \frac{60 \text{ EeV}}{E/Z} \left| \int_0^D \frac{d\vec{x}}{1 \text{ kpc}} \times \frac{\vec{B}}{3\ \mu\text{G}} \right| , \tag{3.6}$$

which shows that it decreases as the CR energy E increases. Therefore only CRs of ultra-high energy are expected to give some hint on the source direction. However, at energies larger than 10^{19} eV, where CRs are not significantly deflected, their flux is of the order of 1 particle/km^2/century, hence very hard to detect. Only recently an indication of the correlation

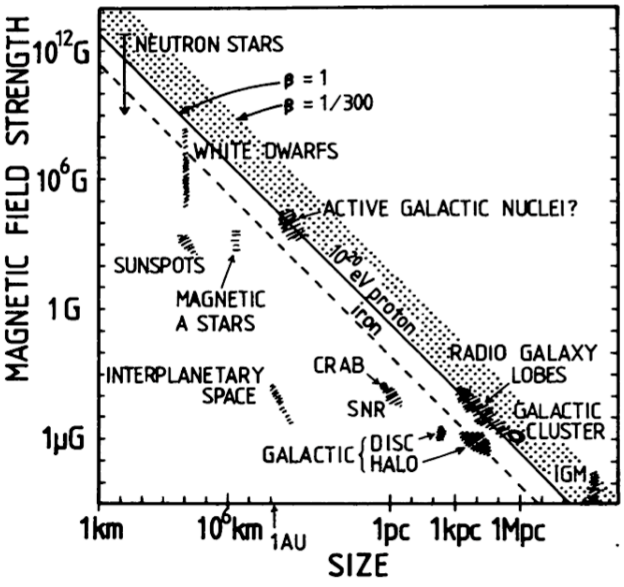

Figure 3.6: Size and magnetic field strength of possible sites of particle acceleration, from [7]. Objects below the diagonal cannot accelerate protons to 10^{20} eV.

between UHECRs and possible source candidates has been claimed [165] (see also [171, 172]) and questioned [173, 174], meaning that the problem is still far from being assessed.

The lack of observational information is accompanied by a corresponding lack of theoretical insights. Theoretically, UHECR source candidates are inferred using the famous Hillas criterion [7] (see fig. 3.6), stating that the maximum attainable energy by charged particles in a region of typical size R filled by a magnetic field of strength B is

$$E_{\max} = ZeBR\,. \tag{3.7}$$

According to the Hillas criterion, only few astrophysical sources are in principle able to power CRs up to 10^{20} eV, e.g. Active Galactic Nuclei, Neutron Stars or Galaxy Clusters, but the observational answer to this question is still far from being achieved.

The origin of lower energy CRs is maybe a less severe problem. Using again the Hillas criterion, we find an entire class of objects, the remnants of SuperNova explosions (SNR), that should be able to accelerate particles up to at least $Z \times 10^{15}$ eV [175]. Moreover, SNRs are known to be highly turbulent

objects, in which strong shocks can form, which makes them suitable for charged particle acceleration. Also, a simple energetic argument points to SNRs as possible CR sources. In fact, given the SN explosion rate in our Galaxy ($\sim (30\ \mathrm{yr})^{-1}$) and their typical kinetic energy output ($\sim 10^{51}$ erg/s), it can be shown that if SNRs are responsible for powering CRs, in order to maintain a steady CR flux at Earth a (quite reasonable) $\sim 10\%$ efficiency for CR acceleration is required [163]. However, the observational evidence of this fact is still lacking. Due to low energy CR diffusion into galactic magnetic fields, it is impossible to obtain *direct* evidence of SNRs being CR sources.

On the other hand, indirect observations are indeed possible. In effect, through observations of local SNR (like CasA, SN1006, RX J1713.7-3946 and others) in the radio, X-ray and γ-ray bands, both features of synchrotron emission and inverse Compton scattering of photons are observed, revealing the presence of a power-law spectrum, with spectral index $p \approx 2$, of shocked electron population in the region. Together with electrons, it is natural to assume that also shock accelerated protons (and in general ions) are present in the same region, although the observational evidence is less clear. The main feature expected in this case is the observation of photons produced by the decay of π^0s formed in hadronic collisions ($p + p_{\mathrm{gas}} \rightarrow p + p + \pi^{0\pm} + ...$) with the surrounding material. This feature can be typically observed in γ-rays in the GeV-TeV bands, but is clearly degenerate, at some extent, with ICS-generated γ-rays. A particularly favourable case is if the γ-ray emission is found to correlate with the density of gas in the region surrounding the accelerator. Indeed, the observation of γ-rays with $E > 1$ TeV from the direction of the Galactic Centre by HESS has excited a wide community of scientists because of its correlation with molecular hydrogen gas, as inferred from CS maps [176].

However, as pointed out in many works (see e.g. [19, 177, 178]) a multi-messenger approach will be more suitable to disentangle the two possibilities. In fact, in hadronic interactions also neutrinos, with energies of the order of few TeV, comparable to that of γ-rays, are expected to be produced together with γ-rays due to the decay of charged pions $\pi^{\pm}$, while they are not expected in presence of ICS radiation. Therefore, if very-high-energy neutrinos were detected from some γ-ray source we could be reasonably sure that the source is a CR accelerator.

Unfortunately, the expected neutrino fluxes from candidate sources are very low, as they are expected to produce only ~ 1 event/yr in a km-scale Neutrino Telescope (like NEMO [179] or IceCube [180]) [19, 177, 178].

3.4 Galactic Cosmic Rays: a possible propagation model

As we already argued, the high isotropy of low energy CRs and the large number of secondary nuclei, together with data from radioactive isotopes, suggest that high-energy particles travel long time in the Galaxy effectively interacting with the ISM. An important role here must be played by the galactic magnetic field, but due to lack of information about the physical conditions of the ISM, the details of the specific mechanism regulating the propagation of CRs in the Galaxy are still unknown. Therefore, approximate semiempirical models have been developed, that allow to classify and correlate numerous experimental facts and to interpret some properties of composition, spectra and anisotropy of different components of CRs.

Being the galactic magnetic field chaotic at some level, charged particles are generally expected to diffuse into it. It is well known, since the pioneering work of Ginzburg and Syrovatskii [181], that in the absence of continuos energy losses, re-acceleration and convection, the diffusive transport of stable nuclei in the ISM is described by the following equation

$$\frac{\partial N_i}{\partial t} + \boldsymbol{\nabla}\left(\boldsymbol{D}\cdot\boldsymbol{\nabla}\ N_i\right) = Q^i(E_k,r,z) - c\beta n_{\rm gas}(r,z)\sigma_{\rm in}(E_k)N_i + \sum_{j>i} c\beta n_{\rm gas}(r,z)\sigma_{ji}\ N_j\ . \tag{3.8}$$

where N_i is the density of the species i, $E_k \equiv (E - m_A)/A$ (E is the total energy of a nucleus with mass $m_A \simeq A \times m_{\rm nucleon}$) is the kinetic energy per nucleon E_k, which is constant during propagation, D is the diffusion tensor, $Q^i(E_k, r, z)$ the distribution of CR sources. In the 2nd term of the r.h.s. of eq. (3.8), which describes fragmentation losses, σ_i is the total inelastic cross section onto the ISM gas with density $n_{\rm gas}(r, z)$. In the third term σ_{ij} is the cross-section for the production of the nuclear species j by the fragmentation of the i-th one.

To solve eq. (3.8) in general is a hard task. For this reason, many simplified models have been adopted. Before describing the most recent numerical models, it is worth referring to one of the most widely known and used analytical models, the so called "leaky-box" model [163].

The "leaky-box" model assumes that diffusion occurs very fast in the Galaxy, so that the CR density over the whole Galaxy is constant and the CR transport can be described by replacing the diffusion term in eq. (3.8) with a "leakage" one, of the form $N_i/\tau_{\rm esc}$, accounting for the escape of CRs out of the Galaxy and all other quantities, like gas density or source distribution,

with averaged ones. The resulting transport equation, derived from (3.8), is

$$\frac{\partial N_i}{\partial t} + N_i/\tau_{\rm esc} = \bar{Q}^i(E_k) - c\beta\bar{n}_{\rm gas}\sigma_{\rm in}(E_k)N_i + \sum_{j>i} c\beta\bar{n}_{\rm gas}\sigma_{ji}\ N_j\ . \tag{3.9}$$

Within this framework, the most important properties of low-energy CRs depend essentially on the average thickness of material crossed by CRs during propagation $x_l = n_{\rm gas} v \tau_{\rm esc}$. For example, if we want to calculate the stationary state density of a secondary species (which we label with the subscript 2) assuming it is produced only by spallation of the primary species 1, we have

$$N_2 \times (1/\tau_{\rm esc} + c\beta\bar{n}_{\rm gas}\sigma_2(E_k)) = c\beta\bar{n}_{\rm gas}\sigma_{12}\ N_1\ , \tag{3.10}$$

whose solution for the secondary/primary ratio is

$$\frac{N_2}{N_1} = \frac{\sigma_{12}}{\sigma_2 + 1/(\tau_{\rm esc} c\beta\bar{n}_{\rm gas})} = \frac{\sigma_{12}}{\sigma_2 + 1/x_l}\ . \tag{3.11}$$

By using this kind of relationships and our knowledge of nuclear cross-sections it is possible to infer the properties of x_l as a function of the kinetic energy per nucleon E_k. In fig. 3.7 the observed B/C ratio is shown. From the energy dependence of B/C ratio it is possible to infer a scaling of the form $x_l \propto E^{-\delta}$ with $\delta \in [0.3, 0.7]$ depending on the details of the model used to fit data. If one recalls the definition of the escape time (3.2) and, from eq. (3.11), the definition of $x_l \propto \tau_{\rm esc}$, it is remarkable that the best fit value is $\delta \approx 0.6$, which is precisely needed to account for the overall CR energy spectrum.

Furthermore, it is possible, introducing some simplification in the more general diffusion model, to relate the matter thickness x_l to the mean CR diffusion coefficient D [163]. If the gas is confined in a layer in the galactic disk whose height h_g is much smaller than the galactic halo one h_h, it can be shown that

$$x_l = \frac{n_g v h_g h_h}{D}\ . \tag{3.12}$$

Therefore, secondary/primary ratio measurements also give relevant information on the diffusion properties of galactic CRs, implying $D \propto E^\delta$, $\delta \approx 0.6$ in this simple model.

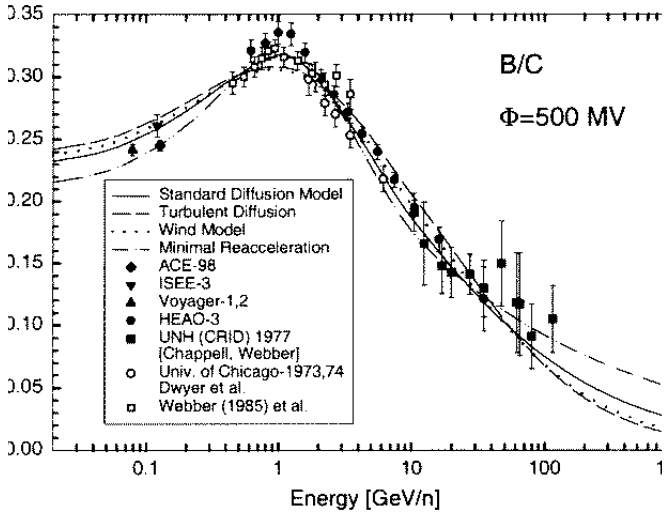

Figure 3.7: Compilation of data of B/C energy spectrum, from [8].

3.4.1 The need of a more refined model

As usual in science, when more refined data were available, this simple "leaky-box" model became inadequate to correctly reproduce them. In particular, more realistic diffusion models are required to provide a comprehensive description of multi-channel observations (including heavy nuclei, electrons, γ-rays and antimatter particles), accounting for the growing amount of available astrophysical data.

The *two-zone model* [182, 183] introduces further details in the diffusion model still trying to obtain analytical results, while on the numerical side the GALPROP code[6] [184, 185] has been developed extensively. In the case of GALPROP, the adoption of a realistic gas and radiation field distributions allows to model also the spectrum and angular distribution of the γ-ray secondary emission.

Although these models allow a significant step forward with respect to previous analyses, they still perform a number of simplifications with respect to a more realistic physical scenario. In particular, they assume diffusion to be statistically isotropic and homogenous, *i.e.* they adopt the same single value (or at most two values in the two-zone model) diffusion coefficient all over the propagation volume.

However, such assumptions may not always be justified, as diffusion coefficients generally depend on the regular magnetic field orientation and on the ratio between the regular and chaotic magnetic field energy densities. Although these quantities are poorly known, several observations and theoretical arguments suggest that they are far from being spatially homogeneous in the Galaxy (see sec. 3.4.2 for more details). This may have relevant consequences for the CR spatial distribution in the Galaxy, for the angular distribution of the secondary γ-ray and neutrino emissions [20] and to interpret the CR anisotropy.

In order to be able to test some of those effects, as well as to verify previous results which have been derived in the literature under more conventional conditions, we developed a new numerical code, DRAGON (Diffusion of cosmic RAys in Galaxy modelizationON). DRAGON is especially designed to account for a spatially in-homogeneous and an-isotropic diffusion coefficient. In its present version it allow to model CR nuclei transport at energies $E_{\rm min} \gtrsim 1$ GeV/n as well as the secondary γ-ray and neutrino emission produced by their interaction with the ISM. We disregard CR convection and re-acceleration (i.e. we work in a plain diffusion (PD) regime) and show that most relevant measurements can be reproduced under these conditions. Above $E_{\rm min}$ we expect that no other physical input than source spectra, dif-

[6] See also the GALPROP website http://galprop.stanford.edu/

fusion and fragmentation processes can determine secondary/primary ratios, hence a comparison of our prediction with experimental data should allow to fix the slope delta of the diffusion coefficient for some assumed slope of the CR injection spectra (see [186] for a detailed discussion about this issue).

In our analysis we will mainly refer to measurements of the secondary/primary flux ratios of several nuclear species (the most relevant are B/C, N/O and sub-Fe/Fe) and the antiproton and $\bar{p}/p$ spectra, performed by several satellite and balloon experiments.

In order to test our code, we firstly study the conventional case of a uniform diffusion coefficient. Afterwards, we will analyse the previously unconsidered case in which D grows exponentially with the distance from the Galactic Plane (GP) and traces the radial distribution of supernova remnants.

3.4.2 Theoretical and observational motivations for inhomogeneous diffusion models

Charged particles diffuse in chaotic magnetic fields due to their scattering onto hydro-magnetic fluctuations. The presence of a regular component of the magnetic field, which is the case in the Milky Way, is expected to break isotropy so that spatial diffusion has to be described in terms of a diffusion tensor $D_{ij}(\mathbf{x})$. According to [187] this can be conveniently decomposed as

$$D_{ij}(\mathbf{x}) = \left(D_{\perp}(\mathbf{x}) - D_{\parallel}(\mathbf{x})\right) \hat{B}_i \hat{B}_j + D_{\parallel}(\mathbf{x})\delta_{ij} + D_A(\mathbf{x})\epsilon_{ijk}\hat{B}_k \ , \qquad (3.13)$$

where $\hat{B}_i$ are the components of the regular magnetic field versor. The symmetric components $D_{\parallel}$ and $D_{\perp}$ are the diffusion coefficients along and perpendicularly to the regular field $\mathbf{B}_0$, while D_A is the antisymmetric (Hall) diffusion coefficient which accounts for the drift due to the interplay of $\mathbf{B}_0$ and CR density gradient. Since D_A is relevant only at very high energies ($E \gtrsim 1$ PeV, see e.g. [20, 188]) we will disregard it in the following.

Since diffusion is related to magnetic processes, diffusion coefficients depend on the particle rigidity $\rho = p(E)/Ze$. Moreover, in general $D_{\parallel}$ and $D_{\perp}$ depend differently on ρ and on the strength of hydro-magnetic fluctuations. In the quasi-linear theory (QLT)

$$D_{\parallel}(\mathbf{x}, \rho) \simeq \frac{1}{3} v r_L(\rho)\ \mathcal{P}^{-1}(k) \qquad (3.14)$$

where $r_L(\rho) = \rho/B_0$ is the Larmor radius and $\mathcal{P}(k) \equiv \delta B(k)^2/B_0^2$ is the normalised power spectrum of the turbulent hydromagnetic modes with wave-

number $k \geq 2\pi r_L^{-1}(\rho)$. A power-law behaviour $\mathcal{P}(k) \propto k^{-\gamma}$ is generally assumed, with $\gamma = 5/3$ (3/2) for Kolmogorov (Kraichnan) turbulence spectrum. In QLT the perpendicular diffusion coefficient is

$$D_\perp(\mathbf{x}, \rho) \sim D_\parallel(\mathbf{x}, \rho)\ \mathcal{P}(k) \ll 1\ , \tag{3.15}$$

meaning that diffusion takes place mainly along the regular magnetic field lines.

Although QLT may not be applicable to the conditions presents in the ISM, more realistic computations [163] confirmed that expectation, finding $D_\perp \simeq 0.1\ D_\parallel$. MonteCarlo simulations of particle propagation in turbulent fields [189, 188, 190] also found a similar result (although computation time limits allowed to test it only at energies above 100 TeV).

What is most relevant here, however, is the different behaviour of $D_\parallel$ and $D_\perp$ as a function of the turbulent power. Simulations of propagation in strongly turbulent fields agree with QLT predicting $D_\parallel$ ($D_\perp$) decreasing (increasing) when $\mathcal{P}(k)$ increases. It should be noted that if, as it is generally assumed, the CR source distribution can be approximated to be cylindrically symmetric, and the regular field to be purely azimuthal $\boldsymbol{B} = (0, B_\phi, 0)$, parallel diffusion plays no physical role[7].

Clearly, under this approximation and in absence of an *a priori* criterion to fix the normalisation and energy dependence of the diffusion coefficients, the substitution of an isotropic diffusion coefficient with $D_\perp$ would produce no physical effects. This conclusion is no more true, however, if the homogeneous diffusion approximation is relaxed and one tries to correlate spatial variations of the relevant diffusion coefficients to those of the hydro-magnetic fluctuation energy density, as $D_\parallel$ and $D_\perp$ have an opposite behaviour as functions of $\mathcal{P}(k)$.

Spatial behaviour of $\boldsymbol{D_\perp}$ in the Milky Way

Very little is known about the spatial distribution of hydro-magnetic fluctuations in the Galaxy. From a theoretical point of view, this quantity is quite unlikely to be uniform, as fluctuations are expected to be correlated, via particle-wave resonant scattering, to CRs, which in turn are correlated to the non-uniform source distribution. Observationally, very little is known. There are, however, evidences both for a longitude [192] and latitude [193, 194] dependence of the fluctuation power.

[7] This conclusion is not expected to change significantly if a possible spiral shape and a tiny dipole component of the regular magnetic fields are accounted for (though more complex scenarios have been considered [191]).

A radial variation of the diffusion coefficient may have relevant consequences on the CR spatial distribution in the galactic disk. In [20] some of us already pointed out that in-homogeneous diffusion may help reconciling the discrepancy between the rather smooth diffuse γ-ray longitude profile observed by EGRET [16] with the quite steep SNR (the most likely CR sources) radial distribution (*CR gradient problem*). That can be understood as a back-reaction effect: a larger CR density nearby sources induces a larger $\mathcal{P}(k)$, hence a larger $D_\perp$, which in turn implies a faster CR diffusion out of those regions (note that the effect would be opposite for $D_\parallel$). In sec. 3.4.5 we will show the possible consequences of this effect on the γ-ray angular distribution.

Concerning the vertical profile of the diffusion coefficient we assume here

$$D(\rho, r, z) = D(\rho)\ f(r)\ \exp\{|z|/z_t\}\ . \tag{3.16}$$

This is motivated by the requirement to get a physically more reasonable behaviour of the CR density at large $|z|$ (see fig. 3.8). In fact, a vertically growing $D_\perp$ may be justified if the regular component of the galactic magnetic field B_0 decreases more rapidly than the turbulent one, so that $\mathcal{P}(k)$ grows with $|z|$ in spite of the decreasing CR density. Indeed, this seems to correspond to the actual physical situation, as RMs of polarised radio sources point to a vertical height scale z_r for the regular magnetic field as large as $z_r \simeq 1.5$ kpc [195], while dating of unstable CR species (mainly the ^{10}Be) constraints the halo vertical hedge to be in the interval $4-6$ kpc [184]. An exponentially growing profile of the diffusion coefficient has been also considered in [196].

We verified that, as far as stable secondary nuclei are concerned, replacing an exponentially vertically growing $D_\perp$ with a uniform one has almost no effects, as expected because spallation takes place mainly in the thin Galactic disk where the CR density is only marginally affected by the choice between these two options. Observable effects may however be expected in the latitude profile of the γ-ray emission.

3.4.3 Description of the model

We solve equation (3.8) numerically in the stationary limit $\partial N_i/\partial t = 0$ using a Cranck-Nicholson scheme [184, 197, 20] with null boundary conditions. This corresponds to free escape of CRs at the outer limit of the Galaxy, defined by $R_{\rm max} = 20$ kpc and $z_{\rm max}$. While $R_{\rm max}$ is fixed, $z_{\rm max}$ is set to $z_{\rm max} = 2 \times z_t$ (cf. eq. 3.16) to avoid border effects.

We describe below our assumptions for the terms appearing in eq. (3.8).

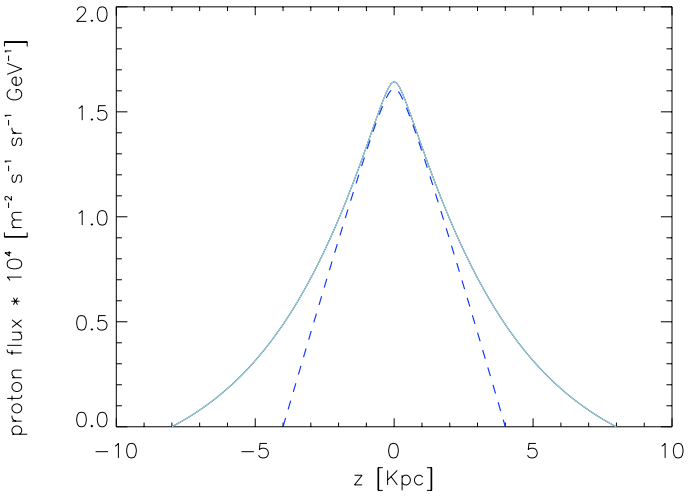

Figure 3.8: The proton flux vertical profile at 1 GeV obtained with DRAGON assuming a uniform diffusion coefficient (blue, dashed line) is compared with that obtained adopting the exponential profile in equation 3.16 for $z_t = 4$ kpc (light blue, continuos line). In both cases D is normalised so to reproduce the B/C (see section 3.4.4).

Spatial diffusion The l.h.s. of eq. (3.8) describes spatial diffusion. As we discussed above, we assume cylindrical symmetry and that the regular magnetic field is azimuthally oriented ($\mathbf{B_0} = B_\phi(r,z)\,\hat{\boldsymbol{\phi}}$). Under these conditions CR diffusion out of the Galaxy takes place only perpendicularly to $\mathbf{B_0}$. Therefore in the following it is understood that D represents in fact the perpendicular diffusion coefficient $D_\perp$. The dependence of D on the particle rigidity ρ is (see e.g. [198])

$$D(\rho, r, z) = D_0\ f(r)\ \beta \left(\frac{\rho}{\rho_0}\right)^{\delta}\ \ \exp\{|z|/z_t\}\ . \tag{3.17}$$

The function $f(r)$ describes a possible radial dependence of D. We define it to be unity at Sun position ($r = r_\odot$) so that D_0 corresponds to the local value of the diffusion coefficient at the reference rigidity $\rho_0 = 3$ GV.

CR sources For the source term we assume the general form

$$Q_i(E_k, r, z) = f_S(r,z)\ q_0^i\ \left(\frac{\rho}{\rho_0}\right)^{-\alpha_i}\ , \tag{3.18}$$

imposing $Q_i(E_k, r_\odot, z_\odot) = 1$. While the exact form of $f_S(r, z)$ has little influence on the charged secondary species spectra, it is very important in shaping the γ-ray angular distribution. We assume $f_S(r, z)$ to trace the SNR distribution as modelled in [199] on the basis of pulsar and progenitor star surveys [20]. In the galactic disk such a distribution is similar to that adopted in [17], but shows an excess in the Galactic Bulge due to the contribution of type-Ia SNe, not accounted for in [17]. Both distributions are significantly more peaked than those empirically determined [200, 184] by matching the γ-ray longitude profile measured by EGRET [16].

The injection abundances q_0^i are tuned so that the propagated spectra of primary and secondary (or their ratio) species fit the observed ones (see below). Even though our code allows to consider different power-law indexes α_i for the different nuclear species, in this work we only consider the same $\alpha_i \equiv \alpha$ for all species, when not differently stated. For each value of δ of eq. (3.17) the source spectral slope α is fixed by the requirement that at high energy $E_k \gg 100$ GeV/n, at which spallation processes are almost irrelevant, the equality $\alpha + \delta = 2.7$ is satisfied[8], in order to match the observed slope.

Nuclear cross sections As in GALPROP the spallation cross sections and the spallation network are based on a compilation of experimental data and semi-empirical energy dependent interpolation formulas as provided e.g. in [201, 202, 203].

Target gas The IS gas is composed mainly by molecular, atomic and ionised hydrogen (respectively, H_2, HI and HII). Although more realistic distributions are known, for $r > 2$ kpc we adopt the same distributions as in GALPROP, for essentially two reasons. First of all, since CRs propagate for million years in the Galaxy, in the stationary limit they just probe a smoothed, mean gas distribution. Secondly, we can have a more direct comparison with GALPROP results.

However, in the central region of the Galaxy, where GALPROP assumes an interpolated density, we use the the H_2 and HI distributions as modelled in [204]. While the flux and composition of charged CR reaching the Earth are not sensitive to the central gas distribution, this choice allows us to better model the γ-ray emission in the Galactic Centre (GC) region, as we will discuss in more details in sec. 3.4.5.

[8] In this regime, the theoretical expectation for the observed flux Φ on Earth is $\Phi(E) \approx Q(E)/D(E) \sim E^{-(\alpha+\delta)}$ [163].

Following [205] we take the He/H numerical fraction in the ISM to be 0.11. We neglect heavier nuclear species.

Here we neglect ionisation and Coulomb energy losses, which, however, are estimated to be irrelevant at energies higher than $1 - 2$ GeV/n [163].

3.4.4 Testing DRAGON: the case of a radially uniform diffusion coefficient

In order to test our code, we ran it under similar conditions to those already considered in the literature. In this section we show the results we obtained assuming that the diffusion coefficient does not depend on the galactocentric radius r. As we mentioned in sec. 3.4.2, the adoption of an exponential vertical profile for D does not affect significantly the results presented in this section with respect to the case of isotropic and uniform diffusion mostly considered in literature. Indeed, passing from a spatially uniform D to the profile described by eq. (3.17) only amounts to a small re-scaling of D_0.

In the following, every label indicating a nuclear species refers in fact to the sum of all its isotopes, unless otherwise stated.

The B/C ratio

As we already mentioned, the Boron to Carbon ratio (B/C) is one of the most useful tracers of CR propagation in the Galaxy. In fact, since Boron is entirely secondary, its observed abundance strongly depends on the residence time of primary CRs in the Galaxy. Moreover, measurements of Boron and Carbon fluxes are of better quality than those of other secondary/primary ratios, and the B production cross sections from its main primaries (^{12}C and ^{16}O) are known better than for other secondary nuclides.

Fixing free parameters Once the spatial distributions of the CR sources and the ISM gas have been chosen, the main parameters determining the B/C in a PD model are the C/O and N/O injection ratios and the quantities δ, D_0 and z_t in eq. (3.17). As it was already shown in several papers, secondary/primary ratios for stable species depend on the ratio D_0/z_t (which will be always expressed in units of 10^{28} cm^2 s^{-1} kpc^{-1} in the following) rather than on the two parameters separately.

While primary/primary ratios are usually disregarded in the literature, as they do not give direct relevant information on CR propagation, we use

them to fix the C/O and N/O[9] injection ratios, while we fix the abundances of primaries heavier than oxygen by requiring that they match the observed abundances in CRs at $E \sim 1 - 10$ GeV/n.

To this aim, we define two different χ^2. We compute the former (which we label $\chi^2_{\{\mathrm{C/O,N/O}\}}$) by comparing our predictions for the C/O and N/O modulated ratios to experimental data over the energy range of our interest. The latter (which we label $\chi^2_{\{D_0/z_t,\,\delta\}}$) is computed comparing our predicted modulated B/C ratio to the observed one. Solar modulation is taken into account here in the "force-field" approximation [206] using a modulation potential of magnitude $\Phi = 500$ MV. In order to study potential energy dependent effects we consider two different minimum kinetic energies per nucleon E_k^{min} for comparison to data: 1 GeV/n and 2 GeV/n. The low statistical significance of the data set above this energy prevents us from going further up the energy scale.

For each pair of values $(D_0/z_t,\, \delta)$, we determine the $\chi^2_{\{\mathrm{C/O,N/O}\}}$ distribution in the space (C/O, N/O) scanning over a wide range of C/O and N/O injection ratios. For the set of parameters that minimises $\chi^2_{\{\mathrm{C/O,N/O}\}}$, we compute $\chi^2_{\{D_0/z_t,\,\delta\}}$ and we repeat this procedure for several values of $(D_0/z_t, \delta)$. Finally, we analyse the distribution of $\chi^2_{\{D_0/z_t,\,\delta\}}$ to obtain our best fit values for $(D_0/z_t,\, \delta)$ with the appropriate confidence regions.

Thus, this strategy allows us to fix best values of the C/O and N/O injection ratios and to consistently determine the best propagation parameters that will be used as our best model for the analysis of antiproton and γ-ray fluxes.

We notice here that this procedure, which corresponds essentially to split the whole $4-D$ parameter space into two separate ones, is physically motivated by the weak dependence of primary/primary ratios on $(D_0/z_t, \delta)$.

Experimental data So far the best B/C measurements above 1 GeV/n have been provided by the HEAO-3 [9] and CRN [10] experiments in the range $1 < E_k < 30$ GeV/n and 70 GeV/n $< E_k \lesssim 1.1$ TeV/n. New data should be released soon by the CREAM [207] and TRACER [208] experiments significantly improving the available statistics at high energy. Here we use only HEAO-3, CRN data.

For consistency, we take also C/O and N/O data from the same experiments.

[9]Note that N = ^{14}N + ^{15}N is a combination of primary and secondary nuclides

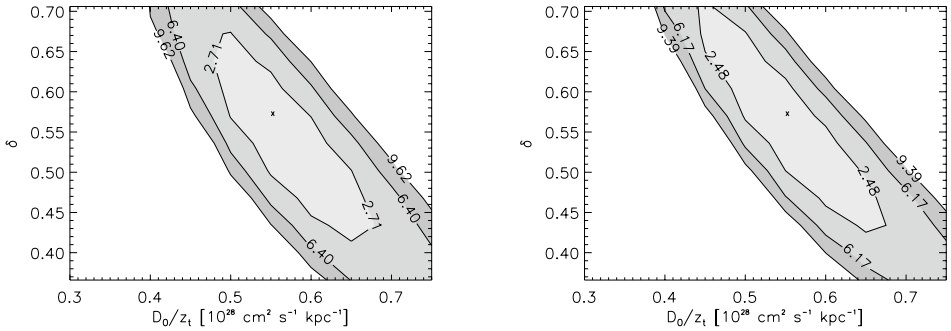

(a) (b)

Figure 3.9: The distribution of $\chi^2_{\{D_0/z_t,\delta\}}$ is shown for the case $E_k^{\rm min} = 1$ GeV/n (left) and 2 GeV/n (right). Contours limit 1, 2 and 3 σ confidence regions.

Results We show in figures 3.9(a) and 3.9(b) the main results of our procedure. In fig. 3.9(a) the distribution of $\chi^2_{\{D_0/z_t,\delta\}}$ for $E_k^{\rm min} = 1$ GeV/n is shown, together with confidence regions at 68%, 95% and 99% Confidence Level (CL). Our best-fit values for $(D_0/z_t, \delta, {\rm C/O}, {\rm N/O})$ if $E_k^{\rm min} = 1$ GeV/n are (0.55, 0.57, 0.79, 0.04). The projection of this point in the $(D_0/z_t, \delta)$ plane is highlighted by the cross in figure 3.9(a). Remarkably, the best-fit value for δ favours a Kraichnan turbulence spectrum, rather than a Kolmogorov one. Changing the minimum energy $E_k^{\rm min}$ from 1 GeV/n to 2 GeV/n indeed produces no relevant effect. In particular, the best-fit values for D_0/z_t and δ are not moved (see fig. 3.9(b)). It is interesting to notice that the particular value of $\delta = 0.57$ we obtain is consistent with findings of other authors (see [8] and references therein). The best-fit C/O and N/O injection ratios (0.79,0.04) should be compared with the solar system ones [205] 0.76 and 0.11 respectively.

We do not include the sub-Fe/Fe (sub-Fe = V + Ti + Sc) ratio in our statistical analysis because of the large uncertainties on the knowledge of the spallation cross sections for heavy elements. However, we found that we consistently obtain a reasonable match of experimental data also for this observable. In order to improve the fit to this ratio a careful fine tuning of nuclear cross section parametrizations seems to be needed. In fig. 3.10 we show the B/C, C/O and N/O ratios as obtained with our best-fit model, and assuming $z_t = 4$ kpc.

A comment is in order here: the particular observables we are considering are not sensitive to D_0 and z_t independently. A possible way to estimate z_t is

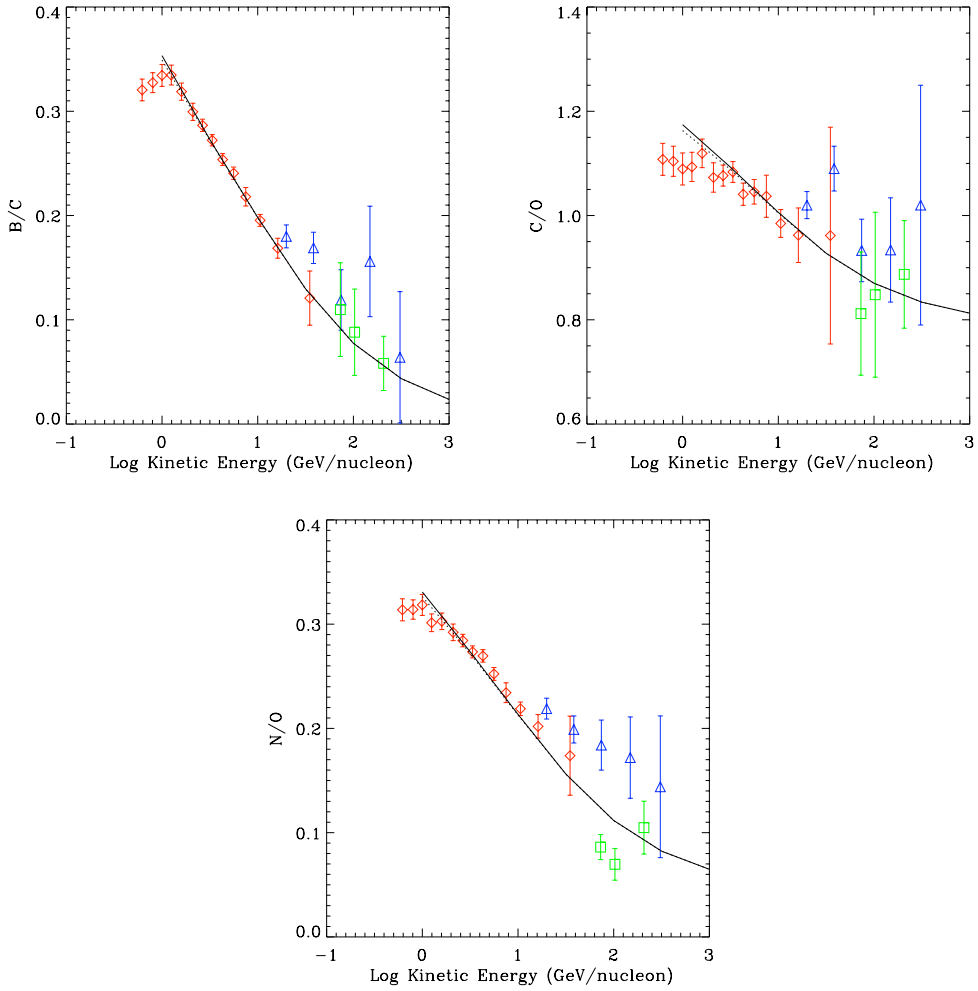

Figure 3.10: In these panels we show our best fit for the B/C, C/O and N/O compared with HEAO-3 [9] (red diamonds), CRN [10] (green, triangle) and ATIC-II [11] (blue) experimental data (though the latter are not used in our statistical analysis). Continuos curves: local interstellar (LIS); dashed lines: top of atmosphere (TOA) ($\Phi = 500$ MV).

offered by unstable/stable ratios (e.g. ^{10}Be/^{9}Be), which are known to probe the vertical height of the Galaxy [163]. Unfortunately, the best experimental data for this particular ratio have been obtained at energies $\lesssim 100$ MeV/n, while only 2 experimental points with large errors are available at 1 GeV/n [209]. Since our code does not allow us to have reliable predictions down to few hundreds MeV/n, because we do not account for continuous energy losses, it is impossible for us to draw any firm conclusion about our best value for z_t. However, by considering only the ^{10}Be/^{9}Be points around 1 GeV/n we infer that z_t should lie between 3 and 5 kpc, in agreement with previous findings [210].

Antiprotons

Most antiprotons reaching the Earth are expected to be a product of CR hadronic collisions with the IS gas. Their measured spectra provide, therefore, valuable information on CR propagation which are complementary to that coming from secondary nuclei (see e.g. [211, 212, 213]).

The main processes responsible for $\bar{p}$ production are p $p_{\rm gas}$, p $\mathrm{He}_{\rm gas}$, He $p_{\rm gas}$ and He $\mathrm{He}_{\rm gas}$, plus a negligible contribution from other nuclei. Similarly to [212, 213] we use the $\bar{p}$ production cross-section calculated using the parametrization given in Tan & Ng [214]. We account for the contribution of heavier nuclei in the CRs and the ISM by using the effective correction function determined by Simon *et al.* [215] with the MonteCarlo model DTUNUC. Inelastic scattering, annihilation and tertiary $\bar{p}$ (antiprotons which have been inelastically scattered) are treated as in [213]. For the local interstellar spectrum (LIS) of primary nuclei we adopt $\Phi_p = 1.6\times10^4\ (E_k/1\ \mathrm{GeV})^{-2.73}\ (\mathrm{m^2\ s\ sr\ GeV})^{-1}$ as measured by BESS during the 1998 flight [216] by accounting for a solar modulation potential $\Phi = 550$ MV in the "force-field" approximation [206].

We use DRAGON to simulate the primary proton distribution in the Galaxy and the LIS of secondary antiprotons. Normalisation is imposed by requiring that the simulated proton LIS coincides with $\Phi_p(r_\odot, 0)_{\rm obs}$[10]. In figures 3.11(b) and 3.11(a) we compare our results with the experimental data released by BESS for the periods 1995-97 [12] and 1998 [13] in the energy interval $1-4$ GeV, and by CAPRICE (1998) [14] in the range $3-49$ GeV. All these data refer to a period of low solar activity (the minimum was in 1997) and same positive phase of the solar cycle, with a mean value of the modulation potential for the period 1995-1998 of $\Phi = 550$ MV [13]. Hence we will also use $\Phi = 550$ MV to obtain $\bar{p}$ modulated spectra.

[10] Only the absolute $\bar{p}$ flux is dependent on such normalisation.

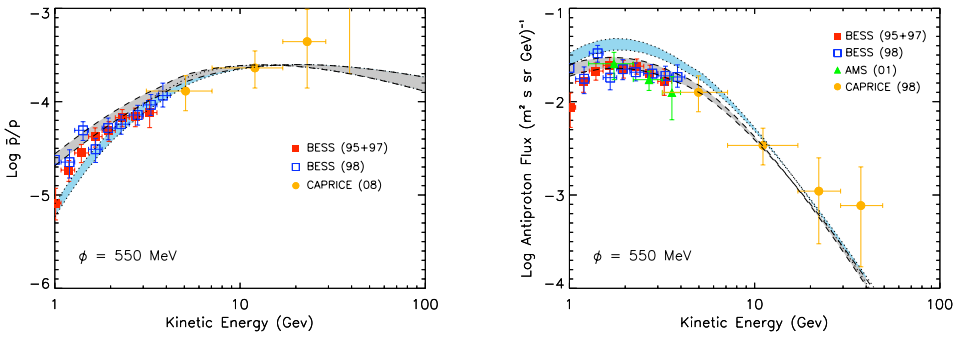

(a) (b)

Figure 3.11: The $\bar{p}/p$ ratio (left) and antiproton absolute spectrum (right) are compared with BESS 95+97 [12], BESS98 [13], CAPRICE [14], and AMS [15] experimental data. The shadowed regions correspond to models matching the B/C data within 1σ. LIS: grey band, short dashes; modulated ($\Phi = 550$ MV): light blue band, long dashed.

The shaded regions correspond to the uncertainty on the antiproton flux due to the uncertainty on the propagation parameters, and are constructed using values of $(D_0/z_t, \delta)$ within the 1σ region of fig. 3.9(a). The figures shown in this section are derived using $z_t = 4$ kpc, but we checked that, similarly to the B/C case, different choices of this parameter do not affect the antiproton spectrum provided that D_0/z_t is kept constant.

In fig. 3.11(a) we also show the LIS and TOA energy behaviour of the $\bar{p}/p$ ratio obtained with the parameters corresponding to minimum of the χ^2 distribution shown in fig. 3.9(a). It is evident that the models which fit the B/C data within 1σ are also compatible with the antiproton measurements. A statistically poor excess of the predictions of our best-fit model respect to the BESS data, which was also found in [213], is probably not significant due to the large systematic uncertainties. At higher energies, we have a small tension between our predictions and the highest energy CAPRICE data. A better agreement may be found if preliminary PAMELA [217] results will be confirmed.

3.4.5 Radial dependent diffusion and the γ-ray longitude distribution

In this section we model the secondary γ-ray emission originated, via π^0 decay, by the interaction of the hadronic component of CRs with the IS

gas. Along the GP, where the gas column density is higher, this process is expected to give the dominant contribution to the total diffuse emission above the GeV. At the energies of our interest a simple scaling model for the differential production cross section can still reliably be used. In this regime the energy spectrum of secondary γ's is a power law with the same slope as the primary nuclei (only protons and He nuclei give a significant contribution).

The main gas (target) components are the molecular (H_2) and atomic (HI) hydrogen, and He atoms. The contribution of ionised hydrogen is almost irrelevant in the GP. For $r > 2$ kpc, we adopt the same HI spatial distribution as [184]. For the H_2 we assume

$$n_{H_2}(r,z) = \epsilon_0(r)\ X_{CO}(r)\ \exp\left\{-\ln 2(z-z_0)^2/z_h(r)\right\}, \tag{3.19}$$

where $\epsilon(r)$ is the CO (a widely used H_2 tracer) volume emissivity, $z_0(r)$ and $z_h(r)$ are the midplane displacement and scale heights respectively, and $X_{CO}(r)$ is the CO - H_2 conversion factor. All these quantities, with the exception of $X_{CO}(r)$, are the same as in [218, 184, 185] for $r > 2$ kpc, while for smaller radii we adopt the Ferriere *et al.* model [204]. The adoption of Ferriere's model for the molecular and atomic hydrogen for $r < 2$ kpc allows us to avoid the interpolation of the γ-ray flux profile in the GC region and to reproduce naturally the peaked emission observed by EGRET toward the GC as we already pointed out in [219]. For the 11% He fraction we adopt the same spatial distribution as for the HI.

The CR gradient problem

The main issue we want to address here is the so called *CR gradient problem*. This originates from the well known discrepancy between the theoretical flux profile obtained by assuming SNRs to be the sources of galactic CRs and that inferred from EGRET γ-ray diffuse observations [16]. Under mild assumptions on the distribution of the galactic gas, it was found [200, 184] that the inferred CR radial profile should be much flatter than the theoretically expected one.

A former proposed solution and a test for DRAGON A possible way out was suggested in [17] in terms of a radially variable X_{CO}. While in [184, 185] this quantity was assumed to be uniform ($X_{CO} = 1.8 \times 10^{20}$ cm^{-2}/(K kms^{-1}))[11], in [17] it was taken to increase gradually

[11]For clarity, in the following we will drop units in quoting values of X_{CO}. They are always understood to be cm^{-2}/(K km s^{-1}).

by more than one order of magnitude from 4×10^{19} at $r = 2$ kpc to 1×10^{21} at $r > 10$ kpc. However, while the growth of this parameter with r is suggested by both theoretical arguments and observations of external galaxies, its actual behaviour is rather uncertain so that in [17] it had to be tuned into 5 steps to match EGRET observations.

To test our code against possible failures in reproducing the γ-ray longitude profile, we try to reproduce the results of [17]. We adopt the same $X_{\rm CO}(r)$ which was used in [17] and a CR model giving the best-fit of the B/C in the case of a radially uniform diffusion coefficient. We use $\delta = 0.57$ (see sec. 3.4.4) but our results do not change appreciably by using any value in the interval $0.45 - 0.65$. In fig. 3.13(a) we compare our results with EGRET measurements along the GP for $4 < E_\gamma < 10$ GeV [16].

We reasonably reproduce both the normalisation and the main features of the observed longitude profile. Smaller structures may only be reproduced using a detailed $3-D$ model of gas distribution which we are planning to do in a forthcoming paper. For comparison, in the same figure we also show the emission profile which we would obtain using a constant $X_{\rm CO}(r) = 1.8 \times 10^{20}$ for $r > 2$ kpc.

An alternative solution of the CR gradient problem As an alternative possibility we explore the case in which the diffusion coefficient traces the radial dependence of the SNR distribution as we motivated in sec. 3.4.2. According to the arguments explained in the same section we expect the CR radial profile to be smoothed with respect to the one obtained in the case of constant diffusion coefficient. Hence, we expect to be able to fit EGRET longitude profile without fine tuning the parameter $X_{\rm CO}$. Indeed, this is what we find.

We assume a constant $X_{\rm CO} = 1.8 \times 10^{20}$ for $r > 2$ kpc, while in the bulge ($r < 2$ kpc), where physical conditions are much different from the outer disk, we take $X_{\rm CO} = 0.5 \times 10^{20}$ [204]. For the diffusion coefficient, we assume that the function $f(r)$, as defined in eq. (3.17), is

$$f(r) = f_S(r, 0)^\tau \ . \tag{3.20}$$

The function $f_S(r, 0)$ describing the radial distribution of the Galactic SNRs is taken by [199] and is the same as in [20]. The exponent τ is practically unknown, hence it will be fixed by the requirement to reproduce observations. We verified that, as long as $\tau < 1$, we are still able to obtain a good fit of the B/C and antiproton data with nearly the same parameter values as in section 3.4.4. In particular, we find that for $\tau = 0.75$ the best-fit value for D_0/z_t is 0.52 while δ, the C/O and N/O injection abundances are unchanged

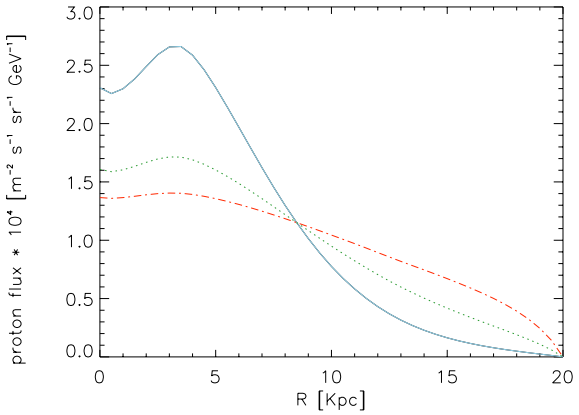

Figure 3.12: Proton differential flux at $E = 1$ GeV for three different choices of the parameter τ setting the radial dependence of the diffusion coefficient on the SNR distribution (see eq. (3.20)). $\tau = 0$ (radially uniform D): blue, continuous curve; $\tau = 0.5$: green, dotted; $\tau = 0.75$: red, dot-dashed. In all cases $z_t = 4$ kpc and the D normalisation giving the best fit to B/C data is chosen.

with respect to the radially uniform diffusion case discussed in the previous sections.

It is worth noticing, however, that the CR spatial distributions corresponding to these models are considerably different. In fig. 3.12 we show the radial profile of the proton differential flux at 1 GeV for three different values of the parameter τ: 0.75, 0.5 and 0 (the latter corresponds to a radially uniform D). It is remarkable that the smoothing effect of relating D to the SNR distribution can be quite significant without spoiling the successful predictions for the charged secondary CR at Earth. Interesting observable effects, however, are expected for what concerns the diffuse γ-ray emission.

In fig. 3.13(b) we show the simulated γ-ray longitude profiles as obtained using $\tau = 0.75$ (smaller values of τ produce a less pronounced flattening). It is clear that our model is able to reproduce EGRET observation without invoking a fine tuning of the $X_{\rm CO}$[12].

It is worth noticing that there is a potential degeneracy between the radial dependence of $X_{\rm CO}$ and that of the diffusion coefficient, as evident comparing figures 3.13(a) and 3.13(b). This should be taken into account when interpreting observations of γ-ray diffusion emission of the Galaxy.

[12] Although we achieved this result by phenomenologically introducing the free parameter τ, it should be noticed that, differently from the $X_{\rm CO}(r)$, τ is the only single value parameter which does need to be tuned in this model.

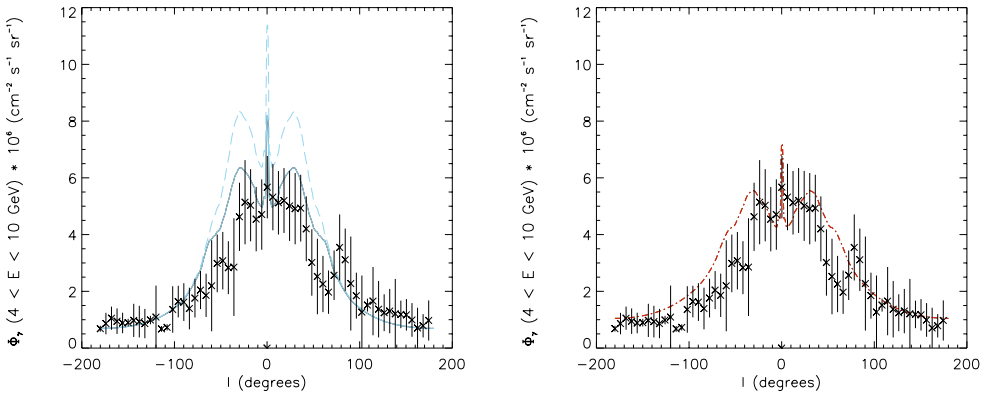

(a) (b)

Figure 3.13: Our predictions for the longitudinal profiles of the γ-ray hadronic emission integrated for $|b| < 1^\circ$ are compared with EGRET measurements [16]. Left panel: radially uniform D with $X_{\rm CO} = 1.8 \times 10^{20}$ cm^{-2}/(K kms^{-1}) for $r > 2$ kpc (long dashed curve), and $X_{\rm CO}$ as in [17] for $r > 2$ kpc (continuous curve). Right panel: $D(r)$ tracing the SNR distribution with $\tau = 0.75$. In both cases $z_t = 4$ kpc and D normalisation is chosen to best-fit the B/C data.

3.4.6 Final remarks

We modelled CR transport in the Galaxy assuming a plain diffusion model. We study two main cases: in the first one the diffusion coefficient D is assumed to be uniform along the Galactic Plane, while in the second case we consider, for the fist time, a $D(r)$ which traces the radial profile of SNRs (which we assume to be the CR sources).

The fact that we can consistently reproduce the observed antiproton spectra and the main secondary/primary nuclear ratios for $E \gtrsim 1$ GeV/n makes us quite confident of the validity of our approach. By using only the B/C, C/O and N/O data we found that the preferred range (1σ) of values of the slope of diffusion coefficient is 0.43-0.65. The best fit value is $\delta \simeq 0.57$. This is in agreement with findings of other authors. A Kolmogorov spectrum is disfavoured and re-acceleration seems to be unnecessary to interpret data above $1 - 2$ GeV/n. Forthcoming experiments like CREAM [207] and TRACER [208] for what concerns nuclei and PAMELA [217] and AMS [15] for antiprotons may soon allow to strengthen this conclusion by improving both statistics and quality of data.

While in both cases we obtain substantially the same successful predic-

tions for what concerns nuclei and antiprotons reaching the Earth, the corresponding CR primary spatial distributions in the Galaxy can be considerably different. This may have a number of interesting effects, including a possible role in the solution of the problem which plain diffusion models face predicting a too high CR anisotropy above 100 TeV.

We focused also on the effects on the expected secondary γ-ray diffuse emission. We showed that the longitude distribution of that emission can be significantly affected by in-homogeneous diffusion. In [20] we already noticed that the effect goes in the right direction to provide a viable solution of the CR gradient problem. Here we confirm this claim and succeed reproducing EGRET observations for $4 < E < 10$ GeV and $|b| < 1^\circ$ for a reasonable choice of the relevant parameters. The extension of our predictions to larger latitudes would require to implement in DRAGON electron propagation (and losses) and more detailed gas and radiation distributions. We conclude by noticing that our predicted neutrino flux above 1 TeV along the GP is almost coincident with that derived in [20].

Chapter 4

Ultra-high-energy Cosmic Rays and LV

"Permitte divis cetera"

Q. Horatius Flaccus

UHECRs observations can be used to further constrain LV at unprecedented levels. In particular, two different observables can be exploited. One is the fact that no modification seems to occur to the propagation of UHE photons ($E > 10^{19}$ eV), which will be exploited in sec. 4.1. The second relevant observation is that of the GZK cut-off, which has been briefly discussed in sec. 1.5.6.

Since we have so high energies at our disposal, we take the opportunity of exploring also higher dimension LV operators, suppressed by $O(E^2/M_{\rm Pl}^2$. From a purely logical point of view, it could seem unreasonable to study $O(E^2/M_{\rm Pl}^2)$ LV corrections (those leading to 4−MDR), as these will be always subdominant with respect to those at $O(E/M_{\rm Pl})$ (those leading to 3−MDR). However, the reasons for this interest are both empirical and theoretical.

On the observational side, the LV parameters $\eta_{\pm}^{(3)}$ are presently constrained to be less than $O(10^{-5})$ at 95% confidence level (CL) by a detailed analysis of the synchrotron component of the Crab Nebula broadband spectrum [21], while so far the best constraint on $|\xi^{(3)}| \lesssim 6 \times 10^{-10}$ at 95% CL is obtained by considering the absence of vacuum birefringence effects in the propagation of hard-X ray polarised light from the Crab Nebula (see sec. 2.7).

On the theoretical side, a reasonably good motivation for focussing on $O(E^2/M_{\rm Pl}^2)$ LV corrections is related to the so called "naturalness problem" [58], which we have already exposed in sec. 1.3.3.

Let us recall it briefly. It is generic that, even starting with an EFT

with only mass dimension 5 or 6 LV operators for free particles, radiative corrections due to particle interactions will generate lower dimension Lorentz violating terms without introducing any further suppression [60]. Hence extra LV terms in p and p^2 will be generically dominant on the higher order LV terms and lead to extremely stringent constraints on the dimensionless LV coefficients $\xi^{(n)}, \eta^{(n)}$.

However, it has been shown [62] that if the theory includes SuperSymmetry (SUSY), then dimension 3 and 4, renormalizable, LV operators are forbidden. As a consequence, renormalisation group equations for Supersymmetric QED with dimension 5 LV operators à la Myers & Pospelov were shown not to generate lower dimensional operators, if SUSY is unbroken.

SUSY soft-breaking does lead to LV terms in p and p^2, however characterised only by a suppression of order $m_s^2/M_{\rm Pl}$ $(n = 3)$ or $(m_s/M_{\rm Pl})^2$ $(n = 4)$, where $m_s \simeq 1$ TeV is the scale of SUSY soft breaking [62]. Nonetheless, given the present constraints, dimension 5 LV operators would induce dimension 3 ones which are already tremendously constrained. Hence, in the $n = 3$ case one would have to require unnaturally small LV coefficients in order to have a viable model. On the contrary, if $n = 4$ then the induced dimension 4 terms are suppressed enough, provided $m_s < 100$ TeV, so to be compatible with current constraints without requiring $\xi^{(4)}, \eta^{(4)}$ much less than one. Therefore, missing an alternative "custodial symmetry" for Lorentz violation with respect to SUSY, QED dimension 5 LV operators seem problematic, while dimension 6 LV, CPT even, ones are favoured.

At the moment, a clear general argument, as to why LV dimension 5 operators should not appear, is missing. However, if we assume, together with SUSY symmetry with $m_s < 100$ TeV, also CPT invariance for the Planck scale theory, then not only dimension 3 and 4 but also dimension 5, CPT odd, LV operators would be forbidden and only CPT even, dimension 6 ones would appear [63] [1].

4.1 UHE photons and LV

Let us consider again the case of Effective Field Theory (EFT) with LV operators. We shall here deal with modified QED via non-renormalizable, Planck suppressed LV operators (the analogue theory with renormalizable operators being already severely constrained [31]). It has been shown in sec. 1.3 that the addition of the two lowest order non-renormalizable LV operators (mass dimension 5 and 6 respectively) to the effective Lagrangian of

[1] It is however important to stress that the SUSY LV operators considered in [62] do not lead to dispersion relations of the form presented here.

QED leads to the following high-energy modified dispersion relations (MDR) (since the LV correction is proportional to p^n we call them $n-$MDR with $n = 3$ for dimension 5 operators and $n = 4$ for dimension 6 ones)

$$\omega_{\pm}^2 = k^2 + \xi_{\pm}^{(n)} k^n / M^{n-2} \tag{4.1}$$

$$E_{\pm}^2 = p^2 + m_e^2 + \eta_{\pm}^{(n)} p^n / M^{n-2} \,, \tag{4.2}$$

where (4.1) refers to photons while (4.2) refers to fermions. As usual, in the following we will assume M to be comparable to the Planck mass $M_{\rm Pl} \simeq 1.22 \times 10^{19}$ GeV. The constants $\xi_{\pm}^{(n)}$ and $\eta_{\pm}^{(n)}$ indicate the strength of the LV and take values on the whole real axis. In (4.1) the + and − signs denote right and left circular polarisation, while in (4.2) they indicate opposite helicity fermion states.

As already detailed in sec. 1.3, a crucial difference between the $n = 3$ and $n = 4$ cases is the fact that the former is characterised by LV terms which break CPT invariance while the relevant ones for the $4-$MDR are CPT even [63]. This difference implies that for the $3-$MDR there is an effective breaking of the symmetry between the two helicity states of the photon. Indeed one finds that $\xi_{+}^{(3)} = -\xi_{-}^{(3)} \equiv \xi^{(3)}$, while $\xi_{+}^{(4)} = \xi_{-}^{(4)} \equiv \xi^{(4)}$ [63]. On the other hand, it can be shown that the coefficients of electrons and positrons are related as $\eta_{\pm}^{e^-} = (-)^n \eta_{\mp}^{e^+}$, exploiting the argument given in [58, 63].

Since suitable powers of the suppressing scale $M_{\rm Pl}$ have been already factored out in eq.(4.1, 4.2), natural values of the LV, dimensionless coefficients in (4.1, 4.2) are expected to be $O(1)$.

It has been recently pointed out [220] that if Lorentz symmetry was violated, then the absorption of ultra-high-energy (UHE) photons ($E > 10^{19}$ eV) on the Cosmic Microwave Background (CMB) and the Universal Radio Background (URB) could be forbidden, so leading to large photon fluxes reaching Earth. This would violate limits put by current experiments [221, 222] on the photon fraction in UHECR. Hence, very strong constraints $|\xi^{(3)}| \lesssim 10^{-15}$ and $\xi^{(4)} \gtrsim -10^{-7}$ were claimed [220]. An underlying assumption in [220] is that $\eta^{(n)} \simeq 0$ in order to prevent competing reactions with respect to photon absorption. This is an important limitation, as we will show below.

We extend here the idea given in [220] to the full LV QED framework described by the equations (1.31) and (1.32). While the original constraints [220] are weakened, we shall see that, when used together with other EFT reactions, this method has the potentiality not only to basically rule out the $n = 3$ case but also to strongly constrain, for the first time, the CPT-even (hence possibly theoretically favoured) $n = 4$ LV QED.

4.1.1 Basic facts on UHE photons

UHE photons originate in the interactions of UHECRs with the CMB, leading to the production of neutral pions which subsequently decay into photon pairs. Pion production occurs only if the interacting UHECR energy is above $E_{\rm th} \simeq 5 \times 10^{19}\ (\omega_b/1.3\ \text{meV})^{-1}$ eV (ω_b is the target photon energy). Hence, it has long been thought to be responsible for a cut off in the UHECR spectrum, the Greisen-Zatsepin-Kuzmin (GZK) cut-off [110, 111].

Experimentally, the presence of a suppression of the UHECR flux has been confirmed only recently with the observations by the HiReS detector [44] and the Pierre Auger Observatory (PAO) [43]. Although the cut off could be also due to the finite acceleration power of the UHECR sources, the fact that it occurs at the expected energy favours the GZK explanation. The results shown in [165] further strengthen this hypothesis.

The PAO and the Yakutsk and AGASA experiments also imposed limits on the presence of photons in the UHECR spectrum. In particular, the photon fraction is less than 2.0%, 5.1%, 31% and 36% (95% C.L) at $E = 10$, 20, 40, 100 EeV respectively [221, 222]. Although its theoretical computation is quite uncertain and depends on many unknowns related to source and propagation effects [221], it is established that photons are mainly attenuated by pair production onto CMB and URB.

However, pair production is strongly affected by LV. In particular, the (lower) threshold energy can be slightly shifted and in general an upper threshold (a finite energy above which pair production is no more allowed by energy-momentum conservation) can be introduced [102]. Therefore, if the upper threshold energy happens to be lower than 10^{19} eV, then UHE photons are no more attenuated by the CMB and can reach the Earth constituting a significant fraction of the total UHECR flux, thereby violating present experimental limits[2] [220].

However, this argument is not stringent enough to cast constraints on LV in EFT, because in this framework two competitive processes, forbidden in LI physics, are allowed and can effectively dump the photon flux: photon decay in vacuum and photon splitting ($\gamma \to N\gamma$). In [220] the special case $\eta^{(n)} \sim 0$ and $\xi^{(n)} < 0$ was considered, in order to prevent these extra processes. In the following we will study the full parameter space.

[2]This conclusion could be evaded if the GZK process was not effective. However, the large mass difference between pions and electrons implies that, at comparable energies and LV coefficients, the GZK reaction must be much less affected than pair production. Moreover, it can be shown [220] that LV does not affect the kinematics of π^0 decay.

4.2 LV reactions

In order to perform a consistent analysis in LV EFT, we have to consider three processes related to photon attenuation: pair production, γ-decay and photon splitting.

4.2.1 Pair production

This well known process occurs whenever the center-of-mass energy of the $\gamma\gamma$ system is sufficient to produce a e^+/e^- pair, i.e. it is larger than $2m_e$. This condition corresponds to $k \geq k_{\rm th} = m_e^2/\omega_b$.

In the following, we exploit the above mentioned relation $\eta_{\pm}^{e^-} = (-)^n \eta_{\mp}^{e^+}$, as on average the initial state is unpolarised. This is justified as π^0 decay produces photons with opposite polarisation and the CMB is unpolarised on average. Moreover, the interaction at threshold must occur in S-wave, because the particles' momenta need to be aligned [102]. Nevertheless, it is possible that, if the S-wave channel is forbidden, higher partial mode interactions occur in off-threshold configuration. In this case, however, the reaction rate is suppressed by partial mode suppression and because only suitably polarised initial states can contribute to it.

Within this framework, and exploiting energy-momentum conservation, the kinematics equation governing pair production is the following [58]

$$\frac{m^2}{k^n y\,(1-y)} = \frac{4\omega_b}{k^{n-1}} + \tilde{\xi} - \tilde{\eta}\left(y^{n-1} + (-)^n\,(1-y)^{n-1}\right) \tag{4.3}$$

where $\tilde{\xi} \equiv \xi^{(n)}/M^{n-2}$ and $\tilde{\eta} \equiv \eta^{(n)}/M^{n-2}$ are respectively the photon's and electron's LV coefficients divided by powers of M, $0 < y < 1$ is the fraction of momentum carried by either the electron or the positron with respect to the momentum k of the incoming high-energy photon and ω_b is the energy of the target photon (we will assume in the following $\omega_b = \omega_{\rm CMB} \simeq 6 \times 10^{-4}$ eV and will not consider pair production onto the URB, as our main conclusions can be drawn using just CMB). Note that the symmetry of (4.3) under the exchange $e^+ \leftrightarrow e^-$ is manifested in its symmetry under $y \leftrightarrow 1-y$ and $\tilde{\eta} \leftrightarrow (-)^n \tilde{\eta}$.

Pair production can be severely affected by LV. In particular, it has been shown [102] that, rather surprisingly, not only the threshold energy $k_{\rm th}$ is modified, but also an upper threshold is introduced. Physically, this means that at sufficiently high momentum the photon does not carry enough energy to create a pair and simultaneously conserve energy and momentum. However, an upper threshold can only be found in regions of the parameter

space in which the γ-decay is forbidden, because if a single photon is able to create a pair, then *a fortiori* two interacting photons will do [102].

The structure of the lower and upper thresholds for $n = 3, 4$ has been studied in [102] if $\eta_+ = \eta_-$. The same kind of analysis can be extended to the full EFT case. However, being the computation rather cumbersome, we shall evaluate it numerically. The structure of the constraint is different depending on n. If $n = 3$, since $\xi_+^{(3)} = -\xi_-^{(3)}$ and the constraint is imposed on both left and right polarised photons, it is symmetric with respect to $\xi \leftrightarrow -\xi$. If $n = 4$ such a symmetric structure is lost.

4.2.2 γ-decay

While forbidden in LI theory, this reaction is allowed in a LV framework if the photon energy is above a certain threshold. The latter can be easily derived by solving the relative energy-momentum conservation equation which can be readily inferred from (4.3) by noticing that it corresponds to the limit $\omega_b \to 0$.

4.2.3 Photon splitting

This is forbidden for $\xi^{(n)} < 0$ while it is always allowed if $\xi^{(n)} > 0$ [102]. When allowed, the relevance of this process is simply related to its rate. The most relevant cases are $\gamma \to \gamma\gamma$ and $\gamma \to 3\gamma$, because processes with more photons in the final state are suppressed by more powers of the fine structure constant.

The $\gamma \to \gamma\gamma$ process is forbidden in QED because of kinematics and C-parity conservation. In LV EFT neither condition holds. However, we can argue that this process is suppressed by an additional power of the Planck mass, with respect to $\gamma \to 3\gamma$. In fact, in LI QED the matrix element is zero due to the exact cancellation of fermionic and anti-fermionic loops. In LV EFT this cancellation is not exact and the matrix element is expected to be proportional to at least $(\xi E/M_{\rm Pl})^p$, $p > 0$, as it is induced by LV and must vanish in the limit $M_{\rm Pl} \to \infty$.

Therefore we have to deal only with $\gamma \to 3\gamma$. This process has been studied in [102, 223]. In particular, in [223] it was found that, if the "effective photon mass" $m_\gamma^2 \equiv \xi E_\gamma^n / M_{\rm Pl}^{n-2} \ll m_e^2$, then the splitting lifetime of a photon is approximately $\tau^{n=3} \simeq 0.025\, \xi^{-5} f^{-1} \left(50 \text{ TeV}/E_\gamma\right)^{14}$ s, where f is a phase space factor of order 1. This rate was rather higher than the one obtained via dimensional analysis in [102] because, due to integration of loop factors, additional dimensionless contributions proportional to m_e^8 enhance the splitting rate at low energy.

This analysis, however, does not apply to our case, because for photons around 10^{19} eV $m_\gamma^2 \gg m_e^2$ if $\xi^{(3)} > 10^{-17}$ and $\xi^{(4)} > 10^{-8}$. Hence the above mentioned loop contributions are at most logarithmic, as the momentum circulating in the fermionic loop is much larger than m_e. Moreover, in this regime the splitting rate depends only on m_γ, the only energy scale present in the problem.

We then expect the analysis proposed in [102] to be correct and we infer that the splitting time scale at $E_\gamma \simeq 10^{19}$ eV is larger than the propagation one (100 Myr for GZK photons) if $\xi^{(3)} < 0.08$, while if $n = 4$ it is well above 100 Myr even for $\xi^{(4)} \sim O(1)$.

4.3 Results

We have demonstrated so far that only γ-decay and pair production are relevant to our analysis. By considering these processes three kinds of constraints are possible.

On the one hand, since at present we have stringent upper bounds on photon fluxes up to 10^{20} eV [222], then any upper threshold energy introduced by LV in pair production must be larger than this figure. This leads to the constraint represented by the black thick solid lines in fig. 4.1, where the allowed region is obviously the one including the origin and in the case $n = 3$ is the intersection of the upper threshold allowed region with the ones allowed by already existing constraints (red lines). We confirm the claim by [220] that, for $\eta^{(3,4)} = 0$, $|\xi^{(3)}| \lesssim 10^{-15}$ and $\xi^{(4)} \gtrsim -10^{-7}$. However, fig. 4.1 shows that this is a rather special (and favourable) case.

On the other hand, if some photons were detected above 10^{19} eV, then it could be deduced that the threshold energy for γ-decay is larger than this energy (once allowed, photon decay is basically instantaneous [58]). Indeed, the PAO will reach the required sensitivity to probe such theoretically expected fluxes [224] within the next few years [221]. In this case the allowed region would be the "clepsydra" delimited by the black solid line in fig. 4.2 and by the two horizontal red lines corresponding to the birefringence constraint. As it can be inferred from fig. 4.2, for $n = 3$ the combination of the above mentioned constraints would cast the very strong bound $|\eta^{(3)}| < 10^{-7}$. Conversely, no significant limit would be placed for $n = 4$.

Finally, we notice that these two methods do not in principle exclude each other (although the physical effects are mutually exclusive). This is the case if a lower limit to the photon flux at 10^{19} eV is imposed by the experiments (thus implying the absence of γ-decay), while the upper limit at 10^{20} eV is confirmed. The constraint obtained in this case would be very strong, as the

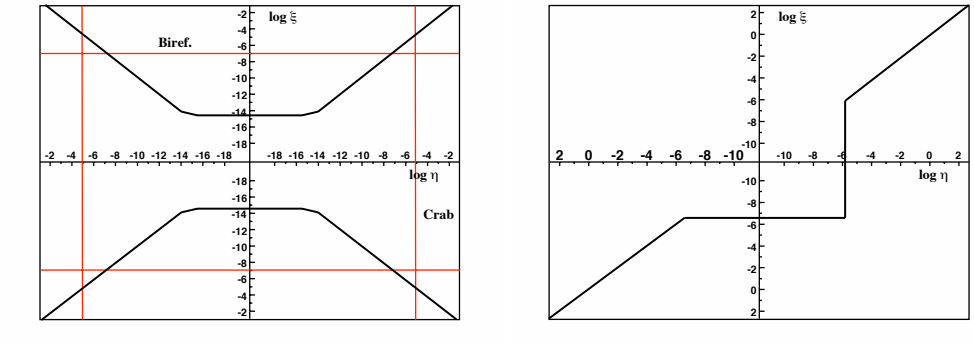

Figure 4.1: Left panel: $n = 3$ LV. Right panel: $n = 4$ LV. Constraints from the absence of pair production upper threshold. The best constraints to date are shown in red, if they exist. The allowed region includes the origin and corresponds to the intersection of the regions bounded by the red and black lines.

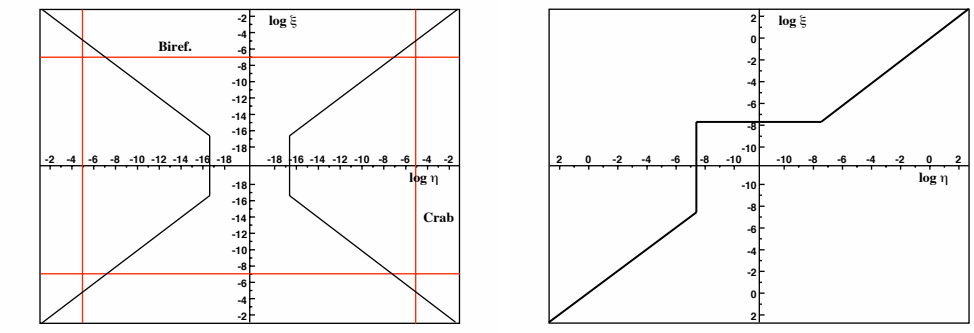

Figure 4.2: Left panel: $n = 3$ LV. Right panel: $n = 4$ LV. γ-decay threshold structure. The best constraints to date are shown in red, if they exist.

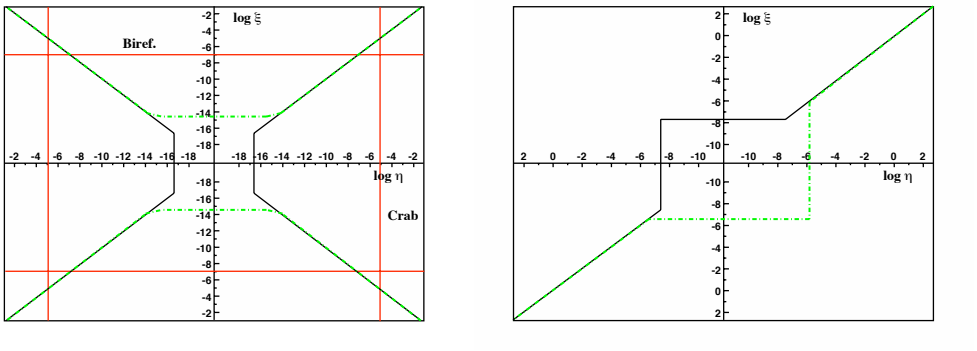

Figure 4.3: Left panel: $n = 3$ LV. Right panel: $n = 4$ LV. The LV parameter space is shown. The current best constraints (when they exist) are drawn in red. Black solid lines represent values of (η, ξ) for which the γ-decay threshold $k_{\gamma-dec} \simeq 10^{19}$ eV. Dot-dashed, green lines indicate pairs (η, ξ) for which the pair production upper threshold $k_{\rm up} \simeq 10^{20}$ eV.

allowed region is given by the intersection of the two regions bounded by the green dot-dashed and the black solid lines in fig. 4.3. Figure 4.3 shows that in this case, for $n = 3$ one would get $|\xi^{(3)}|, |\eta^{(3)}| \lesssim 10^{-14}$, basically ruling out this model. Remarkably, also the case $n = 4$ would be strongly constrained as in this case one could deduce $|\xi^{(4)}|, |\eta^{(4)}| \lesssim 10^{-6}$.

This would be the first strong and robust limit on the $n = 4$, CPT even LV QED, which, as we explained before is also favoured from a theoretical point of view. Accidentally, as a methodological remark, this result also shows that while much attention was focussed on the detection of single event at GZK energies for constraining LV, full spectral information could be more effective.

Conclusions

"There is nothing more
deceptive than an obvious fact"

Sherlock Holmes

This thesis has been devoted to the study of the phenomenology of possible models of Quantum Gravity. In particular, we exploited the consequences of intermediate energy effects induced by Quantum Gravity being described in the context of Effective Field Theory. This framework is known to be able to reproduce successfully most of low energy physics. In the absence of a model of Quantum Gravity mature enough to compute consistently predictions on low energy processes, a reasonable guess is to assume that these processes are described in Effective Field Theory. Indeed, any model of Quantum Gravity should succeed in describing at least the established physics of the Standard Model of particle interactions, hence it should admit an EFT low energy limit.

In particular, we have studied the phenomenology of the violation of Lorentz invariance, a common feature of many QG models. In the context of EFT, LV is expressed through the addition of LV operators to the Lagrangian of the Standard Model. Although both renormalizable and non-renormalizable operators are possible in general, we focused mainly on the latter ones. There are many reasons for this fact: on the one hand, renormalizable operators induce LV at very low energy (comparable to the mass of involved particles), hence they are very strongly constrained by terrestrial experiments; on the other hand, the presence of non-renormalizable operators is somehow theoretically expected, if they are originated by freezing out of high-energy degrees of freedom. These latter operators are naturally suppressed by a mass scale (which is assumed to be of the order of the Planck mass $M_{\rm Pl}$), hence their effects are evident at substantially higher energy than former ones. Since the interesting energy scale for LV effects to be relevant is of the order of at least few TeV if we study electromagnetic interactions of electrons/positrons and photons, observations of high energy radiation from

astrophysical objects are mostly suited for the purpose of studying LV effects.

Throughout this work, we have shown the importance of high-energy astrophysics observations in constraining LV. Indeed, several observations of high energy radiation from a well known galactic object, the Crab Nebula, have been exploited. The most interesting region of the Crab Nebula radiation spectrum is the one with frequencies ranging between ~ 1 MeV$/h$ and ~ 100 MeV$/h$ (h is the Planck's constant). This portion of the spectrum is usually interpreted as due to synchrotron emission of electrons and positrons accelerated at extremely high energies $E \gtrsim 100$ TeV.

In order to study the LV effects on the radiation spectrum, we needed to reconsider the LI model for the Crab Nebula emission. We looked at any model assumption and implication in which Lorentz invariance could play a crucial role and checked whether the same consequences could be kept in presence of LV. In particular, we studied the modifications induced by LV on the Fermi first order acceleration mechanism, which is thought to be responsible for electron and positron acceleration in the Crab Nebula, and the effects of some processes usually forbidden in LI physics, but allowed by LV: the emission of Čerenkov radiation in vacuum and the so called Helicity Decay. In fact, due to the broken CPT invariance of our model, the radiation produced by charged particles depends in general on the helicity state and on the sign of the charge. A thorough analysis has been needed to this aim: on the one hand, we have carried on a detailed computation of the involved QED processes, on the other hand, we needed to set up a complex numerical program and several analysis tools to obtain the Nebula radiation spectrum and analyse data.

Present-day observations do not provide, at the moment, any evidence of violation of Lorentz invariance suppressed by one power of the Planck mass. Therefore, strong constraints on the strength of this violation (that can be readily turned into lower limits on the mass scale suppressing the effective LV operators) have been placed. Furthermore, by considering the physics of Ultra-High-Energy Cosmic Rays and the present observations, we obtained indications that also LV suppressed by two powers of the Planck mass could be disfavoured.

An important methodological result achieved in this thesis is related to the way limits on LV are placed. While former works on this subject just considered observations at single energies (typically, at the highest possible energy at which significant observations were made), we exploited, when possible, broadband, full spectral information, together with a careful LV analysis of each process at work in the astrophysical objects we studied. This allowed us not only to place robust limits on the complete LV parameter space, but also to significantly strengthen existing ones to unprecedented

levels, allowing to basically rule out the model under consideration.

Future observations will allow significant improvements. The first observations in the new field of hard X-ray polarimetry already implied tight limits on photon vacuum birefringence induced by QG. The forthcoming observations by AUGER will probably allow to turn the "indications" mentioned in chap. 4 into stringent limits on the viability of Planck scale suppressed LV.

However, it should be admitted that most of the forthcoming work on Quantum Gravity modeling should be on the theoretical, rather than phenomenological side. The stringent limits discussed in this thesis represent a true challenge for theorists, and a model of QG should address them convincingly. Indeed, limits of the order of 10^{-5}, or 10^{-10} on the magnitude of dimensionless parameters, that should in principle be of the order of 1, need to be explained by a viable theoretical model of QG: either the true description of low energy QG effects is not through EFT, or the actual mechanism by which the high energy degrees of freedom affect the low energy world produces stronger suppressions than what we expected.

We are not able at present to guess what the answer to these questions is. Only a thorough study of the low energy implications of Quantum Gravity, if it definitely exists, might solve this problem.

Bibliography

[1] The HEGRA, F. Aharonian *et al.*, Astrophys. J. **614**, 897 (2004), astro-ph/0407118.

[2] E. Costa *et al.*, (2002), astro-ph/0207440.

[3] L. Anchordoqui, T. Paul, S. Reucroft, and J. Swain, Int. J. Mod. Phys. **A18**, 2229 (2003), hep-ph/0206072.

[4] J. A. Simpson, Annual Review of Nuclear and Particle Science **33**, 323 (1983).

[5] The KASCADE, K.-H. Kampert *et al.*, Nucl. Phys. Proc. Suppl. **136**, 273 (2004), astro-ph/0410559.

[6] K.-H. Kampert, (2008), 0801.1986.

[7] A. M. Hillas, Ann. Rev. Astron. Astrophys. **22**, 425 (1984).

[8] A. W. Strong, I. V. Moskalenko, and V. S. Ptuskin, Ann. Rev. Nucl. Part. Sci. **57**, 285 (2007), astro-ph/0701517.

[9] W. R. Binns *et al.*, Astrophys. J. **346**, 997 (1989).

[10] S. P. Swordy, D. Mueller, P. Meyer, J. L'Heureux, and J. M. Grunsfeld, Astrophys. J. **349**, 625 (1990).

[11] A. D. Panov *et al.*, (2007), 0707.4415.

[12] BESS, S. Orito *et al.*, Phys. Rev. Lett. **84**, 1078 (2000), astro-ph/9906426.

[13] BESS, T. Maeno *et al.*, Astropart. Phys. **16**, 121 (2001), astro-ph/0010381.

[14] WiZard/CAPRICE, M. Boezio *et al.*, Astrophys. J. **561**, 787 (2001), astro-ph/0103513.

[15] L. Arruda *et al.*, (2008), 0801.4957.

[16] S. D. Hunger *et al.*, Astrophys. J. **481**, 205 (1997).

[17] A. W. Strong, I. V. Moskalenko, O. Reimer, S. Digel, and R. Diehl, Astron. Astrophys. **422**, L47 (2004), astro-ph/0405275.

[18] S. Sarkar, Mod. Phys. Lett. **A17**, 1025 (2002), gr-qc/0204092.

[19] V. Cavasinni, D. Grasso, and L. Maccione, Astropart. Phys. **26**, 41 (2006), astro-ph/0604004.

[20] C. Evoli, D. Grasso, and L. Maccione, JCAP **0706**, 003 (2007), astro-ph/0701856.

[21] L. Maccione, S. Liberati, A. Celotti, and J. Kirk, Journal of Cosmology and Astroparticle Physics **2007**, 013 (2007), arXiv:0707.2673 [astro-ph].

[22] L. Maccione and S. Liberati, (2008), 0805.2548.

[23] C. Evoli, D. Gaggero, D. Grasso, and L. Maccione, (2008), 0807.4730.

[24] L. Maccione, S. Liberati, A. Celotti, J. G. Kirk, and P. Ubertini, (2008), 0809.0220.

[25] N. E. Mavromatos, Lect. Notes Phys. **669**, 245 (2005), gr-qc/0407005.

[26] S. Weinberg, Phys. Rev. **D72**, 043514 (2005), hep-th/0506236.

[27] T. Damour and A. M. Polyakov, Nucl. Phys. **B423**, 532 (1994), hep-th/9401069.

[28] J. D. Barrow, (1997), gr-qc/9711084.

[29] M. Bleicher, S. Hofmann, S. Hossenfelder, and H. Stoecker, Phys. Lett. **B548**, 73 (2002), hep-ph/0112186.

[30] V. A. Kostelecky, Phys. Rev. **D69**, 105009 (2004), hep-th/0312310.

[31] D. Mattingly, Living Rev. Rel. **8**, 5 (2005), gr-qc/0502097.

[32] O. W. Greenberg, Phys. Rev. Lett. **89**, 231602 (2002), hep-ph/0201258.

[33] S. Liberati, S. Sonego, and M. Visser, Annals Phys. **298**, 167 (2002), gr-qc/0107091.

[34] R. Lehnert, (2006), hep-ph/0611177.

[35] V. A. Kostelecky and S. Samuel, Phys. Rev. **D39**, 683 (1989).

[36] G. Amelino-Camelia, J. R. Ellis, N. E. Mavromatos, D. V. Nanopoulos, and S. Sarkar, Nature **393**, 763 (1998), astro-ph/9712103.

[37] R. Gambini and J. Pullin, Phys. Rev. **D59**, 124021 (1999), gr-qc/9809038.

[38] S. M. Carroll, J. A. Harvey, V. A. Kostelecky, C. D. Lane, and T. Okamoto, Phys. Rev. Lett. **87**, 141601 (2001), hep-th/0105082.

[39] J. Lukierski, H. Ruegg, and W. J. Zakrzewski, Ann. Phys. **243**, 90 (1995), hep-th/9312153.

[40] G. Amelino-Camelia and S. Majid, Int. J. Mod. Phys. **A15**, 4301 (2000), hep-th/9907110.

[41] C. P. Burgess, J. Cline, E. Filotas, J. Matias, and G. D. Moore, JHEP **03**, 043 (2002), hep-ph/0201082.

[42] C. Barcelo, S. Liberati, and M. Visser, Living Rev. Rel. **8**, 12 (2005), gr-qc/0505065.

[43] Pierre Auger, M. Roth, (2007), arXiv:0706.2096 [astro-ph].

[44] HiRes, R. Abbasi *et al.*, (2007), astro-ph/0703099.

[45] G. Amelino-Camelia, Int. J. Mod. Phys. **D11**, 35 (2002), gr-qc/0012051.

[46] G. Amelino-Camelia, Phys. Lett. **B510**, 255 (2001), hep-th/0012238.

[47] H. P. Robertson, Reviews of Modern Physics **21**, 378 (1949).

[48] R. Mansouri and R. U. Sexl, General Relativity and Gravitation **8**, 497 (1977).

[49] C. M. Will, Living Rev. Rel. **4**, 4 (2001), gr-qc/0103036.

[50] V. A. Kostelecky and M. Mewes, Phys. Rev. **D66**, 056005 (2002), hep-ph/0205211.

[51] G. Amelino-Camelia, (2003), gr-qc/0309054.

[52] J. Lukierski, (2004), hep-th/0402117.

[53] G. Amelino-Camelia, (2008), 0806.0339.

[54] S. Judes and M. Visser, Phys. Rev. **D68**, 045001 (2003), gr-qc/0205067.

[55] Particle Data Group, W. M. Yao *et al.*, J. Phys. **G33**, 1 (2006).

[56] R. C. Myers and M. Pospelov, Phys. Rev. Lett. **90**, 211601 (2003), hep-ph/0301124.

[57] P. A. Bolokhov and M. Pospelov, (2007), hep-ph/0703291.

[58] T. Jacobson, S. Liberati, and D. Mattingly, Annals Phys. **321**, 150 (2006), astro-ph/0505267.

[59] T. A. Jacobson, S. Liberati, D. Mattingly, and F. W. Stecker, Phys. Rev. Lett. **93**, 021101 (2004), astro-ph/0309681.

[60] J. Collins, A. Perez, D. Sudarsky, L. Urrutia, and H. Vucetich, Phys. Rev. Lett. **93**, 191301 (2004), gr-qc/0403053.

[61] S. Groot Nibbelink and M. Pospelov, Phys. Rev. Lett. **94**, 081601 (2005), hep-ph/0404271.

[62] P. A. Bolokhov, S. G. Nibbelink, and M. Pospelov, Phys. Rev. **D72**, 015013 (2005), hep-ph/0505029.

[63] D. Mattingly, (2008), 0802.1561.

[64] M. Gasperini, Class. Quant. Grav. **4**, 485 (1987).

[65] D. Mattingly and T. Jacobson, (2001), gr-qc/0112012.

[66] N. Arkani-Hamed, H.-C. Cheng, M. A. Luty, and S. Mukohyama, JHEP **05**, 074 (2004), hep-th/0312099.

[67] J. W. Moffat, Int. J. Mod. Phys. **D12**, 1279 (2003), hep-th/0211167.

[68] C. Eling, T. Jacobson, and D. Mattingly, (2004), gr-qc/0410001.

[69] O. Bertolami and J. Paramos, Phys. Rev. **D72**, 044001 (2005), hep-th/0504215.

[70] J. W. Elliott, G. D. Moore, and H. Stoica, JHEP **08**, 066 (2005), hep-ph/0505211.

[71] T. Jacobson, (2008), 0801.1547.

[72] J. R. Ellis, N. E. Mavromatos, and A. S. Sakharov, Astropart. Phys. **20**, 669 (2004), astro-ph/0308403.

[73] J. R. Ellis, N. E. Mavromatos, and D. V. Nanopoulos, Phys. Lett. **B293**, 37 (1992), hep-th/9207103.

[74] J. R. Ellis, N. E. Mavromatos, D. V. Nanopoulos, and A. S. Sakharov, Int. J. Mod. Phys. **A19**, 4413 (2004), gr-qc/0312044.

[75] J. Polchinski, (1996), hep-th/9611050.

[76] MAGIC, J. Albert *et al.*, (2007), 0708.2889.

[77] Y.-Z. Fan, D.-M. Wei, and D. Xu, Mon. Not. Roy. Astron. Soc. **376**, 1857 (2006), astro-ph/0702006.

[78] L. S. Brown and G. Gabrielse, Rev. Mod. Phys. **58**, 233 (1986).

[79] R. Bluhm, V. A. Kostelecky, and N. Russell, Phys. Rev. **D57**, 3932 (1998), hep-ph/9809543.

[80] V. A. Kostelecky and N. Russell, (2008), 0801.0287.

[81] R. K. Mittleman, I. I. Ioannou, H. G. Dehmelt, and N. Russell, Phys. Rev. Lett. **83**, 2116 (1999).

[82] V. W. Hughes, H. G. Robinson, and V. Beltran-Lopez, Phys. Rev. Lett. **4**, 342 (1960).

[83] R. W. P. Drever, Philosophical Magazine **6**, 683 (1961).

[84] D. Bear, R. E. Stoner, R. L. Walsworth, V. A. Kostelecky, and C. D. Lane, Phys. Rev. Lett. **85**, 5038 (2000), physics/0007049.

[85] V. A. Kostelecky and C. D. Lane, Phys. Rev. **D60**, 116010 (1999), hep-ph/9908504.

[86] O. Bertolami and J. G. Rosa, Phys. Rev. **D71**, 097901 (2005), hep-ph/0412289.

[87] D. F. Phillips *et al.*, Phys. Rev. **D63**, 111101 (2001), physics/0008230.

[88] R. Bluhm and V. A. Kostelecky, Phys. Rev. Lett. **84**, 1381 (2000), hep-ph/9912542.

[89] E. . Kostelecky, V. Alan, Singapore, Singapore: World Scientific (1999) 256 p.

[90] B. R. Heckel, Prepared for 3rd Meeting on CPT and Lorentz Symmetry (CPT 04), Bloomington, Indiana, 4-7 Aug 2004.

[91] L.-S. Hou, W.-T. Ni, and Y.-C. M. Li, Physical Review Letters **90**, 201101 (2003).

[92] V. A. Kostelecky, Phys. Rev. **D64**, 076001 (2001), hep-ph/0104120.

[93] H. Nguyen, (2001), hep-ex/0112046.

[94] KLOE, A. Di Domenico, Frascati Phys. Ser. **41**, 79 (2006).

[95] G. Gwinner *et al.*, Prepared for 3rd Meeting on CPT and Lorentz Symmetry (CPT 04), Bloomington, Indiana, 4-7 Aug 2004.

[96] C. D. Lane, Phys. Rev. **D72**, 016005 (2005), hep-ph/0505130.

[97] M. E. Tobar, P. Wolf, A. Fowler, and J. G. Hartnett, Phys. Rev. **D71**, 025004 (2005), hep-ph/0408006.

[98] J. R. Ellis, N. E. Mavromatos, D. V. Nanopoulos, A. S. Sakharov, and E. K. G. Sarkisyan, Astropart. Phys. **25**, 402 (2006), astro-ph/0510172.

[99] S. D. Biller *et al.*, Phys. Rev. Lett. **83**, 2108 (1999), gr-qc/9810044.

[100] R. J. Gleiser and C. N. Kozameh, Phys. Rev. **D64**, 083007 (2001), gr-qc/0102093.

[101] D. Mattingly, T. Jacobson, and S. Liberati, Phys. Rev. **D67**, 124012 (2003), hep-ph/0211466.

[102] T. Jacobson, S. Liberati, and D. Mattingly, Phys. Rev. **D67**, 124011 (2003), hep-ph/0209264.

[103] T. Jacobson, S. Liberati, and D. Mattingly, Nature **424**, 1019 (2003), astro-ph/0212190.

[104] R. Montemayor and L. F. Urrutia, Phys. Rev. **D72**, 045018 (2005), hep-ph/0505135.

[105] G. Amelino-Camelia, J. Kowalski-Glikman, G. Mandanici, and A. Procaccini, Int. J. Mod. Phys. **A20**, 6007 (2005), gr-qc/0312124.

[106] J. R. Ellis, N. E. Mavromatos, and D. V. Nanopoulos, Phys. Rev. **D61**, 027503 (2000), gr-qc/9906029.

[107] J. R. Ellis, N. E. Mavromatos, and D. V. Nanopoulos, Phys. Rev. **D62**, 084019 (2000), gr-qc/0006004.

[108] G. Amelino-Camelia, New J. Phys. **6**, 188 (2004), gr-qc/0212002.

[109] P. L. Nolan *et al.*, Astrophys. J. **409**, 697 (1993).

[110] K. Greisen, Phys. Rev. Lett. **16**, 748 (1966).

[111] G. T. Zatsepin and V. A. Kuz'min, On the interaction of cosmic rays with photons., in *Cosmic rays, Moscow, No. 11, p. 45 - 47* Vol. 11, pp. 45–47, 1969.

[112] S. R. Coleman and S. L. Glashow, (1998), hep-ph/9808446.

[113] R. Aloisio, P. Blasi, P. L. Ghia, and A. F. Grillo, Phys. Rev. **D62**, 053010 (2000), astro-ph/0001258.

[114] R. Aloisio, P. Blasi, A. Galante, P. L. Ghia, and A. F. Grillo, (2002), astro-ph/0210402.

[115] J. Ellis, N. Harries, A. Meregaglia, A. Rubbia, and A. Sakharov, (2008), 0805.0253.

[116] J. G. Kirk, Y. Lyubarsky, and J. Petri, (2007), astro-ph/0703116.

[117] A. Achterberg, Y. A. Gallant, J. G. Kirk, and A. W. Guthmann, Mon. Not. Roy. Astron. Soc. **328**, 393 (2001), astro-ph/0107530.

[118] M. F. Bietenholz, J. J. Hester, D. A. Frail, and N. Bartel, Astrophys. J. **615**, 794 (2004), astro-ph/0408061.

[119] K. Mori *et al.*, Astrophys. J. **609**, 186 (2004), astro-ph/0403287.

[120] F. D. Seward, W. H. Tucker, and R. A. Fesen, Astrophys. J. **652**, 1277 (2006), astro-ph/0608485.

[121] M. G. F. Kirsch *et al.*, (2006), astro-ph/0604097.

[122] C. F. Kennel and F. V. Coroniti, Astrophys. J. **283**, 694 (1984).

[123] J. Clear *et al.*, Astron. & Astrophys. **174**, 85 (1987).

[124] O. C. de Jager and A. K. Harding, Astrophys. J. **396**, 161 (1992).

[125] A. M. Hillas *et al.*, Astrophys. J. **503**, 744 (1998).

[126] J. Kildea and et al., Observations of the Crab Nebula and Pulsar with STACEE, in *International Cosmic Ray Conference*, , International Cosmic Ray Conference Vol. 4, pp. 89–+, 2005.

[127] MAGIC, R. M. Wagner *et al.*, Prepared for 29th International Cosmic Ray Conference (ICRC 2005), Pune, India, 3-11 Aug 2005.

[128] H.E.S.S., F. Aharonian *et al.*, Astron. Astrophys. **457**, 899 (2006), astro-ph/0607333.

[129] Tibet Gamma, M. Amenomori *et al.*, (1999), astro-ph/9909172.

[130] Milagro, R. W. Atkins *et al.*, Astrophys. J. **595**, 803 (2003), astro-ph/0305308.

[131] C. F. Kennel and F. V. Coroniti, Astrophys. J. **283**, 710 (1984).

[132] M. J. Rees and J. E. Gunn, Mon. Not. Roy. Astron. Soc. **167**, 1 (1974).

[133] P. Goldreich and W. H. Julian, Astrophys. J. **157**, 869 (1969).

[134] R. T. Emmering and R. A. Chevalier, Astrphys. J. **321**, 334 (1987).

[135] Z.-Y. Li and M. C. Begelman, Astrophys. J. **400**, 186 (1992).

[136] E. van der Swaluw, Astron. Astrophys. **404**, 939 (2003), astro-ph/0303661.

[137] P. L. Marsden *et al.*, Astrophys. J. Lett. **278**, L29 (1984).

[138] A. M. Atoyan and F. A. Aharonian, MNRAS **278**, 525 (1996).

[139] C. M. Reyes, L. Urrutia, and J. D. Vergara, (2007), 0712.3489.

[140] L. D. Landau and E. M. Lifshitz, *Relativistische Quantentheorie* (Lehrbuch der theoretischen Physik, Berlin: Akademie-Verlag, 1970, 1970).

[141] J. G. Kirk, (2005), astro-ph/0503316.

[142] G. Morlino, P. Blasi, and M. Vietri, Astrophys. J. **658**, 1069 (2007), arXiv:astro-ph/0701173.

[143] J. G. Kirk, A. W. Guthmann, Y. A. Gallant, and A. Achterberg, Astrophys. J. **542**, 235 (2000), arXiv:astro-ph/0005222.

[144] R. Lieu and W. I. Axford, Astrophys. J. **416**, 700 (1993).

[145] P. R. Bevington and D. K. Robinson, *Data reduction and error analysis for the physical sciences* (New York: McGraw-Hill, —c1992, 2nd ed., 1992).

[146] A. J. Dean *et al.*, Science **321**, 1183 (2008).

[147] A. N. Parmar *et al.*, INTEGRAL Mission, in *X-Ray and Gamma-Ray Telescopes and Instruments for Astronomy. Edited by Joachim E. Truemper, Harvey D. Tananbaum. Proceedings of the SPIE, Volume 4851, pp. 1104-1112*, 2003.

[148] M. Forot, P. Laurent, I. A. Grenier, C. Gouiffes, and F. Lebrun, (2008), 0809.1292.

[149] S. McGlynn *et al.*, (2007), astro-ph/0702738.

[150] J. Petri and J. G. Kirk, Astrophys. J. **627**, L37 (2005), astro-ph/0505427.

[151] M. C. Weisskopf, E. H. Silver, H. L. Kestenbaum, K. S. Long, and R. Novick, ApJL **220**, L117 (1978).

[152] C. Y. Ng and R. W. Romani, Astrophys. J. **601**, 479 (2004), astro-ph/0310155.

[153] G. Kanbach, A. Slowikowska, S. Kellner, and H. Steinle, AIP Conf. Proc. **801**, 306 (2005), astro-ph/0511636.

[154] Y. Kanai *et al.*, Nuclear Instruments and Methods in Physics Research A **570**, 61 (2007).

[155] E. Costa *et al.*, (2006), astro-ph/0609576.

[156] J. Knodlseder *et al.*, (2007), 0707.4627.

[157] P. Auger, P. Ehrenfest, R. Maze, J. Daudin, and A. F. Robley, Rev. Mod. Phys. **11**, 288 (1939).

[158] W. Heitler, Royal Society of London Proceedings Series A **166**, 529 (1938).

[159] S. Sarkar, (2002), hep-ph/0202013.

[160] T. K. Gaisser and T. Stanev, Nucl. Phys. **A777**, 98 (2006).

[161] D. R. Bergman and J. W. Belz, J. Phys. **G34**, R359 (2007), 0704.3721.

[162] E. Fermi, Phys. Rev. **75**, 1169 (1949).

[163] V. S. Berezinskii, S. V. Bulanov, V. A. Dogiel, and V. S. Ptuskin, *Astrophysics of cosmic rays* (Amsterdam: North-Holland, 1990, edited by Ginzburg, V.L., 1990).

[164] J. Candia, S. Mollerach, and E. Roulet, JCAP **0305**, 003 (2003), astro-ph/0302082.

[165] Pierre Auger, J. Abraham *et al.*, Science **318**, 938 (2007), 0711.2256.

[166] T. K. Gaisser, *Cosmic rays and particle physics* (Cambridge and New York, Cambridge University Press, 1990, 292 p., 1990).

[167] H. Reeves, W. A. Fowler, and F. Hoyle, Nature **226**, 727 (1970).

[168] Y. e. a. Fedorova, Hires collaboration, in *Proc. 30th ICRC, Mérida, p.1236*, 2007.

[169] M. e. a. Unger, Pierre auger collaboration, in *Proc. 30th ICRC, Mérida, p.594*, 2007.

[170] R. Aloisio *et al.*, Astropart. Phys. **27**, 76 (2007), astro-ph/0608219.

[171] M. R. George, A. C. Fabian, W. H. Baumgartner, R. F. Mushotzky, and J. Tueller, (2008), 0805.2053.

[172] G. Ghisellini, G. Ghirlanda, F. Tavecchio, F. Fraternali, and G. Pareschi, (2008), 0806.2393.

[173] D. Gorbunov, P. Tinyakov, I. Tkachev, and S. Troitsky, (2007), 0711.4060.

[174] D. S. Gorbunov, P. G. Tinyakov, I. I. Tkachev, and S. V. Troitsky, (2008), 0804.1088.

[175] P. O. Lagage and C. J. Cesarsky, Astron. & Astrophys. **125**, 249 (1983).

[176] H.E.S.S., F. Aharonian *et al.*, Nature **439**, 695 (2006), astro-ph/0603021.

[177] M. D. Kistler and J. F. Beacom, Phys. Rev. **D74**, 063007 (2006), astro-ph/0607082.

[178] F. Vissani, Astropart. Phys. **26**, 310 (2006), astro-ph/0607249.

[179] NEMO, E. Migneco *et al.*, Prepared for VLVnT Workshop on Technical Aspects of a Very Large Volume Neutrino Telescope in the Mediterrenean Sea, Amsterdam, The Netherlands, 5-8 Oct 2003.

[180] IceCube, A. Achterberg *et al.*, Astropart. Phys. **26**, 155 (2006), astro-ph/0604450.

[181] V. L. Ginzburg and S. I. Syrovatskii, *The Origin of Cosmic Rays* (The Origin of Cosmic Rays, New York: Macmillan, 1964, 1964).

[182] D. Maurin, F. Donato, R. Taillet, and P. Salati, Astrophys. J. **555**, 585 (2001), astro-ph/0101231.

[183] D. Maurin, R. Taillet, and F. Donato, Astron. Astrophys. **394**, 1039 (2002), astro-ph/0206286.

[184] A. W. Strong and I. V. Moskalenko, Astrophys. J. **509**, 212 (1998), astro-ph/9807150.

[185] A. W. Strong, I. V. Moskalenko, and O. Reimer, Astrophys. J. **613**, 962 (2004), astro-ph/0406254.

[186] A. Castellina and F. Donato, Astropart. Phys. **24**, 146 (2005), astro-ph/0504149.

[187] V. S. Ptuskin *et al.*, Astron. & Astrophys. **268**, 726 (1993).

[188] J. Candia and E. Roulet, JCAP **0410**, 007 (2004), astro-ph/0408054.

[189] F. Casse, M. Lemoine, and G. Pelletier, Phys. Rev. **D65**, 023002 (2002), astro-ph/0109223.

[190] D. De Marco, P. Blasi, and T. Stanev, JCAP **0706**, 027 (2007), 0705.1972.

[191] D. Breitschwerdt, V. A. Dogiel, and H. J. Volk, (2002), astro-ph/0201345.

[192] X.-H. Sun and J. L. Han, (2004), astro-ph/0402180.

[193] A. W. Clegg, J. M. Cordes, J. M. Simonetti, and S. R. Kulkarni, Astrophys. J. **386**, 143 (1992).

[194] M. Haverkorn *et al.*, Astrophys. J. **637**, L33 (2006), astro-ph/0512456.

[195] J. L. Han and G. J. Qiao, Astron. & Astrophys. **288**, 759 (1994).

[196] T. Shibata, M. Hareyama, M. Nakazawa, and C. Saito, Astrophys. J. **642**, 882 (2006).

[197] J. Candia, E. Roulet, and L. N. Epele, JHEP **12**, 033 (2002), astro-ph/0206336.

[198] V. S. Ptuskin, H. J. Voelk, V. N. Zirakashvili, and D. Breitschwerdt, Astron. & Astrophys. **321**, 434 (1997).

[199] K. M. Ferriere, Rev. Mod. Phys. **73**, 1031 (2001), astro-ph/0106359.

[200] A. W. Strong and J. R. Mattox, Astron. & Astrophys. **308**, L21 (1996).

[201] J. R. Letaw, R. Silberberg, and C. H. Tsao, Astrophys. J. Suppl. **51**, 271 (1983).

[202] W. R. Webber, J. C. Kish, and D. A. Schrier, Phys. Rev. **C41**, 520 (1990).

[203] R. Silberberg and C. H. Tsao, Phys. Rept. **191**, 351 (1990).

[204] K. Ferriere, W. Gillard, and P. Jean, Astron. Astrophys. **467**, 611 (2007), astro-ph/0702532.

[205] M. Asplund, N. Grevesse, and J. Sauval, Nucl. Phys. **A777**, 1 (2006), astro-ph/0410214.

[206] L. J. Gleeson and W. I. Axford, Astrophys. J. **154**, 1011 (1968).

[207] H. S. Ahn *et al.*, Nucl. Instrum. Meth. **A579**, 1034 (2007).

[208] D. Muller *et al.*, Prepared for 30th International Cosmic Ray Conference (ICRC 2007), Merida, Yucatan, Mexico, 3-11 Jul 2007.

[209] T. Hams *et al.*, Astrophys. J. **611**, 892 (2004).

[210] I. V. Moskalenko, S. G. Mashnik, and A. W. Strong, (2001), astro-ph/0106502.

[211] L. Bergstrom, J. Edsjo, and P. Ullio, Astrophys. J. **526**, 215 (1999), astro-ph/9902012.

[212] F. Donato *et al.*, Astrophys. J. **536**, 172 (2001), astro-ph/0103150.

[213] I. V. Moskalenko, A. W. Strong, J. F. Ormes, and M. S. Potgieter, Astrophys. J. **565**, 280 (2002), astro-ph/0106567.

[214] L. C. Tan and L. K. Ng, Phys. Rev. **D26**, 1179 (1982).

[215] M. Simon, A. Molnar, and S. Roesler, Astrophys. J. **499**, 250 (1998).

[216] T. Sanuki *et al.*, Astrophys. J. **545**, 1135 (2000), astro-ph/0002481.

[217] PAMELA, P. Picozza and M. Casolino.

[218] L. Bronfman, R. S. Cohen, H. Alvarez, J. May, and P. Thaddeus, Astrophys. J. **324**, 248 (1988).

[219] C. Evoli, D. Gaggero, D. Grasso, and L. Maccione, Prepared for 5th Workshop on Science with the New Generation High Energy Gamma-ray Experiments (SciNe-GHE07): The Light of the Dark: Solving the Mysteries of the Universe, Frascati, Rome, Italy, 18-20 Jun 2007.

[220] M. Galaverni and G. Sigl, Phys. Rev. Lett. **100**, 021102 (2008), 0708.1737.

[221] Pierre Auger, J. Abraham *et al.*, Astropart. Phys. **29**, 243 (2008), 0712.1147.

[222] G. I. Rubtsov *et al.*, Phys. Rev. **D73**, 063009 (2006), astro-ph/0601449.

[223] G. Gelmini, S. Nussinov, and C. E. Yaguna, JCAP **0506**, 012 (2005), hep-ph/0503130.

[224] G. Gelmini, O. Kalashev, and D. V. Semikoz, (2005), astro-ph/0506128.